

Unlocking Galactic Wolf-Rayet stars with *Gaia* DR2 I: Distances and absolute magnitudes

Gemma Rate,^{*} Paul A. Crowther

Department of Physics and Astronomy, University of Sheffield, Sheffield, S3 7RH, UK

Accepted XXX. Received YYY; in original form ZZZ

ABSTRACT

We obtain distances to 383 Galactic Wolf-Rayet (WR) stars from *Gaia* DR2 parallaxes and Bayesian methods, with a prior based on H_{II} regions and dust extinction. Distances agree with those from Bailer-Jones et al. for stars up to 2 kpc from the Sun, though deviate thereafter due to differing priors, leading to modest reductions in luminosities for recent WR spectroscopic results. We calculate visual and K-band absolute magnitudes, accounting for dust extinction contributions and binarity, and identify 187 stars with reliable absolute magnitudes. For WR and O stars within 2 kpc, we find a WR/O ratio of 0.09. The distances are used to generate absolute magnitude calibrations and obtain the *Gaia* colour magnitude diagram for WR stars. Average v^{WR} -band absolute magnitudes for WN stars range from −3.6 mag (WN3–4) to −7.0 mag (WN8–9ha), and −3.1 (WO2–4) to −4.6 mag (WC9), with standard deviations of ∼0.6 mag. Using H_{II} region scale heights, we identify 31 WR stars at large ($3\sigma, |z| \geq 156$ pc) distances from the mid-plane as potential runaways accounting for the Galactic warp, of which only 4 involve WN8–9 stars, contrary to previous claims.

Key words: stars: Wolf-Rayet – stars: massive – stars: distances – Galaxy: disc

1 INTRODUCTION

Wolf-Rayet (WR) stars are the final stages of evolution for massive O stars (>25 M_⊙, Crowther 2007). With extremely fast and dense stellar winds, they play an important role in helping to ionize H_{II} regions and disperse natal gas left over from the star formation process. This feedback may drive and quench star formation. Additionally, WR stars are potential progenitors of long Gamma Ray Bursts (Leloudas et al. 2010) and stripped envelope supernovae, although some may collapse directly to black holes (Georgy et al. 2009).

The later stages of massive star evolution depend heavily on parameters such as initial mass and metallicity, which influence mass loss rates (Meynet & Maeder 2005). Such dependencies make modelling massive star evolution challenging. The accuracy of evolutionary models can be tested with observations, which in turn depend on reliable distances. Inaccurate distances can thus lead to an incorrect understanding of massive star evolution.

The Milky Way contains a rich population of WR stars, whose total has been estimated at 1200±200 (Rosslowe &

Crowther 2015b). Over half have been detected thus far¹. Of those, approximately half have been discovered via IR surveys (e.g. Crowther et al. 2006, Hadfield et al. 2007, Shara et al. 2009), whilst the rest are optically visible. Until now, distances to WR stars have relied upon the small subset of the population, which are thought to be members of clusters or associations (e.g. Lundström & Stenholm 1984). These stars, along with the WR population of the Magellanic Clouds (e.g. Smith 1968 and Vacca & Torres-Dodgen 1990), have been used to calculate absolute magnitude calibrations (e.g. van der Hucht 2001, Rosslowe & Crowther 2015a). The calibrations were then applied to estimate distances to field stars. As there is some variation in absolute magnitudes within spectral subtypes, the resulting distances had large uncertainties (50% according to van der Hucht 2001).

Binarity is a key additional piece of the evolutionary puzzle for massive stars. Mason et al. (2009) estimates that 40–70% of all massive stars are in binaries. Additionally, Sana et al. (2012) suggests that 70% of O stars will undergo interaction during their lifetimes. WR stars may form via Roche Lobe overflow (Kippenhahn & Weigert 1967) at the

* garate1@sheffield.ac.uk

¹ <http://pacrowther.staff.shef.ac.uk/WRcat/index.php>, v1.21

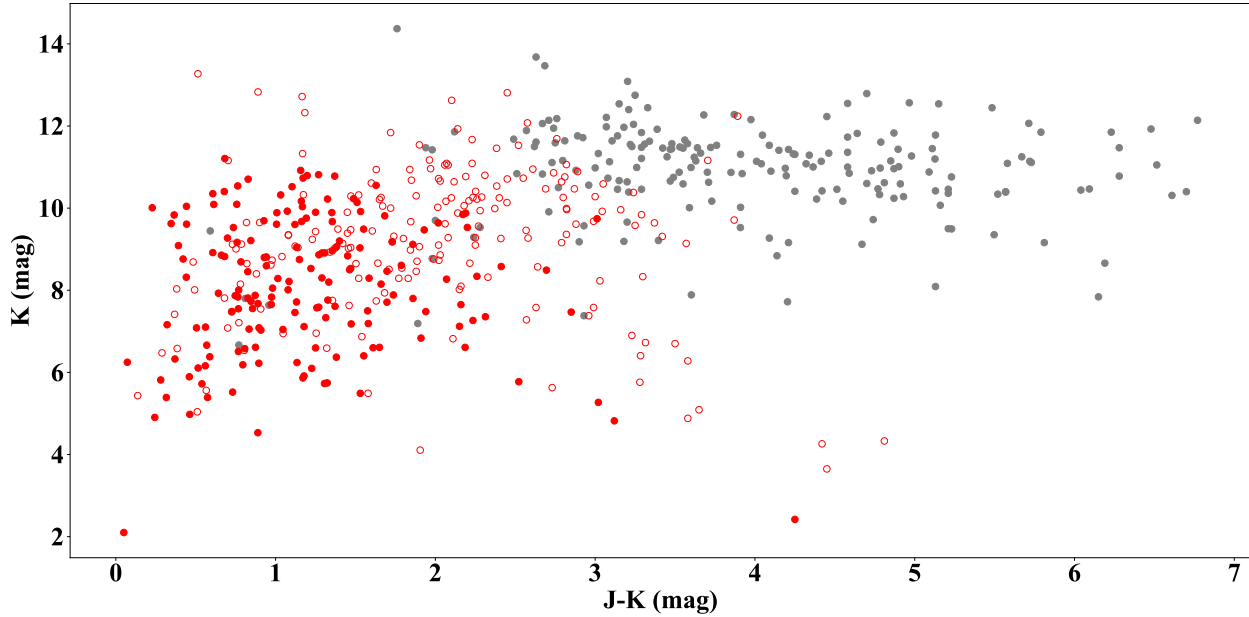


Figure 1. Plot showing the colour magnitude diagram of Galactic WR stars from the catalogue detected by *Gaia* (red) and WR stars only observed at IR wavelengths (grey). Stars not observed by *Gaia* have larger (>3) J–K colours, indicating significant extinction. Filled red circles are stars with the most reliable distances, these are limited to bright sources ($K < 12$) with $J-K < 3$.

upper end of the stripped star regime (Götberg et al. 2018) and may be responsible for the high rate of observed Ibc supernovae, relative to the number of massive stars (Eldridge et al. 2013, Smith et al. 2011).

Binaries therefore have a major influence on the evolutionary trajectory of massive stars. Studying the fractions of runaways can provide an insight into how massive binaries interact and verify models involving binary physics. Here, again, accurate distances are essential to determine how far a WR star has travelled over its lifetime.

The second *Gaia* data release (Gaia Collaboration et al. 2018a, Gaia Collaboration et al. 2016, hereafter referred to as DR2) offers parallaxes, proper motions and positions for over a billion stars in the Galaxy. A large fraction of the Galactic WR population have been detected in the *Gaia* G band, (330–1050nm) and so *Gaia* increases the number of WR with trigonometric parallaxes from just one (WR11 in Hipparcos, van Leeuwen 2007) to almost 400.

In this work (Paper I) we present distances obtained using *Gaia* data and discuss the resulting new insights into Wolf-Rayet absolute magnitudes, runaways and physical parameters. In Section 2, we determine the most likely distances for Galactic WR stars using a Bayesian method and in Section 3, validate these using absolute magnitudes. We compare the new *Gaia* distances to previous values in Section 4. Distances from the Galactic midplane are discussed in section 5 and used to identify potential runaways. Finally, we conclude with an overview and anticipate potential improvements from later *Gaia* data releases.

In Paper II (Rate, Crowther & Parker, submitted), we will use these new distances and other *Gaia* DR2 results to reevaluate WR membership of clusters and associations, and

discuss the implications of the results on our understanding of massive star origins and evolution. Future studies will use our distances and extinctions to calculate updated WR line luminosity calibrations for application to unresolved extra-galactic WR populations.

2 DISTANCE DETERMINATION METHODS

2.1 *Gaia* DR2 catalogue

The parallax and errors used to calculate distances were taken from the *Gaia* DR2 catalogue (Gaia Collaboration et al. 2018a). The calculation also made use of *G* band magnitudes, astrometric excess noise (to identify potentially spurious results) and *Gaia* RA and Declination coordinates.

A python ASTROQUERY (Astropy Collaboration et al. 2013, Astropy Collaboration et al. 2018) script downloaded data from the *Gaia* archive (Salgado et al. 2017) using the ADQL query in Appendix A of the online material. The script searched for stars which were within 1" of the quoted WR coordinates. Almost all known WR stars are isolated enough for this constraint to be sufficient. The majority (370) of 415 successful search coordinates came from van der Hucht (2001). However, 45 coordinates from the catalogue did not lead to correct *Gaia* detections. In these instances, coordinates from SIMBAD were used instead (Wenger et al. 2000, accessed on 23/05/2018). We checked the coordinates for accuracy using images from VPHAS+ DR3 (Drew et al. 2014), IPHAS DR2 (Barentsen et al. 2014, Drew et al. 2005) and 2MASS (Skrutskie et al. 2006), to ensure they corresponded to isolated WR stars. The remaining 243 WR stars yielded no successful results with either coordinate set. Fig-

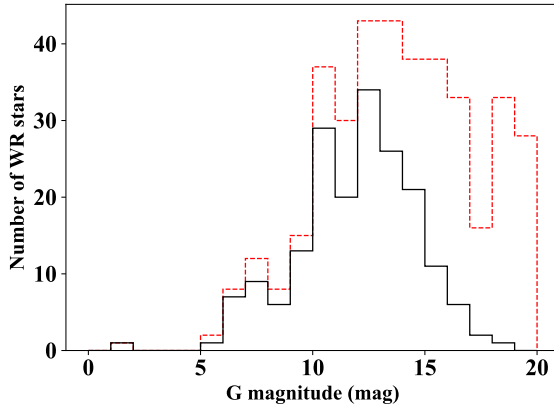


Figure 2. Histogram of G band magnitudes for Gaia DR2 detected WR stars. The solid line (black) involves 187 WR stars with reliable absolute magnitudes (Section 3) and the dashed line (red) involves the full sample of 383 WR stars.

ure 1 shows most of these (>230) have $J-K > 3$ mag, indicating significant foreground dust extinction and are therefore inaccessible to Gaia.

383 stars (58% of the total) from the Galactic WR catalogue¹ have *Gaia* parallaxes. Of those, 305 have positive parallaxes. Figure 2 shows that both the total WR population, and the sample containing only the results with reliable distances, appear to be relatively complete up to $G \sim 13$ mag. However, for results with robust absolute magnitudes, the distribution falls off more quickly beyond $G \sim 13$ mag. This is because fainter magnitudes are preferentially removed due to their larger astrometric excess noise and increased incidence of negative parallaxes (which are more likely to produce unacceptable absolute magnitudes).

2.2 Bayesian methods

The conversion of *Gaia* parallaxes to distances significantly modifies the shape of the original parallax (ω) probability distribution, which means uncertainties do not transform symmetrically. This occurs unless the parallax errors (σ_ω) are very small ($\sigma_\omega/\omega < 0.1$, Bailer-Jones 2015), which is not the case for most of our DR2 sources. Additionally, many sources have negative parallaxes; a consequence of the data processing algorithm fitting noisy observations (Luri et al. 2018) and of the variation in parallax zero points (see Section 2.2.1). Obtaining the WR star distances should therefore be done carefully using Bayesian methods.

Bayesian inference is therefore the recommended way to transform parallaxes to distances (Luri et al. 2018). The end result is a probability distribution with correct uncertainties, reflecting the non symmetric transformation of parallax to distance. Bayesian methods are also capable of elegantly accounting for unphysical parallaxes and so there is no need to cut negative data from the sample (Luri et al. 2018).

The technical details of the Bayesian method used, including equations and plots of the model HII region and dust maps, are in Appendices B, C and D in the online material.

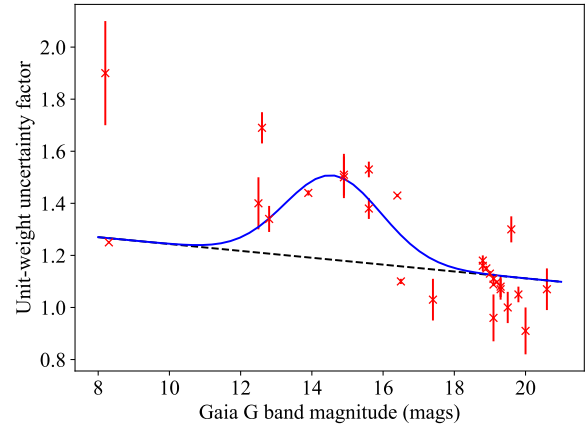


Figure 3. Weighted fit to the unit weight uncertainty factors from Arenou et al. (2018), used to increase the uncertainties σ_ω , to account for underestimation in the *Gaia* catalogue. The dotted line is the linear component of the fit, whilst the solid line is the total fit and the red crosses are the unit weight uncertainties of the external data.

2.2.1 Likelihoods

The likelihood can be constructed by assuming the parallax distribution is Gaussian, with a mean at the parallax measured by *Gaia* and the parallax error as the standard deviation (Hogg 2018, Luri et al. 2018, Bailer-Jones 2015).

The parallaxes quoted by *Gaia* are not corrected for the global zero point. As our sample of WR stars is spread over the sky and the zero point will therefore not be dominated by regional systematics, we choose to apply this global correction to the distance calculation (Arenou et al. 2018). In light of the variation in measured zero points and the fact that Lindegren et al. (2018a) states that the zero point is likely multivariate, with no general process currently available to calculate it, we choose to use the globally measured QSO zero point of -0.029 mas (Lindegren et al. 2018b, Luri et al. 2018). One possible effect of this on the final distances is that if the full multivariate zero point could be used, some small negative parallaxes could be converted to positive values. We discuss further effects of this choice in Section 4.1.

Additionally, analysis from Arenou et al. (2018) suggests that, when compared to external data, the errors of DR2 parallaxes in the catalogue are underestimated. This is because they are consistent with the internal uncertainties, and do not account for systematics. The underestimation varies with G band magnitude and is particularly acute for results in the range $12 < G < 15$, which could be underestimated by 30–50% (Gaia Collaboration et al. 2018a).

To account for this, we calibrate the uncertainties of *Gaia* parallaxes using parallaxes from previous surveys. Arenou et al. (2018) provide in their Table 1 the unit weight error calculated using a variety of comparative surveys and the median G band of these surveys. Using this data, we present the conversion curve shown in Figure 3. This is similar to the approach of Lindegren et al. (2018a), although our model neglects the HST measurement (1.9 unit weight error at $G=8$ mag). It is possible to fit a combined Gaussian

4 Rate & Crowther

and straight line which can increase the size of the uncertainties in proportion to the G band magnitude. Details of the equation used for this fit and the impact of increasing the uncertainties on the distances are in Appendices B and E in the online material.

These increased uncertainties were applied to our WR parallaxes and lead to a likelihood that is appropriate for the WR population.

2.2.2 Prior

The prior is a probability distribution of the expected distances for a given WR star. Previous work with *Gaia* (Bailer-Jones et al. 2018) has opted for a smooth, exponentially decreasing prior, with a single parameter that can be tuned based on galactic latitude and longitude. This is designed to follow the distribution of all observed stars within the Milky Way and to provide a distance derived purely from a geometric model.

Almost all WR stars are found at large (kiloparsec) distances and lie preferentially in the Galactic plane, so their observed distribution will be significantly affected by extinction. Previous priors do not properly account for this, which could be problematic for our sample.

Instead, we build a prior using H_{II} regions and a dust model for extinction. H_{II} regions approximate the spatial distribution of massive stars. They are independent of previous WR distribution maps, avoiding any bias from previous incorrect results and are well sampled across the galaxy (as they are detectable at a broad range of wavelengths).

To find the overall distribution, we considered H_{II} region density along each line of sight. Figure 4 shows a mixture of Gaussians fitted to binned Galactic latitude and longitude distributions, which gave normalised numbers of H_{II} regions at a given latitude or longitude coordinate. These were then multiplied together to get a total number density along the line of sight.

We apply a simple dust model (Rosslowe & Crowther 2015a) to account for the effects of extinction. This consists of both molecular and atomic gas, to replicate the thin and thick disks. For the Sun, we chose a distance of 8.122 kpc (Gravity Collaboration et al. 2018) to the Galactic Centre and a height of 20.8 pc (Bennett & Bovy 2019) above the plane. The resulting distribution is shown in the online supplementary material, in Appendix C.

The prior covered distances between 0 and 15 kpc, at a resolution of 1 pc. The probability is zero below 300 pc, as we do not expect to find any WR stars detected with Gaia closer than this distance. The final form of the prior therefore varies from Gaussian like in regions with a pronounced H_{II} region peak or low extinction, to exponential like in regions with a less pronounced peak or high extinction.

2.2.3 Posterior

We then calculated the posterior distribution. Figure 5 shows an example of this for WR4, together with the prior and its components.

Use of the numerical dust model meant we could not differentiate the posterior and produce an analytical solution for the maximum likelihood. Instead the peak of the

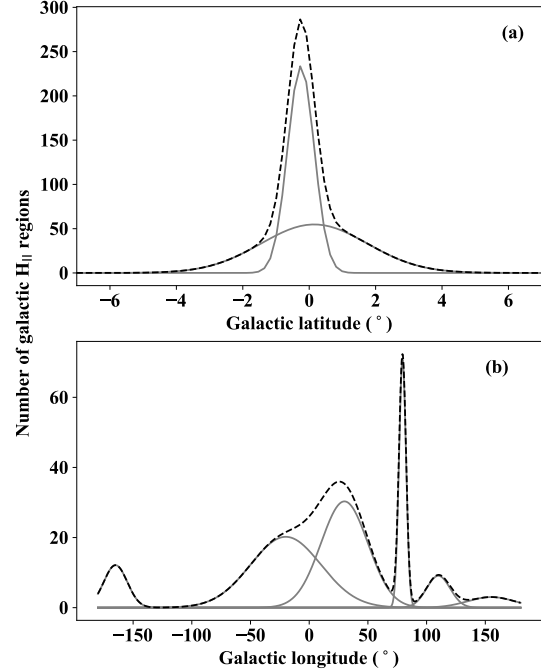


Figure 4. A mixture of Gaussians showing the number of H_{II} regions over (a) Galactic latitude and (b) Galactic longitude, based on Figure 6 and data from Paladini et al. (2003). The solid lines are the individual Gaussians and the black dotted line is the over-fit. The peak around $l=75-90^\circ$ is the Cygnus X region.

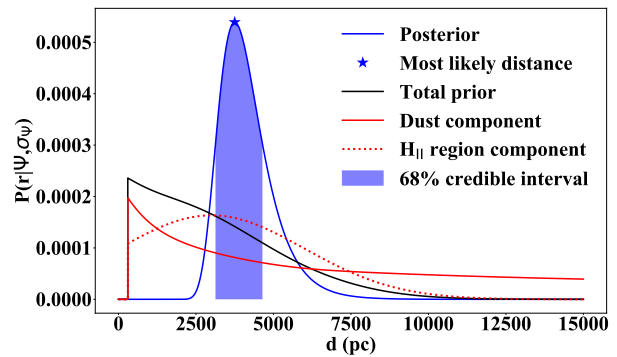


Figure 5. Posterior distribution for WR4, shown alongside the prior components and credible interval. The filled star is the most likely distance to WR4 ($3.75^{+0.89}_{-0.62}$ kpc, compared to $3.71^{+0.65}_{-0.49}$ kpc from Bailer-Jones et al. 2018).

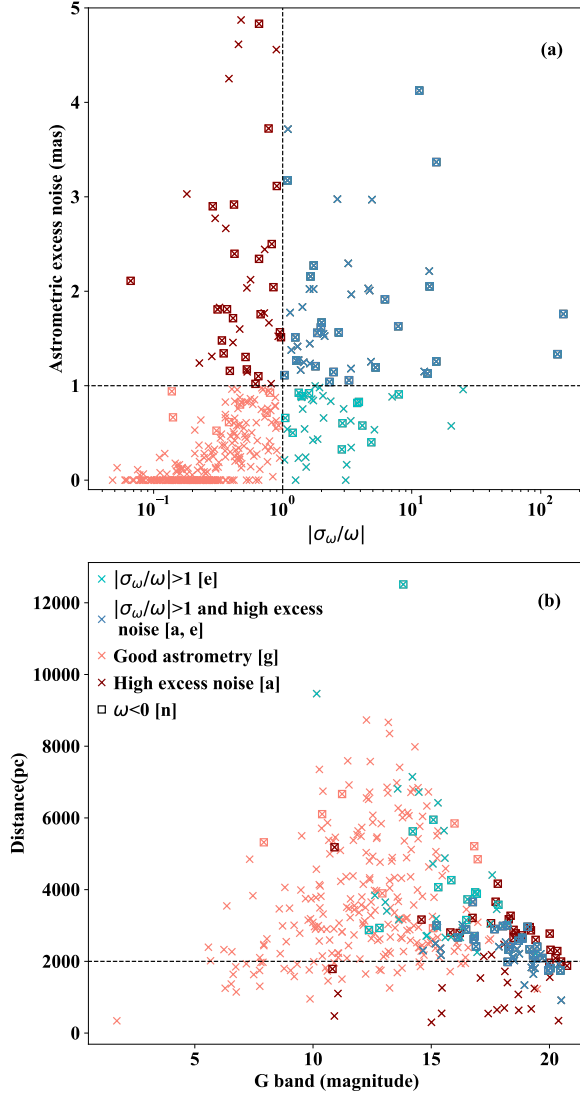


Figure 6. (a) Comparison between parallax error $|\sigma_\omega/\omega|$ and astrometric excess noise (mas) for Galactic WR stars from *Gaia* DR2, for which dotted lines indicate values of unity for each parameter to highlight data quality flags a, e, g, n; (b) Comparison between G band magnitudes and inferred distances (pc) for Galactic WR stars from *Gaia* DR2, with the dotted line marking a distance of 2 kpc.

distribution was taken as the most likely distance. Credible intervals (similar to those used in Bailer-Jones et al. 2018) give distances which, when used as integral limits, cover 68% of the area below the curve. The one sigma errors are the differences between the peak and these distances.

2.3 Flags from *Gaia*

The validity of the distances is determined by the quality of the parallax data. A significantly negative parallax (less than the zero point), will result in a smaller likelihood than

a positive parallax and will increase the proportional size of the prior. Negative parallaxes can also indicate unreliable *Gaia* data. Similarly, a large error (on the scale of the data itself) will also result in a much smaller likelihood and a greater influence from the prior.

These issues mainly arise from badly fitted parallax solutions, which can be identified using parameters in the *Gaia* catalogue. We chose astrometric excess noise (the observational noise which needs to be added to the data to match the solution residuals) as this identifier. Large values can indicate that a solution does not fit the data well. We chose to use this parameter, as it was the quality indicator with the clearest cut-off and acted as a good benchmark for removing bad values when calculating absolute magnitudes. The excess noise can also account for modelling errors, which are not included in the observational noise. Significant astrometric excess noise is mainly applied to fainter objects, in particular those with brighter neighbours.

The *Gaia* documentation (Hambly et al. 2018) states that high excess noise will be present in early releases and suggests that users apply their own cut-offs to determine erroneous values. The ideal excess for results with distances is zero, which indicates a good fit. However, excluding an outlier with excess noise 18 mas, the average value for our sample is 0.71 mas and the standard deviation is 0.98 mas. Therefore, we flag all results with noise above 1 mas.

Combined, our three criteria for flagging *Gaia* data quality are

$$\begin{aligned} a &= \text{astrometric_excess_noise} > 1 \\ e &= |\sigma_\omega/\omega| > 1 \\ n &= \omega < 0. \end{aligned}$$

Results without any of these issues are given the 'g' flag. These flags are applied to the distances in Table 1.

We apply the flags to the zero point corrected parallaxes and the increased errors, as these are the values used to calculate distance. A star can be flagged if it satisfies one or more of the criteria. If all three are applied, then 37% of the WR stars with parallaxes have an a, e or n flag.

59% of the flagged results had more than one negative flag. This reflects the way such errors are intertwined, where a poor solution fit due to noisy observations can lead to a large astrometric excess noise, sizeable errors and negative parallaxes all at once.

The relations between flags are shown in Figure 6. In general, WR stars with large astrometric excess noise are supposedly located closer than 4 kpc, and in many cases closer than 2 kpc. This latter group further breaks down into brighter objects at around $G=11$ mag (WR146 and WR115) and $G=15$ mag (including WR77p) and fainter objects with $G>17$ mag. The fainter objects may have high excess noise because of astrometric modelling difficulties, caused by issues like binarity or a badly determined spacecraft attitude during a given time interval (Hambly et al. 2018, Lindegren et al. 2018b). These problems would make it difficult for the *Gaia* AGIS algorithm to reliably extract astrometric parameters. The brighter objects may have high excess noise for a variety of reasons, such as issues with instrument calibration (Lindegren et al. 2018b). High astrometric excess noise can also occur if the stars are in binaries (WR146) or potential binaries (WR115).

The other two flags show a less clear breakdown. Negative parallaxes can occur at all magnitudes and distances,

6 Rate & Crowther

Table 1. Gaia DR2 astrometric, photometric and parallax properties for 383 Galactic WR stars, including WR11 using a parallax and photometry from Hipparcos (van Leeuwen 2007). The distance for WR11 was calculated in the same manner as WR with *Gaia* results, except the adjustments to calculate ω and σ_ω were not applied. Stellar luminosities, updated from Hamann et al. (2019) and Sander et al. (2019) according to our revised distances, are restricted to sources with no error flags. The full table is available in the online supplementary material.

WR Number	Spectral Type	Alias	RA J2015	Dec J2015	$\omega \pm \sigma_\omega$	d kpc	$ z $ pc	G mag	$G_{BP} - G_{RP}$ mag	Excess Noise	$\log L$ L_\odot	Flags
WR1	WN4b	HD 4004	00 43 28.39	+64 45 35.4	0.314 ± 0.040	$3.15^{+0.47}_{-0.36}$	125^{+15}_{-12}	9.79	1.05	0.00		g
WR3	WN3ha	HD 9974	01 38 55.62	+58 09 22.6	0.342 ± 0.051	$2.90^{+0.52}_{-0.39}$	188^{+37}_{-27}	10.58	0.18	0.10	5.56	g
WR4	WC5+?	HD 16523	02 41 11.67	+56 43 49.8	0.258 ± 0.051	$3.75^{+0.89}_{-0.62}$	174^{+46}_{-32}	9.68	0.51	0.06	5.72	g
WR5	WC6	HD 17638	02 52 11.66	+56 56 07.1	0.334 ± 0.042	$2.97^{+0.43}_{-0.33}$	90^{+16}_{-12}	10.06	0.94	0.00	5.53	g
WR6	WN4b	EZ CMa	06 54 13.04	-23 55 42.0	0.441 ± 0.065	$2.27^{+0.42}_{-0.31}$	376^{+73}_{-53}	6.57	0.04	0.18	5.78	g
WR7	WN4b	HD 56925	07 18 29.13	-13 13 01.5	0.221 ± 0.051	$4.23^{+1.08}_{-0.74}$	11^{+2}_{-1}	11.17	0.73	0.00	5.33	g
WR8	WN7o/CE	HD 62910	07 44 58.22	-31 54 29.5	0.263 ± 0.038	$3.74^{+0.63}_{-0.48}$	226^{+41}_{-31}	9.92	0.84	0.00		g
WR9	WC5+O7	HD 63099	07 45 50.40	-34 19 48.5	0.212 ± 0.035	$4.57^{+0.84}_{-0.63}$	256^{+70}_{-52}	10.14	1.30	0.00		g
WR10	WN5h	HD 65865	07 59 46.24	-28 44 03.0	0.162 ± 0.040	$5.46^{+1.25}_{-0.91}$	75^{+12}_{-9}	10.94	0.60	0.09	5.78	g
WR11	WC8+O7.5III-V	γ Vel	08 09 31.96	-47 20 11.8	2.920 ± 0.300	$0.34^{+0.04}_{-0.03}$	24^{+5}_{-4}	1.70				
WR12	WN8h	Ve5-5	08 44 47.29	-45 58 55.4	0.154 ± 0.037	$5.71^{+1.24}_{-0.92}$	175^{+42}_{-31}	10.36	1.15	0.00	5.93	g

Columns are: (1) WR Number, (2) Spectral type, (3) Alternative name, (4) *Gaia* Right Ascension, (5) *Gaia* Declination, (6) Zero point corrected parallax ω and inflated error σ_ω , (7) Distance from the Sun, (8) Distance from the midplane, (9) *Gaia* G band apparent magnitude, (10) *Gaia* colour index, (11) Astrometric excess noise, (12) Stellar luminosity, (13) Error flags, a = astrometric excess noise > 1 mas; e = large parallax uncertainty $|\sigma_\omega/\omega| > 1$; n = negative parallax $\omega < 0$, g = good astrometry.

Table 2. Intrinsic colours of WR stars from PoWR models (Hamann & Gräfener 2004 and Todt et al. 2015 for WN, Sander et al. 2012 for WC) for $(b - v)_0^{\text{WR}}$ and monochromatic $(J - K_s)_0^{\text{mono}}$ and $(H - K_s)_0^{\text{mono}}$, and Rosslowe & Crowther (2015a) for $(J - K_s)_0$ and $(H - K_s)_0$.

WR subtype	PoWR model	$\log(T/k)$	$\log(R_t)$	$(b - v)_0^{\text{WR}}$	$(J - K_s)_0$	$(H - K_s)_0$	$(J - K)_0^{\text{mono}}$	$(H - K)_0^{\text{mono}}$
WN3-4	WNE 12-11	4.95	1.0	-0.32 ± 0.1	-0.11 ± 0.1	-0.03 ± 0.1	0.24	0.16
WN4b-7b	WNE 12-18	4.95	0.3	-0.18 ± 0.1	0.37 ± 0.1	0.27 ± 0.1	0.63	0.40
WN5-6	WNE 08-11	4.75	1.0	-0.28 ± 0.1	0.18 ± 0.1	0.16 ± 0.1	0.30	0.20
WN7-9	WNL 06-13	4.65	0.8	-0.15 ± 0.1	0.13 ± 0.1	0.11 ± 0.1	0.30	0.18
WN6ha	WNL 07-07	4.70	1.4	-0.33 ± 0.1	-0.015 ± 0.1	0.03 ± 0.1	0.00	0.00
WN7ha	WNL 07-07	4.70	1.4	-0.33 ± 0.1	-0.04 ± 0.1	0.01 ± 0.1	0.00	0.00
WN8-9ha	WNL 05-07	4.60	1.4	-0.32 ± 0.1	-0.04 ± 0.1	0.01 ± 0.1	0.01	0.00
Of/WN	WNL 07-06	4.65	1.5	-0.34 ± 0.1	-0.11 ± 0.1	-0.07 ± 0.1	-0.04	-0.03
WO2-3	WC 17-12	5.20	0.9	-0.37 ± 0.1	0.11 ± 0.1	0.00 ± 0.1	0.20	0.11
WC4-7	WC 11-16	4.90	0.5	-0.20 ± 0.2	0.62 ± 0.1	0.58 ± 0.2	0.54	0.33
WC8	WC 09-14	4.80	0.7	-0.37 ± 0.1	0.43 ± 0.1	0.38 ± 0.1	0.38	0.21
WC9	WC 06-12	4.65	0.9	-0.32 ± 0.1	0.23 ± 0.1	0.26 ± 0.1	0.12	0.09
WN/WC				-0.23 ± 0.1	0.37 ± 0.1	0.27 ± 0.1		

but have non zero excess noise. Only a small fraction of results with large error ratios have zero astrometric excess noise and none at all occur below $G=12$ mag. Both flags become increasingly common beyond $G=15$ mag and only a few points beyond $G=18$ mag are not flagged. This is expected given that highly reddened objects at any distance are more difficult for *Gaia* to observe. The flags applied to

the data are listed in Table 1. Any users should note that distances to these flagged stars may be suspect and should account for this in their analysis.

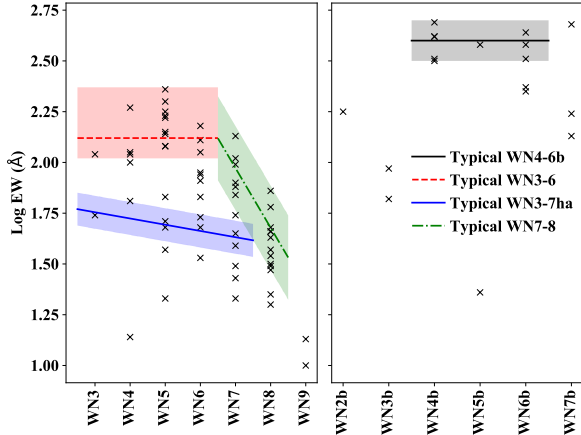


Figure 7. WN stars with HeII 4686Å equivalent widths from Conti & Massey (1989) and Smith et al. (1996). The lines show the equivalent width for a typical single WN star at each subtype. The shaded regions should contain only single stars.

3 ABSOLUTE MAGNITUDES

In addition to the *Gaia* data quality flags, we checked the validity of the distance results by calculating absolute magnitudes in the v^{WR} -band (Smith 1968)², designed to avoid WR emission lines, and the K_s band. As part of this, we calculated extinction using intrinsic colours and an adopted extinction law. The result was then combined with distances and apparent magnitudes to obtain absolute magnitudes.

3.1 Intrinsic colours for single stars

Intrinsic optical colours were taken from PoWR grids (Hamann & Gräfener 2004 and Todt et al. 2015 for WN, Sander et al. 2012 for WC), for single stars in the v^{WR} band (see Table 2). The exception is for WN/WC stars, as the value $(b - v)_0^{WR} = -0.23$ is averaged from the $E(b - v)^{WR}$ values of Sander et al. (2012) and the b^{WR} and v^{WR} apparent magnitudes of each star. Intrinsic colours for the J, H and K_s bands are taken from Rosslowe & Crowther (2015a), with monochromatic near-IR PoWR synthetic colours also included.

3.2 Intrinsic colours for binary systems

16% (61 stars) of our WR sample were classified as binaries. For these systems, we calculated absolute magnitudes in the same manner as single stars, but included the companion in the intrinsic colour by measuring the dilution of the strongest optical emission lines. These are HeII 4686Å for WN stars, and CIV 5808Å and CIII 5696Å for WC stars. We fit the relation of the equivalent width to subtype for single stars (see Figs 7–8), to obtain the equivalent width of a ‘typical’ single star with a particular subtype.

For WC stars, we used CIV 5808Å to obtain the typical

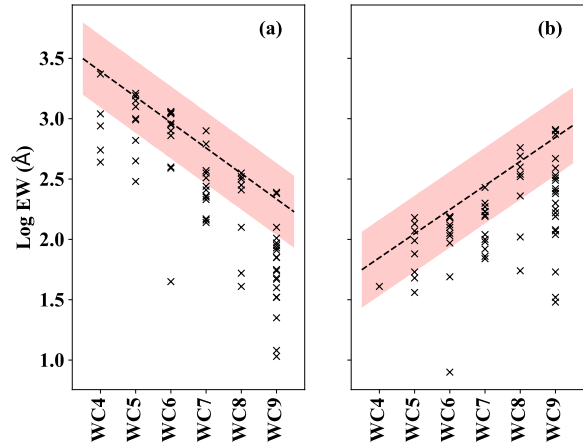


Figure 8. Equivalent widths of (a) CIV 5808Å and (b) CIII 5696Å from Torres et al. (1986), Conti & Massey (1989), Smith et al. (1990), Cohen et al. (1991), Mauerhan et al. (2009) and Zhekov et al. (2014) showing the relation between line strengths and spectral types for both single and binary stars. The dotted line shows the equivalent width for a typical single WC star at each subtype. The shaded region is the one sigma standard deviation and should contain only single stars.

equivalent width of a single WR star with subtype 4, 5 or 6. In subtypes 8 and 9, the dominant line is instead CIII 5696Å. The fractions for WC7, which can contain either line, were the average dilution of the two. The fractional contribution of the WR’s visible light (F_{CWRV}) to the binary was then found using:

$$F_{CWRV} = \frac{EW_b}{EW_s} \quad (1)$$

where EW_b is the WR equivalent width for the binary and EW_s is the equivalent width for a single star. We summed the intrinsic colour of each component, weighted by contribution fraction, to obtain the colour for the system.

WR stars contribute a higher fraction of the continuum flux to the binary at near-IR wavelengths with respect to the visual (see Table 3). To illustrate this, we compare template spectra from WR stars of different subtypes to an O star from a Kurucz ATLAS model ($T_{\text{eff}} = 37500\text{K}$ and $\log g = 5$). Each template spectrum is set to the same V-band continuum flux. The fraction of light contributed by the template O star at IR wavelengths can then be calculated. We use this to obtain the intrinsic colours of the binary in the same way as optical wavelength colours.

For WR11, we used the light ratio derived in De Marco et al. (2000) and for WR104, we used the ratio from Williams & van der Hucht (2000). For WR30a, we estimated the fraction of light contributed by the WR was 10%, based on the emission line strength of similar WO4 star BAT99-123 (Br93, Sand 2). For WR64-4, we used the HeII 1.16μm, 1.69μm and 2.19μm IR lines to find contribution ratios, as no optical data were available. For WR35a, a reverse approach was followed based on the absolute magnitude of the system and assuming an absolute V magnitude for the O8.5V com-

² A ‘WR’ superscript is added to distinguish the Smith v filter from the standard Johnson V-band filter

Table 3. The relative continuum flux contribution of WR stars to O-type companions at near-IR wavelengths for various subtypes, adopting a Kurucz ATLAS O star model with $T_{\text{eff}} = 37500\text{K}$ and $\log g = 5$ for the companion, assuming each contribute 50% of the V-band continuum flux.

WR subtypes	F_{WR}/F_0			
	V	J	H	K
WNE-w	1	1.33	1.56	1.94
WNE-s	1	2.45	3.35	4.56
WN6ha	1	1.22	1.38	1.63
WN8	1	2.03	2.70	3.55
WN9	1	1.33	1.5	1.78
Of/WN	1	1.17	1.22	1.33
WC4-5	1	2.03	2.57	3.55
WC6-7	1	1.94	2.45	3.35
WC8	1	1.86	2.23	3.00
WC9	1	1.70	2.13	2.57

panion (from [Martins & Plez 2006](#)), to calculate the absolute magnitude of the WR component.

3.3 Optical and IR extinctions

We calculate dust extinctions using the intrinsic colours (Table 2) and apparent magnitudes in the v^{WR} band taken from the Galactic Wolf-Rayet catalogue, which was primarily compiled from [van der Hucht \(2001\)](#) and [Torres-Dodgen & Massey \(1988\)](#). J, H and K_s band magnitudes were primarily sourced from the 2MASS catalogue. The K_s band extinction, A_{K_s} , was calculated using the standard extinction law $A_{K_s} = 0.107A_v^{\text{WR}}$ (obtained from $A_{K_s} = 0.118A_V$ from [Cardelli et al. 1989](#) and $A_v^{\text{WR}} = 1.1A_V$ from [Turner 1982](#)), if values of A_v^{WR} were available. Otherwise, A_{K_s} was calculated with the relations of A_H and A_J to A_{K_s} (using parameters from [Fritz et al. 2011](#) towards the Galactic Centre and [Stead & Hoare 2009](#) elsewhere, as in [Rosslose & Crowther 2015a](#)).

For WR25, known to have an anomalous extinction curve, we calculated A_v^{WR} using $R_v^{\text{WR}} = 6.2$ from [Crowther et al. \(1995\)](#).

Since dust extinction preferentially attenuates blue wavelengths, the $G_{BP} - G_{RP}$ can be used as a proxy for extinction. Some stars had unusually high K_s band extinctions (possibly due to incorrect photometry), which led to erroneous absolute magnitudes. Figure 9(a) shows the relationship between $(G_{BP} - G_{RP})$ and A_{K_s} , while Fig 9(b) compares $(G_{BP} - G_{RP})$ and A_v^{WR} . A 5σ (grey dashed lines) cut-off from the line of best fit (black solid line) was used to exclude incorrect extinctions. Some values of A_v^{WR} were also excluded for being outliers, indicating an issue either with some photometry or the $G_{BP} - G_{RP}$ magnitudes.

To obtain meaningful results at low $G_{BP} - G_{RP}$ (where we have no observations) we ensure that the extinction is zero at the intrinsic colour, $(G_{BP} - G_{RP})_0$. We obtain $(G_{BP} - G_{RP})_0$ for a generic blue energy distribution, namely a B0 V spectral type, with $V - I = -0.44$ in the Johnson filter ([Ducati et al. 2001](#)). We transform this relation to the Cousins system ([Bessell 1979](#)) and finally to $(G_{BP} - G_{RP})_0 = -0.43$, using the $V - I$ to $G_{BP} - G_{RP}$ calibration in [Evans et al. \(2018\)](#).

Carrasco & Jordi (priv. comm) (using methodology from [Jordi et al. 2010](#)) provide the transformation from A_V

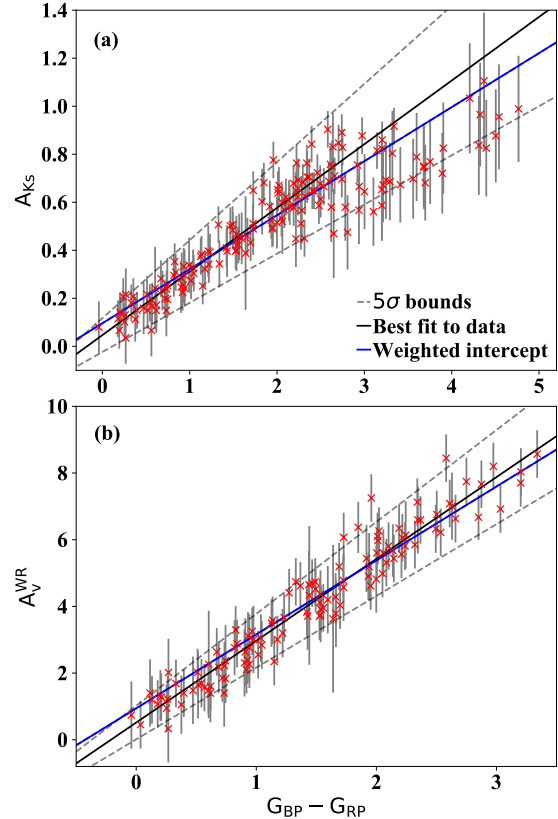


Figure 9. $Gaia G_{BP} - G_{RP}$ colours for Galactic WR stars compared to (a) K_s -band and (b) v^{WR} band extinctions. In (a), the solid black line presents the best fit to data with $G_{BP} - G_{RP} < 3$ while in (b), the solid line is a best fit to all data. The grey dashed lines are the 5σ bounds, based on the uncertainties of the fit parameters. The solid blue line is also the best fit to the data, but weighted so that it passes through $A_v^{\text{WR}} = A_{K_s} = 0$ at $(G_{BP} - G_{RP})_0 = -0.43$, as expected for a generic B0 V star.

to A_G by artificially reddening template PoWR WR spectra with different extinctions (from $A_V \sim 0.5$ to 36 mag). Synthetic photometry for the $Gaia$ ([Maíz Apellániz & Weiler 2018](#)) passbands was then obtained at each A_V . This allowed for the calculation of $E(G_{BP} - G_{RP})$ and A_G . The results from Carrasco & Jordi allow us to find the intrinsic colour $(G_{BP} - G_{RP})_0$ for each WR subtype. The generic B0 V model we have used to calculate $(G_{BP} - G_{RP})_0$ is within the uncertainty of the average WR value $(G_{BP} - G_{RP})_0 = -0.35 \pm 0.14$ of the subtypes in Table 4.

For the K_s band, we obtain the $G_{BP} - G_{RP}$ to A_{K_s} relationship using data with $G_{BP} - G_{RP} < 3$. This is the regime in which A_{K_s} follows the extinction law, as these stars are also observed in the v^{WR} band. At higher $G_{BP} - G_{RP}$, the calculated extinction begins to deviate from this relationship. The empirical fit is shown in blue in Figure 9(a) and has the form:

$$A = X(G_{BP} - G_{RP}) + Y \quad (2)$$

where $G_{BP} - G_{RP}$ is the value from the $Gaia$ catalogue,

Table 4. Conversion equations between narrowband v^{WR} and *Gaia* G band filters for $(G_{BP} - G_{RP})_0$ of different spectral types, using results from Carrasco & Jordi (valid for $A_v < 12$).

WR class	$(G_{BP} - G_{RP})_0$	A_v^{WR} to A_G
WNE-w	-0.421	$-0.0169A_v^2 + 0.894A_v$
WNE-s	-0.136	$-0.0159A_v^2 + 0.871A_v$
WN6ha	-0.406	$-0.0166A_v^2 + 0.891A_v$
WN8	-0.163	$-0.0157A_v^2 + 0.868A_v$
WN9	-0.359	$-0.0163A_v^2 + 0.886A_v$
WC5	-0.619	$-0.0178A_v^2 + 0.933A_v$
WC7	-0.479	$-0.0182A_v^2 + 0.921A_v$
WC8	-0.360	$-0.0178A_v^2 + 0.901A_v$
WC9	-0.159	$-0.0156A_v^2 + 0.870A_v$
B0V SED	-0.430	

Table 5. Average absolute magnitudes for Galactic Wolf-Rayet subtypes in v^{WR} and K_s band filters. In the v^{WR} band, the WC9d sample has been combined with non dusty WC9 stars.

WR subtypes	$M_{v^{WR}}$ (mag)	$N(v^{WR})$	M_{K_s} (mag)	$N(K_s)$
WN3-4	-3.6 ± 0.5	6	-3.1 ± 0.6	7
WN5-6	-4.3 ± 0.6	22	-4.0 ± 0.5	33
WN6-7ha	-6.5 ± 0.3	3	-6.2 ± 0.3	5
WN4-6b	-4.5 ± 0.6	13	-4.6 ± 0.7	15
WN7	-4.6 ± 0.6	10	-4.8 ± 0.3	15
WN8	-5.7 ± 0.6	8	-6.0 ± 0.8	13
WN8-9ha	-7.0 ± 0.4	2	-6.8 ± 0.4	2
WN9	-6.0 ± 0.8	2	-5.7 ± 0.7	6
Of/WN	-5.8 ± 0.1	2	-6.1 ± 0.1	3
WO2-4	-3.1 ± 1.4	3	-2.6 ± 1.0	4
WC4-5	-4.1 ± 0.6	11	-4.3 ± 0.4	11
WC6-7	-3.9 ± 0.4	19	-4.9 ± 0.4	22
WC8	-4.5 ± 0.9	6	-5.3 ± 0.5	7
WC9	-4.6 ± 0.4	12	-4.8 ± 0.5	9
WC9d			-6.6 ± 0.8	13

$X=0.2250$ and $Y=0.0961$. The v^{WR} band, shown in Figure 9(b), was much more closely grouped around the line of best fit, with $X=2.217$ and $Y=0.9436$. The gradient is 9.85 times the gradient for the K_s band. This is slightly larger than the $A_{K_s} = A_v^{WR}/9.35$ extinction law used to calculate values of A_{K_s} with A_v^{WR} . The deviation reflects the fact that some values of A_{K_s} were not calculated using that extinction law.

We can also use the synthetic photometry from Carrasco & Jordi to calculate the conversion relationship from A_v^{WR} to A_G (also shown in Table 4), by converting A_v in their relationship to A_v^{WR} . This enables us to calculate the absolute *Gaia* G magnitude and present the *Gaia* colour magnitude diagram (CMD) in Figure 10, for the most reliable WR results. Fig. 10(a) presents a CMD for Galactic WR stars plus visually bright O stars from v4.1 of the Galactic O Star Catalogue (GOSC, Maíz Apellániz et al. 2013), while Fig. 10(b)

compares the CMD of WR stars to 70,000 DR2 stars from [Gaia Collaboration et al. \(2018b\)](#). Two exceptionally bright stars are the extreme hypergiants He 3-519 (WR31a) and AG Car (WR31b), which exhibit very late WN characteristics at extreme visual minima ([Smith et al. 1994](#)).

3.4 Absolute magnitudes

We used the extinctions, distances and apparent magnitudes to calculate the absolute magnitudes for stars that have reliable extinctions (within the 5σ bounds of Figure 9). Repeating the calculation using a Monte Carlo selection (bootstrapping with replacement) from the distributions of the three parameters, produced a binned histogram of absolute magnitude against frequency. This acted as a proxy for the probability distribution of each absolute magnitude. A Gaussian or Weibull distribution was fit to the binned data, to find the most likely absolute magnitude and uncertainties (more details are available in Appendix F of the online material).

For binaries, the absolute magnitudes of Wolf-Rayet components were separated from the total system magnitude.

A multi step process of sigma clipping allowed us to find reliable absolute magnitudes for all WR stars. First, stars with high astrometric excess noise, or unrealistically low absolute magnitudes (≥ -1 mag) were removed from the sample. We then calculated the averages of the remaining stars in each subtype class. Stars with unusually high or low absolute magnitudes (defined as were greater than one sample standard deviation, from the mean) were then cut from the sample. This cut-off provided a good balance between excluding clearly incorrect values and including valid ones across all subtypes.

The remaining sample contained only the most reliable absolute magnitude results in each subclass and were used to calculate the averages presented in Table 5. LBVs, aside from He 3-519 (WR31a) and AG Car (WR31b), were removed due to variability. WR20-2, WR42-1, WR43-2, WR43-3 were also excluded from the averages, owing to uncertain subtypes.

We obtain K_s band results for dusty subtypes (WC8d and WC9d) by converting A_v^{WR} to A_{K_s} , using the standard extinction law. This method prevents the IR dust emission from contaminating the extinction calculation. The absolute magnitudes could then be calculated for each subtype and in each filter, with the standard deviation providing upper and lower bounds on the typical absolute magnitudes. The WC9d were combined in the v^{WR} band, but not in the K_s band, as their IR excess renders them brighter than dust free WR stars. As there were only three WC8d (WR48a, WR53 and WR113) in the final sample, these stars were grouped with the non dusty WC8 stars and only WR113 was used to calculate the final absolute K_s in Table 5. Excluding WR113 from the average, we obtain $M_{K_s}=-5.3$ mag for WC8 stars, the same result as Table 5.

In Figure 11, we present the final absolute K_s band magnitudes and uncertainties for each subtype. These are compared with corresponding values from [Rosslowe & Crowther \(2015a\)](#). Figure 12 shows the same distribution for the v^{WR} band, compared with [van der Hucht \(2001\)](#). Tables 6 and 7 show results for individual stars (the full lists are in the supplementary online material).

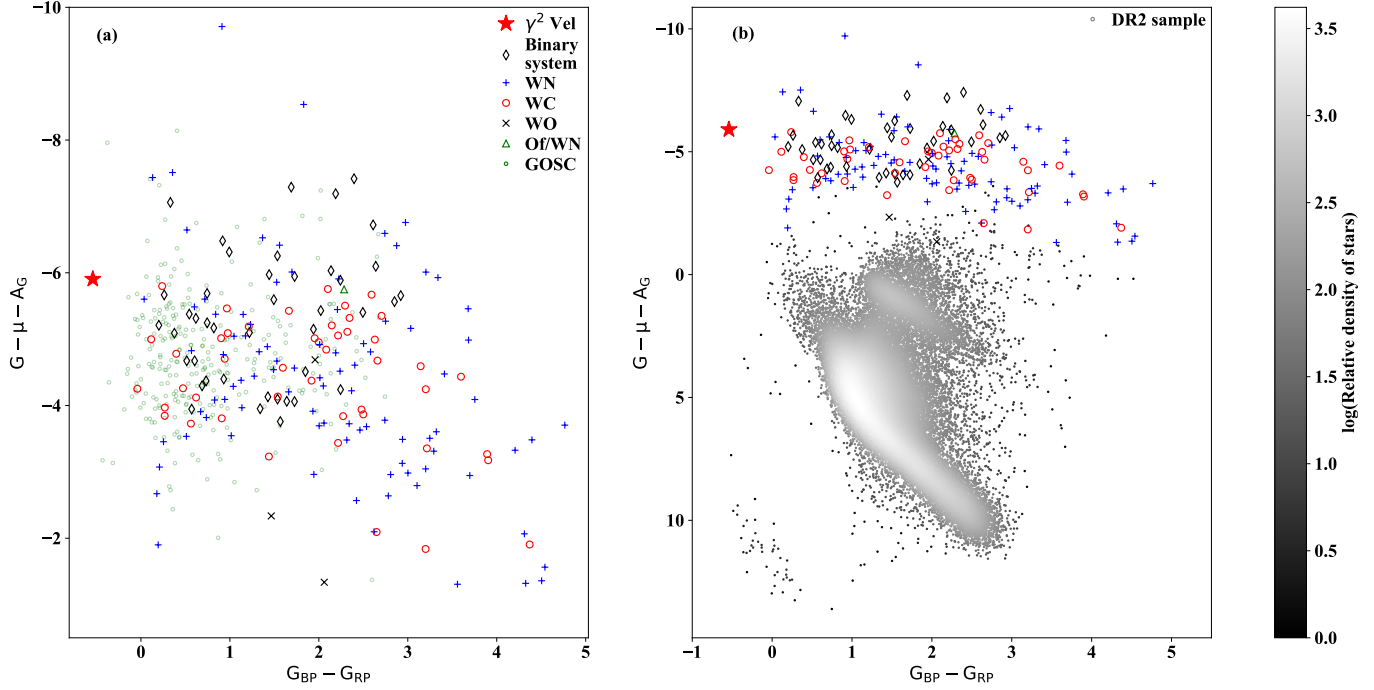
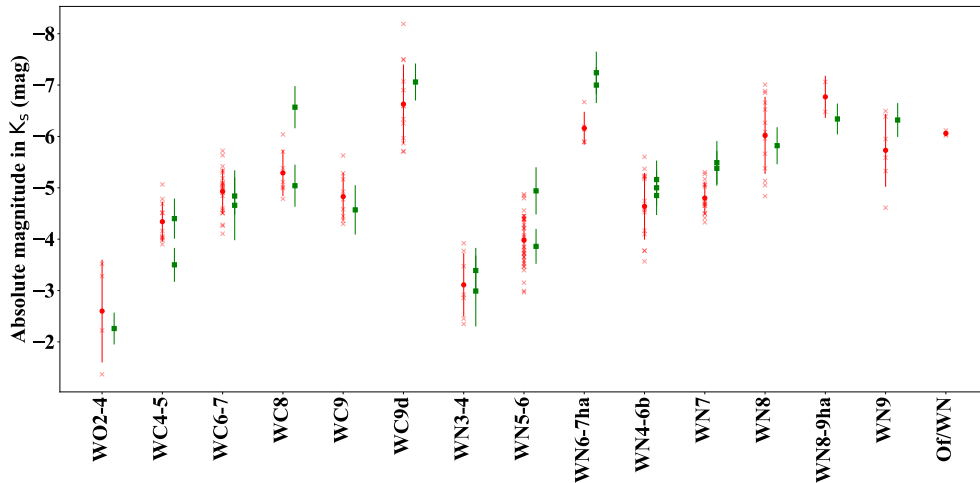


Figure 10. (a) *Gaia* DR2 colour magnitude diagram for Galactic WR stars plus O stars from GOSC (v4.1, Maíz Apellániz et al. 2013). Absolute magnitudes are calculated using our inferred distance moduli μ and A_G (converted from A_v^{WR} using the relation from Carrasco & Jordi). The red star is the WR component of γ Velorum, the only WR star with a trigonometric parallax from *Hipparcos*; (b) *Gaia* DR2 colour magnitude diagram for Galactic WR stars plus 70,000 stars from DR2, satisfying the selection criteria from section 2.1 of Gaia Collaboration et al. (2018b).



We additionally plot the absolute magnitudes for 116 LMC stars in Figure 12, using results from Hainich et al. (2014) for single WN and Of supergiant stars (excluding WN2b), Shenar et al. (2019) for stars in binaries, Crowther et al. (2002) for single WC stars and reddenings from Tram-

per et al. (2015) and v^{WR} band magnitudes from Torres-Dodgen & Massey (1988) for BAT99-123 (WO4). We adopt spectral types of LMC late WN stars from Crowther & Smith (1997) instead of Schnurr et al. (2008).

From Fig. 12, absolute v^{WR} magnitudes of LMC stars are

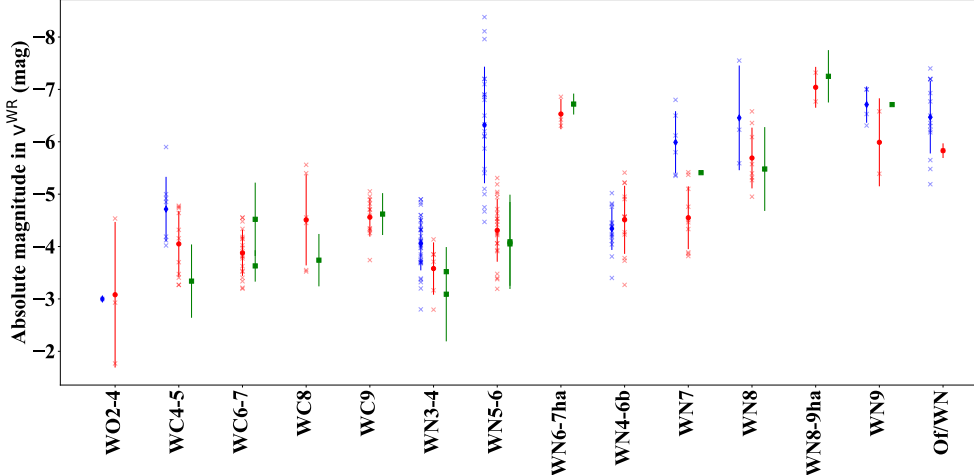


Figure 12. Absolute magnitudes in the v^{WR} band. Red crosses are individual WR star results and the red circle is the average for each spectral subtype (with the sample standard deviation of the data as the uncertainties). Green squares are the comparative data from van der Hucht (2001). Results from the LMC (Hainich et al. 2014, Shenar et al. 2019 and Crowther et al. 2002) are shown in blue, with crosses for individual stars and the diamond the average for each subtype. LMC WN5-6 stars include very luminous H-rich main sequence WN5-6h stars. Results for WO were calculated using Tramper et al. (2015) and Torres-Dodgen & Massey (1988)

Table 6. Absolute K_s -band magnitudes for Galactic WR stars. The full table is available in the online supplementary material.

WR Number	Spectral type	K_s (mag)	μ (mag)	$J-K_s$ (mag)	$H-K_s$ (mag)	A_{K_s} (mag)	$M_{K_s}^{Sys}$ (mag)	$F_{K_s}^{WR}/F_{K_s}^{Sys}$	$M_{K_s}^{WR}$ (mag)	Flags
WR1	WN4b	7.48	12.49	0.73	0.38	0.30 ± 0.08			$-5.4_{-0.3}^{+0.3}$	b:
WR3	WN3ha	10.01	12.31	0.23	0.12	0.11 ± 0.08			$-2.5_{-0.4}^{+0.3}$	b:
WR4	WC5+?	7.88	12.87	0.87	0.69	0.18 ± 0.11			$-5.2_{-0.5}^{+0.4}$	b
WR5	WC6	7.65	12.36	0.98	0.69	0.30 ± 0.11			$-5.1_{-0.3}^{+0.3}$	g
WR6	WN4b	5.89	11.78	0.46	0.34	0.05 ± 0.08			$-6.0_{-0.4}^{+0.3}$	b
WR7	WN4b	9.27	13.13	0.70	0.40	0.24 ± 0.08			$-4.2_{-0.5}^{+0.4}$	g
WR8	WN7o/CE	7.93	12.87	0.64	0.39	0.31 ± 0.08			$-5.3_{-0.3}^{+0.3}$	b:
WR9	WC5+O7	7.54	13.3	0.91	0.57	0.45 ± 0.08	$-6.3_{-0.4}^{+0.3}$	0.60 ± 0.24	$-5.7_{-0.7}^{+0.9}$	b
WR10	WN5h	9.61	13.69	0.44	0.28	0.24 ± 0.17			$-4.4_{-0.5}^{+0.5}$	g

Columns: (1) WR Number, (2) Spectral type, (3) K_s apparent magnitude, (4) Distance modulus μ , (5) $J-K_s$ colour, (6) $H-K_s$ colour, (7) K_s band extinction A_{K_s} , (8) Absolute magnitude of binary system (including companion), (9) Fraction of light contributed to the binary system by the WR component, (10) Absolute magnitude of WR star, (11) Error flags, where $M > upper_{initial}$ or $M < lower_{initial} = b$, $M > upper_{final}$ or $M < lower_{final} = b$: ($initial$ denotes the averages calculated before sigma clipping, $final$ are the final absolute magnitude boundaries) and g are results with no issues.

brighter than their Galactic analogues, so it is inappropriate to apply LMC WR absolute magnitudes to Galactic stars. LMC WN5–6 stars are particularly bright, since this sample includes the luminous H-rich main sequence WN5–6h stars whose closest Galactic analogues are WN6–7ha stars which are amongst the visually brightest WR stars in the Milky Way.

In total, reasonable absolute magnitudes, extinctions and no *Gaia* excess noise flags, were obtained in 187 cases. Absolute magnitudes for almost all WR subtypes revealed standard deviations that overlapped with the uncertainty

range of the previous results in both the v^{WR} and the K_s bands. The differences between values can be attributed to the improved distance estimates and the increased number of stars with distances. Some stars, such as WR2 (the only WN2 star, Chené et al. 2019), were not present in the *Gaia* catalogue.

There is a clear trend across both filters of increasing absolute magnitudes with increasing subtype. In both filters, WN4–6b are brighter than their weak-lined counterparts despite their higher effective temperatures (Hamann

Table 7. Absolute v^{WR} -band magnitudes for Galactic WR stars. The full table is available in the online supplementary material.

WR Number	Spectral type	$v^{WR} \pm 0.1$ (mag)	μ (mag)	$(b - v)^{WR}$ (mag)	A_v^{WR} (mag)	M_{v}^{Sys} (mag)	F_v^{WR} / F_v^{Sys}	M_v^{WR} (mag)	Flags
WR1	WN4b	10.51	12.49	0.51	2.84 ± 0.71			$-4.9_{-0.8}^{+0.8}$	g
WR3	WN3ha	10.70	12.31	-0.06	1.07 ± 0.71			$-2.8_{-0.8}^{+0.8}$	b:
WR4	WC5+?	10.53	12.87	0.20	1.65 ± 1.01			$-4.2_{-1.1}^{+1.1}$	g
WR5	WC6	11.02	12.36	0.47	2.76 ± 1.01			$-4.2_{-1.1}^{+1.1}$	g
WR6	WN4b	6.94	11.78	-0.07	0.45 ± 0.71			$-5.4_{-0.8}^{+0.8}$	b:
WR7	WN4b	11.75	13.13	0.36	2.22 ± 0.71			$-3.8_{-0.9}^{+0.9}$	b:
WR8	WN7o/CE	10.48	12.87	0.47	2.88 ± 0.71			$-5.4_{-0.8}^{+0.8}$	b:
WR9	WC5+O7	10.93	13.3	0.74	4.16 ± 0.72	$-6.6_{-0.8}^{+0.8}$	0.29 ± 0.12	$-5.3_{-1.2}^{+1.4}$	b
WR10	WN5h	11.08	13.69	0.22	2.26 ± 1.61			$-5.0_{-1.7}^{+1.7}$	b:

Columns: (1) WR Number, (2) Spectral type, (3) v^{WR} apparent magnitude and error, (4) Distance modulus μ , (5) $(b - v)^{WR}$ colour, (6) v^{WR} band extinction A_v , (7) Absolute magnitude of binary system (including companion), (8) Fraction of light contributed to the binary system by the WR component, (9) Absolute magnitude of WR star, (10) Error flags, where $M > upper_{initial}$ or $M < lower_{initial} = b$, $M > upper_{final}$ or $M < lower_{final} = b$: ($initial$ denotes the averages calculated before sigma clipping, $final$ are the final absolute magnitude boundaries) and g are results with no issues.

et al. 2006). WNLha stars are known to be highly luminous, and conform to this expectation.

The spread in absolute magnitudes is similar to those previously obtained in the near-IR, but slightly larger in the v^{WR} band. Rosslowe & Crowther (2015a) quote a range of 0.3–0.6 mag, whilst the standard deviation in our K_s band results spans 0.1–1.0 mag, but is also more typically 0.3–0.6 mag. For the v^{WR} band, the standard deviations range from 0.3–1.4 mag and mostly have standard deviations between 0.4–0.6 mag.

We therefore corroborate the findings of Sander et al. (2019) that WC stars of the same subtype have a broader range of absolute magnitudes than expected. We also posit this is true for WN stars (Hamann et al. 2019 also note the relations between absolute magnitude and subtype are not strict). The uncertainties show no systematic differences between WC and WN classes or regular variation across subtypes. However, particularly in the v^{WR} band, some classes suffered from very small numbers of WR stars (only 2 WN9 stars had v^{WR} band magnitudes, for instance). This increases the size of the uncertainties on the mean result.

Due to this intrinsic variation, we advise caution when using averages as absolute magnitude calibrations and recommend accounting for the large uncertainties by exploring other methods, such as a Bayesian approach with a probability distribution centred on the average magnitude. We also recommend continued use of the intrinsic colours in Table 2, rather than calculating new values using our methods and results. The large uncertainties of our absolute magnitudes, mean that propagated uncertainties of any resulting intrinsic colours are correspondingly large. These new uncertainties are far larger than the intrinsic colours from Table 2.

3.5 Sensitivity of results to adopted intrinsic colours

We test the sensitivity of the results to the intrinsic colours. For the v^{WR} band, this is straightforward in that any difference in $(b - v)_0^{WR}$ is propagated through to the extinction (so multiplied by 4.12, Turner 1982). However, within the K_s band, the combination of $(J - K_s)_0$ and $(H - K_s)_0$ complicates this somewhat and we test the effects by calculating M_{K_s} with alternative $J - K_s$ and $H - K_s$ synthetic colours. These are taken from the PoWR grids (Hamann & Gräfener 2004 and Todt et al. 2015 for WN, Sander et al. 2012 for WC), using the same models as Table 2. Unlike the $b - v^{WR}$ colours, these are only valid at the monochromatic wavelengths and not the whole filter bands, which are affected by emission lines, especially for early-type WC stars. The difference in absolute magnitudes are between 0.05 for WN5–6 and 0.2 for WC6–7 and WN2–4 (as emission lines fall within the filter band and are not included in the monochromatic result), with most subtypes falling between 0.1 and 0.2. In all instances, this was well within the uncertainties on individual magnitudes.

3.6 Photometric Flags

In addition to the *Gaia* flag, we identify results with potentially spurious absolute magnitudes. As stars with incorrect extinctions were removed, spurious results can indicate either incorrect apparent magnitudes, or an incorrect *Gaia* parallax, whose distance generates the wrong absolute magnitude. We therefore adopt two different flags, one where the absolute magnitude is implausible and another where the absolute magnitude only just falls outside the uncertainty of the subtype average. The latter does not necessarily indicate a bad result, but these data should be treated with caution.

$M > upper_{initial}$ or $M < lower_{initial} = b$

$M > upper_{final}$ or $M < lower_{final} = b$:

where upper and lower are the upper and lower magni-

Table 8. WR stars within 2 kpc of the Sun, including colour excess, K-band extinction and A_{Ks}/kpc , extinction per kpc.

WR Number	Alias	Spectral type	Distance (kpc)	Flags	E(B-V)	A_{Ks}	A_{Ks}/kpc
WR11	γ Vel	WC8+O7.5III-V	$0.34^{+0.04}_{-0.03}$...	0.00 ± 0.30	0.00 ± 0.11	$0.00^{+0.32}_{-0.32}$
WR94	HD 158860	WN5o	$0.95^{+0.06}_{-0.06}$	g	1.24 ± 0.21	0.45 ± 0.08	$0.47^{+0.09}_{-0.08}$
WR90	HD 156385	WC7	$1.15^{+0.11}_{-0.09}$	g	0.10 ± 0.30	0.04 ± 0.11	$0.03^{+0.09}_{-0.03}$
WR78	HD 151932	WN7h	$1.25^{+0.15}_{-0.12}$	g	0.44 ± 0.21	0.16 ± 0.08	$0.13^{+0.06}_{-0.06}$
WR139	HD 193576	WN5o+O6III-V	$1.31^{+0.07}_{-0.06}$	g	0.81 ± 0.24	0.30 ± 0.09	$0.23^{+0.07}_{-0.07}$
WR79	HR 6265	WC7+O5-8	$1.37^{+0.12}_{-0.10}$	g	0.31 ± 0.26	0.11 ± 0.09	$0.08^{+0.07}_{-0.07}$
WR145	AS 422	WN7o/CE+?	$1.46^{+0.12}_{-0.10}$	g	2.28 ± 0.39	0.83 ± 0.14	$0.57^{+0.11}_{-0.10}$
WR110	HD 165688	WN5-6b	$1.58^{+0.15}_{-0.12}$	g	1.13 ± 0.21	0.41 ± 0.08	$0.26^{+0.05}_{-0.05}$
WR111	HD 165763	WC5	$1.63^{+0.32}_{-0.23}$	g	0.22 ± 0.30	0.08 ± 0.11	$0.05^{+0.07}_{-0.05}$
WR142	Sand 5	WO2	$1.65^{+0.11}_{-0.09}$	g	2.13 ± 0.21	0.78 ± 0.08	$0.47^{+0.06}_{-0.05}$
WR105	NS 4	WN9h	$1.73^{+0.32}_{-0.23}$	g	2.41 ± 0.21	0.88 ± 0.08	$0.51^{+0.10}_{-0.08}$
WR134	HD 191765	WN6b	$1.75^{+0.13}_{-0.11}$	g	0.46 ± 0.21	0.17 ± 0.08	$0.10^{+0.04}_{-0.04}$
WR52	HD 115473	WC4	$1.75^{+0.16}_{-0.13}$	g	0.59 ± 0.30	0.22 ± 0.11	$0.12^{+0.06}_{-0.06}$
WR144	HM19-1	WC4	$1.75^{+0.24}_{-0.19}$	g		0.47 ± 0.19	$0.27^{+0.11}_{-0.11}$
WR93	Th10-19	WC7+O7-9	$1.76^{+0.19}_{-0.15}$	g	1.67 ± 0.23	0.61 ± 0.08	$0.34^{+0.06}_{-0.06}$
WR142-1	HBHalpha 4203-27	WN6o	$1.77^{+0.23}_{-0.18}$	g		0.69 ± 0.16	$0.39^{+0.10}_{-0.10}$
WR113	HD 168206	WC8d+O8-9IV	$1.80^{+0.24}_{-0.19}$	g	0.94 ± 0.21	0.34 ± 0.08	$0.19^{+0.05}_{-0.05}$
WR142a	PCG02 1	WC8	$1.81^{+0.61}_{-0.37}$	g		0.83 ± 0.19	$0.46^{+0.19}_{-0.14}$
WR133	HD 190918	WN5o+O9I	$1.85^{+0.16}_{-0.14}$	g	0.36 ± 0.21	0.13 ± 0.07	$0.07^{+0.04}_{-0.04}$
WR113-2	SMG09 1425_-47	WC5-6	$1.86^{+0.90}_{-0.56}$	g		0.65 ± 0.21	$0.35^{+0.21}_{-0.16}$
WR70-5	WM10 11b	WC9	$1.95^{+0.75}_{-0.47}$	g		1.26 ± 0.26	$0.65^{+0.28}_{-0.21}$
WR98	HDE 318016	WN8o/C7	$1.96^{+0.31}_{-0.24}$	g	1.59 ± 0.21	0.58 ± 0.08	$0.29^{+0.06}_{-0.05}$
WR25	HD 93162	O2.5I* / WN6+O	$1.97^{+0.18}_{-0.15}$	g	0.93 ± 0.32	0.34 ± 0.11	$0.17^{+0.06}_{-0.06}$
WR135	HD 192103	WC8	$1.98^{+0.18}_{-0.15}$	g	0.41 ± 0.21	0.15 ± 0.08	$0.08^{+0.04}_{-0.04}$
WR85	HD 155603B	WN6h	$1.99^{+0.30}_{-0.24}$	g	1.03 ± 0.21	0.37 ± 0.08	$0.19^{+0.05}_{-0.04}$

tude bounds of the absolute magnitude average. $a_{initial}$ denotes the averages calculated before sigma clipping (Section 3), a_{final} are the final absolute magnitude boundaries (as in Table 5) and M is the absolute magnitude of individual WR stars. Results with a 'b' flag are highly implausible and lie well outside the range of acceptable absolute magnitudes, whilst those with a 'b:' flag are still acceptable, but fall outside the 1σ uncertainties of the results in Table 5. Again, results without any of these issues are given the 'g' flag. Results without any absolute magnitudes are flagged with 'u'. These stars were included to provide the reader with the distance moduli of the stars and any other helpful information (e.g apparent magnitudes), if their absolute magnitudes could not be calculated.

For all subsequent analysis we use only the most photometrically reliable results, which have a 'b:' or 'g' flag in either the v^{WR} band, or the K_s band. These data do not have high astrometric excess noise ('a') Gaia data quality flags. Results with, for example, two 'b' flags were excluded. These

flags are applied to the absolute magnitudes in Tables 7 and 6.

We note that 13 objects retained in this selection process had either negative parallax ('n') or high parallax to error ratio ('e') *Gaia* flags. However, the reliable absolute magnitudes mean the distances may still be valid.

4 NEW DISTANCES TO WR STARS AND COMPARISON TO OTHER GAIA DERIVED DISTANCES

We can compare the WR star sample from *Gaia* to the total population. There is no substantial difference between the latitude and longitude distribution of WR stars detected in *Gaia* and the total known WR distribution. The exception is for some regions, such as around Westerlund 1 and towards the Galactic Centre, which went undetected by *Gaia* due to their high extinctions (with $A_V > 30$ mag in the latter case).

Crowding presented an additional challenge. WR 43A and 43B are not included in the final distance catalogue as

the same *Gaia* source was detected for both stars. The detection for WR43C is also spurious, as the position overlaps with other objects. These stars are located in the compact cluster NGC 3603 (Melena et al. 2008, Crowther & Dessart 1998) and therefore blending is to be expected. It is possible that further stars are missing parallaxes due to crowding, as this issue would reduce the quality of the *Gaia* five parameter solution below acceptable limits, and cause it to be excluded from the *Gaia* catalogue.

Finally, some stars may not have been detected due to their close binary companions. Arenou et al. (2018) shows that completeness falls for separations below 2'', to a limit at 0.12''. This may account for three missing stars with narrowband $v^{\text{WR}} < 15$ mag (WR2, WR63 and WR86), two of which (WR63 and WR86) have known companions.

Table 1 includes distances for each WR star with measured parallaxes. Also included are the 68% credible intervals. Table 8 lists the closest WR stars (with reliable results) within 2 kpc of the Sun. We find 25 WR stars within this distance, similar to the 30 WR stars within 2 kpc from Conti et al. (1983). We also calculate distances to O stars using our Bayesian prior and GOSC v4.1 (Maíz Apellániz et al. 2013). For the O star population within 2 kpc, we obtain a WR/O ratio of 0.09. This ratio is within the 0.07–0.10 range of Conti et al. (1983), found by comparing lifetimes of H and He core burning phases from massive star models, as an analogue to O star and WR star phases. However, our ratio includes all O stars, and not just the most massive population that WR stars are descended from. Conti et al. (1983) also calculate a WR/O ratio with only O stars $>40M_{\odot}$, and find a much higher ratio of 0.36 ± 0.15 .

Table 8 also includes K_s -band extinctions, and extinctions per kpc for these nearby WR stars, with $A_{K_s}/\text{kpc} \sim 0.26$ mag, albeit with significant star-to-star variation. Dust extinctions of stars in common with the 3D dust map from Pan-STARRS1 and 2MASS Green et al. (2015) shows reasonable overall agreement.

4.1 Comparison with previous WR distances

Rosslove & Crowther (2015a) provide distance estimates for 228 Galactic WR stars based on previous absolute magnitude calibrations. Of those, 87 have reliable distances from this work. Fig. 13(a) compares distances to Galactic WR stars in common with Rosslove & Crowther (2015a). Agreement is reasonable up to ~ 2 kpc. This is the subset of *Gaia* sources with the lowest uncertainties and extinction, enabling accurate applications of our prior and absolute magnitude calibrations. Beyond 2 kpc, there is significant scatter, with many stars closer than previously thought. These are principally more highly reddened WR stars that have been discovered recently. Conversely many stars that were thought to be nearby based on calibrations, have significantly larger distances (e.g. WR57 is revised from 2.98 ± 0.52 kpc to $5.50^{+1.49}_{-1.06}$ kpc).

All of our 187 stars with reliable absolute magnitudes have distance estimates from Bailer-Jones et al. (2018). Comparisons are presented in Figure 13(b). Again, good agreement is obtained up to ~ 2 kpc, beyond which the Bailer-Jones et al. (2018) distances are generally larger than our results. The average ω/σ_{ω} for stars at distances beyond 2.5 kpc is -0.71 . The error is therefore a substantial propor-

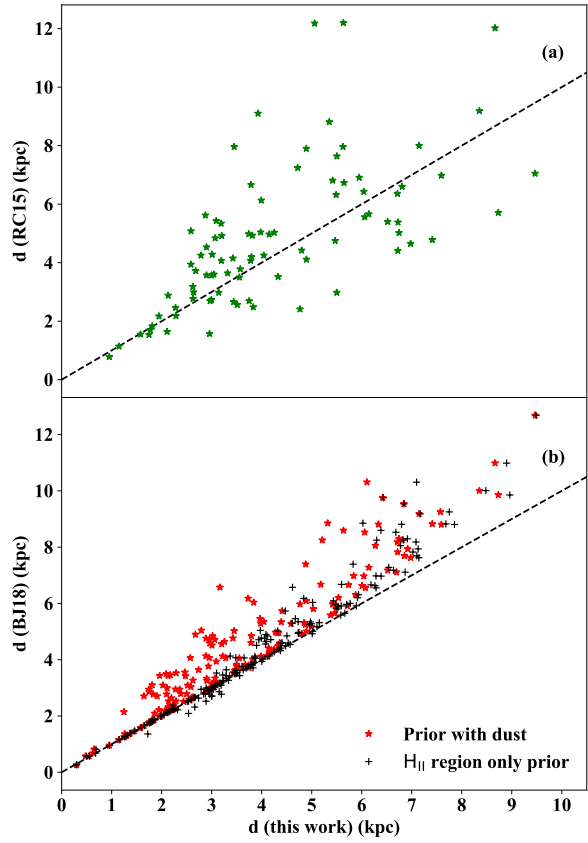


Figure 13. (a) A comparison between distances to Galactic WR stars in common between this work and Rosslove & Crowther (2015a). The black dashed line indicates one-to-one agreement. Error bars from Rosslove & Crowther (2015a) have been omitted for clarity; (b) A comparison between WR distances obtained in this work and Bailer-Jones et al. (2018). We illustrate the effect of extinction by presenting the full prior including both dust and HII regions (red stars) and a prior with only HII regions (black cross).

tion of the total parallax, which suggests disparities stem primarily from limitations in the *Gaia* data and the differences between the two priors. At large distances and so proportionally large parallax errors, the prior dominates the data and the peak of the posterior shifts closer to the peak of the prior.

For this work, the peak of the prior probability defaults to <3 kpc, depending on longitude. If the peak in the Bailer-Jones prior is substantially closer or further, this results in a large divergence between the two measures. Our prior differs significantly from Bailer-Jones et al. (2018) as it more directly accounts for extinction and the specific distribution of massive stars. The red stars/black crosses in Figure 13(b) show the contrast between results calculated with/without the dust extinction model. In most instances, the stars had results more in line with Bailer-Jones et al. (2018) when dust was excluded. Therefore, in the vast majority of cases, dust extinction in the prior is the primary factor leading to different results.

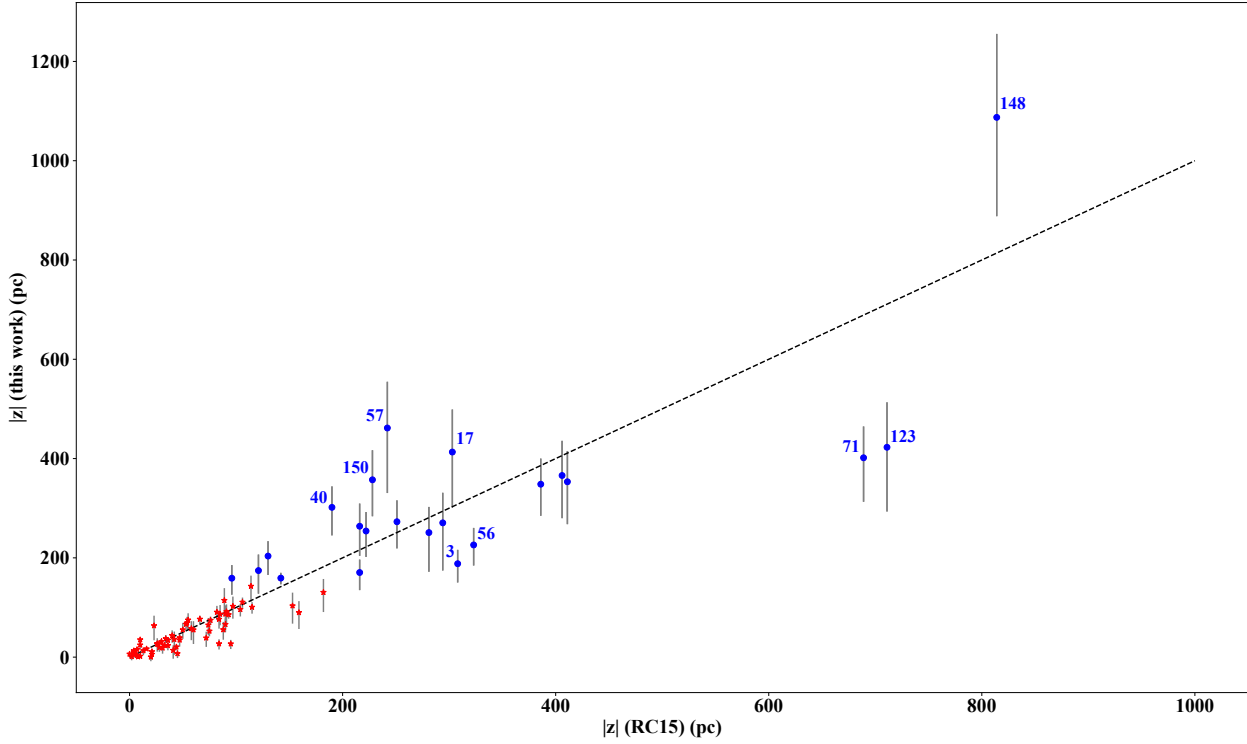


Figure 14. A comparison between the WR distances from the midplane from Rosslowe & Crowther (2015a) and this work. Blue circles are the points from this work with distances greater than 3σ , where σ is the HII region scale height. The dotted line indicates parity between the two measures. Stars with significant disagreement are labelled with their WR numbers.

Since distances from Bailer-Jones et al. (2018) formed the basis of the recent spectroscopic studies of Galactic WR stars by Sander et al. (2019) and Hamann et al. (2019), use of distances from this study with no warning flags would lead to generally modest 0.05 dex reductions in stellar luminosity. These are included in Table 1, with higher reductions for relatively distant stars including WR74 (WN7o, 0.24 dex), WR91 (WN7b, 0.23 dex), WR56 (WC7, 0.20 dex) and WR64 (WC7, 0.20 dex).

We also compare the distances to a Galactic LBV (WR31b = AG Car) and LBV candidate (WR31a = He 3-519) which are in common with Smith et al. (2019). They obtain a distance of $7.12^{+2.53}_{-1.67}$ kpc to WR31a, versus $7.35^{+1.45}_{-1.18}$ kpc from this work, and $4.65^{+1.43}_{-0.92}$ kpc to WR31b, versus $4.85^{+0.93}_{-0.70}$ kpc from this work. These are well within the uncertainties of both stars, particularly given WR31a has a high error to parallax ratio of 0.72 (as measured directly from the catalogue values). Smith et al. (2019) adopt a different zero point to our study, namely -0.05 mas as an initial value and model some uncertainty in this as part of their calculation. This decision is based on the variety of different zero points found in the literature (e.g Riess et al. 2018, Zinn et al. 2019, Stassun & Torres 2018 and Graczyk et al. 2019).

Therefore, these distances are systematically closer than those from Bailer-Jones et al. (2018). This result agrees both with our findings and Schönrich et al. (2019), who also find that Bailer-Jones et al. (2018) appear to systematically overestimate distances. As Smith et al. (2019) adopts a similar

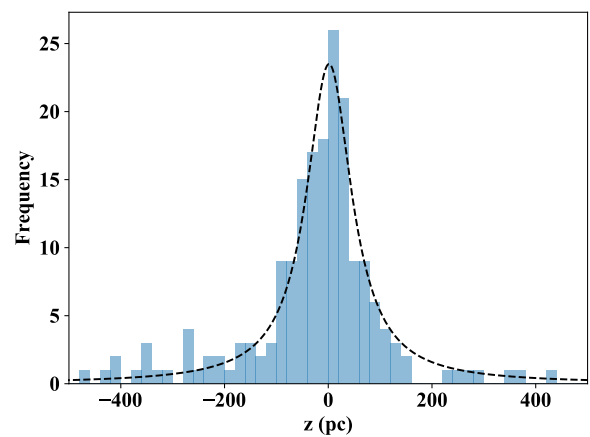


Figure 15. A histogram distribution of WR distances from the Galactic disk. The dotted line shows the Cauchy fit from Equation 3.

prior to that of Bailer-Jones et al. (2018), the overlapping results therefore indicate that the larger zero point is performing much the same function as our dust model, acting to moderate the distances of Bailer-Jones et al. (2018).

5 DISTANCES FROM THE GALACTIC DISK

To identify potential runaway stars, we calculated distances from the Galactic plane using the most likely distance from the Sun and the Galactic latitude of the star, with the addition of the 20.8 pc (Bennett & Bovy 2019) for the Sun’s distance above the midplane. The 68% distance uncertainty intervals were scaled to give height uncertainties.

The new midplane distances in Table 1 are compared with results from Rosslowe & Crowther (2015a) in Figure 14. In general, the deviation from previous results increases with height, reflecting the uncertainty of distances to very remote WR stars. The scale heights, σ , of HII regions loosely trace massive star formation sites and can therefore highlight potential runaways. Based on the median north scale height between 3.9 kpc and 5.6 kpc in Paladini et al. (2004), σ is 52 pc. The south scale heights contained too few points to be reliable.

We additionally calculated the scale height of the WR population. The histogram of WR distances from the midplane is presented in Figure 15 and can be fit with a Cauchy distribution

$$g = \frac{A}{\pi\gamma} \frac{\gamma^2}{(z - c)^2 + \gamma^2} \quad (3)$$

where A is the scale constant, c is the distribution centre and γ is the scale parameter, specifying the half width half maximum (HWHM). Fitting these parameters gives a centre of 1.5 pc and a HWHM of 53.4 pc. The central value of our distribution is similar to Rosslowe & Crowther (2015a) (1.9 pc), though their HWHM is somewhat smaller, at 39.2 pc. The central value would suggest many WR stars are slightly above the plane, but this may be due to planar dust extinction rendering WR stars which sit below the disk being inaccessible to *Gaia*.

Our results are similar to Conti & Vacca (1990), who find a WR scale height of 45 ± 5 pc using an isothermal disk model and Bobylev & Bajkova (2016), who obtained a height 51.3 ± 3.7 pc using the same method. However, this latter value relies on a sample at <4 kpc (excluding distant stars to avoid the effects of Galactic disk warp) and thus only covers about half the WR stars in our sample.

To identify only the most extreme runaways and ensure they did not form in situ, we apply a 3σ cut-off using the HII region scale height. Since a velocity of 1 km s^{-1} equates to 1 pc Myr^{-1} , runaways ($\geq 30 \text{ km s}^{-1}$) will travel in excess of 150 pc over a typical WR lifetime of 5 Myr. 91% of 383 WR stars in *Gaia* reside within three scale heights from the Galactic plane, so 9 % of WR stars are located far from the Galactic plane. Table 9 presents the $|z|$ distances for each of these stars.

However, the resulting runaway list does not account for the known warp in the Galactic disk. Romero-Gómez et al. (2019) estimate the warp begins at a radius of 12-13 kpc from the Galactic centre for their sample of young, bright stars (which they refer to as the OB sample). All but two of our WR stars are within 12 kpc of the Galactic centre and by this measure, would be unaffected. However, their results show some complex structures that in fact suggest some of our sample may be affected by the warp. An alternative measure from Li et al. (2019), estimates that the Galactic disk instead begins to warp at a radius of 9.2 kpc. 20 stars

are further from the centre than this distance, and so their heights would need to account for the warp.

To obtain a robust candidate list of runaways with $\geq 30 \text{ km s}^{-1}$, we used the Galactic warp model and onset from Li et al. (2019) to calculate the height of the Galactic plane at the position of each of the 383 WR stars with distances. We subtracted off the height of this Galactic warp, which produced a distance from the midplane for each star, which accounted for the warp. These distances were then used to exclude any stars which were not 3σ from the plane, once the warp was accounted for. Using this method, we excluded WR8 and WR12 from our runaway list in Table 9. Therefore, 31 stars (8% of WR stars in *Gaia*) are robust runaway candidates.

We do not apply the warp to our full list of distances from the plane in Table 1, as the warp onset and model are still uncertain.

The runaways identified in Rosslowe & Crowther (2015a) generally remain far from the plane. However, many of the more extreme distances from the plane are now moderated, due to reduced distances from the Sun. This suggests that extreme runaways are less common than previously thought. WR93a and WR64 are not included, as they were identified as having abnormal v^{WR} band extinction (Section 3), which meant it was not possible to calculate their absolute magnitudes, so their distances could not be validated.

Two main evolutionary paths may have created these runaways. The first is the disruption of a binary system when the primary star explodes as a supernova and ejects the remaining companion (Blaauw 1961). The second scenario is dynamical ejection from a dense cluster, which can eject both binary and single stars (Poveda et al. 1967). The majority of outliers with $>3\sigma$ distances are apparently single stars, as only WR30 and WR69 have confirmed OB companions.

As both single stars and binaries can be ejected from clusters, it is not possible for us to definitively state which mechanism is dominant. We defer a discussion of the origin of runaways to Paper II which considers the association of WR stars with star clusters or OB associations. However, we note that recent simulations suggest fast runaways from either mechanism are anticipated to be very rare (Renzo et al. 2019; Oh & Kroupa 2016), in stark contrast with the high fraction of WR stars at extreme distances from the Galactic plane.

Two stars merit individual consideration. The high velocity runaway WR124 is now located at $|z|=360$ pc, compared to previous estimates of 217 pc (Rosslowe & Crowther 2015a), 193 pc (Marchenko et al. 2010) and 250 pc (Moffat et al. 1982). This confirms its runaway status, although our work places it significantly further from the Sun (5.9 kpc instead of 3.3 kpc from Marchenko et al. 2010).

WR148 is located furthest from the Galactic plane. Drissen et al. (1986) suggested it as a possible WR+compact object binary disrupted by a SN, however, Munoz et al. (2017) claim it is instead a WN+O binary. If the latter is true, our data suggests that WR148 is a binary system that has been ejected from a cluster, concurring with Munoz et al. (2017). Assuming a lifetime of 5 Myr and a straight vertical trajectory from the Galactic disk, the minimum possible

Table 9. Distance of WR stars from the midplane $|z|$, for which excesses exceed 3σ , where $\sigma=52$ pc, the HII region scale height of 52 pc. Previously identified runaways with $|z| \geq 300$ pc according to [Rosslowe & Crowther \(2015a\)](#) are also indicated

WR Number	Spectral type	Dist (kpc)	$ z $ (pc)	HII σ	Known runaway
WR148	WN8h+	$9.47^{+1.77}_{-1.49}$	1087^{+199}_{-168}	$20.9^{+3.8}_{-3.2}$	Yes
WR57	WC8	$5.50^{+1.49}_{-1.06}$	462^{+131}_{-93}	$8.9^{+2.5}_{-1.8}$	No
WR123	WN8o	$5.35^{+1.56}_{-1.09}$	423^{+129}_{-91}	$8.1^{+2.5}_{-1.7}$	Yes
WR73	WC9d	$6.81^{+1.85}_{-1.47}$	423^{+109}_{-87}	$8.1^{+2.1}_{-1.7}$	No
WR17	WC5	$6.75^{+1.74}_{-1.33}$	413^{+112}_{-86}	$7.9^{+2.1}_{-1.6}$	Yes
WR71	WN6o	$3.19^{+0.67}_{-0.48}$	402^{+89}_{-63}	$7.7^{+1.7}_{-1.2}$	Yes
WR6	WN4b	$2.27^{+0.42}_{-0.31}$	376^{+73}_{-54}	$7.2^{+1.4}_{-1.0}$	No
WR75c	WC9	$7.15^{+1.78}_{-1.45}$	366^{+86}_{-70}	$7.0^{+1.7}_{-1.3}$	Yes
WR124	WN8h	$5.87^{+1.48}_{-1.09}$	360^{+85}_{-63}	$6.9^{+1.6}_{-1.2}$	Yes
WR150	WC5	$8.73^{+1.70}_{-1.38}$	357^{+73}_{-60}	$6.9^{+1.4}_{-1.1}$	No
WR61	WN5o	$5.49^{+1.25}_{-0.91}$	353^{+85}_{-62}	$6.8^{+1.6}_{-1.2}$	Yes
WR49	WN5(h)	$8.35^{+1.44}_{-1.17}$	348^{+64}_{-52}	$6.7^{+1.2}_{-1.0}$	Yes
WR58	WN4b/CE	$5.88^{+1.42}_{-1.04}$	337^{+86}_{-63}	$6.5^{+1.7}_{-1.2}$	No
WR40	WN8h	$3.83^{+0.67}_{-0.50}$	302^{+56}_{-42}	$5.8^{+1.1}_{-0.8}$	No
WR126	WC5/WN	$7.57^{+1.49}_{-1.19}$	300^{+55}_{-44}	$5.8^{+1.1}_{-0.8}$	No
WR103	WC9d+?	$3.46^{+1.28}_{-0.77}$	275^{+109}_{-65}	$5.3^{+2.1}_{-1.3}$	No
WR33	WC5; WC6	$7.59^{+1.62}_{-1.30}$	273^{+54}_{-43}	$5.2^{+1.0}_{-0.8}$	No
WR69	WC9d+OB	$3.48^{+0.64}_{-0.47}$	272^{+54}_{-40}	$5.2^{+1.0}_{-0.8}$	No
WR92	WC9	$3.78^{+1.25}_{-0.79}$	271^{+96}_{-61}	$5.2^{+1.8}_{-1.2}$	No
WR54	WN5o	$6.52^{+1.37}_{-1.05}$	264^{+60}_{-46}	$5.1^{+1.1}_{-0.9}$	Yes
WR129	WN4o	$5.47^{+1.22}_{-0.90}$	254^{+52}_{-38}	$4.9^{+1.0}_{-0.7}$	No
WR83	WN5o	$3.80^{+1.10}_{-0.72}$	251^{+79}_{-52}	$4.8^{+1.5}_{-1.0}$	No
WR131	WN7h+abs	$6.92^{+1.40}_{-1.09}$	227^{+42}_{-32}	$4.4^{+0.8}_{-0.6}$	No
WR56	WC7	$8.67^{+1.46}_{-1.20}$	226^{+41}_{-34}	$4.3^{+0.8}_{-0.7}$	Yes
WR30	WC6+O6-8	$5.09^{+0.99}_{-0.74}$	211^{+45}_{-33}	$4.1^{+0.9}_{-0.6}$	No
WR20	WN5o	$6.98^{+1.18}_{-0.93}$	204^{+38}_{-30}	$3.9^{+0.7}_{-0.6}$	No
WR3	WN3ha	$2.90^{+0.52}_{-0.39}$	188^{+38}_{-28}	$3.6^{+0.7}_{-0.5}$	Yes
WR4	WC5+?	$3.75^{+0.89}_{-0.62}$	174^{+47}_{-32}	$3.4^{+0.9}_{-0.6}$	No
WR128	WN4(h)	$2.90^{+0.54}_{-0.39}$	170^{+35}_{-26}	$3.3^{+0.7}_{-0.5}$	No
WR52	WC4	$1.75^{+0.16}_{-0.13}$	159^{+13}_{-11}	$3.1^{+0.2}_{-0.2}$	No
WR34	WN5o	$7.41^{+1.37}_{-1.09}$	159^{+33}_{-26}	$3.1^{+0.6}_{-0.5}$	No

velocity for WR148 is 212 km s^{-1} , making it a very rapid cluster ejection.

Moffat (1989) suggested WN8-9 were over represented amongst runaways, a finding which was corroborated by Rosslowe & Crowther (2015a). However amongst our sample, only 4 out of 31 stars are of the WN8-9 subtype. The previous over representation disappears with the drop in extreme runaways. If our sample is representative of the wider WR star population, this suggests that the observed dis-

tribution was due to overestimated distance measurements, which would have made the stars appear further from the plane than they truly are.

6 CONCLUSIONS

We have calculated distances and absolute magnitudes of the Galactic WR population using data from *Gaia* DR2:

- 383 WR stars (58% of the known Galactic population) have full five parameter astrometric solutions (proper motions and parallaxes) in the *Gaia* catalogue. WR stars with large $J-K > 3$ colours, indicating high dust extinctions, were generally not detected by *Gaia*.
- We used the *Gaia* parallaxes to calculate distances to the 383 WR stars detected by *Gaia*. We use Bayesian methods to properly transform the parallax uncertainties to distance uncertainties and to obtain distances from negative parallaxes. Our Bayesian prior accounts for extinction using a Galactic dust model and the specific distribution of massive stars using HII regions. Potential underestimates of parallax uncertainties and the zero point error are accounted for in our calculation.
- The resulting distances agree well with both the previous calibration (Rosslowe & Crowther 2015a) and DR2 distances from Bailer-Jones et al. (2018) up to 2 kpc. Deviations above 2 kpc are due primarily to the large uncertainties of the *Gaia* parallaxes. Distances from Bailer-Jones et al. (2018) formed the basis of recent spectroscopic studies of Galactic WR stars by Sander et al. (2019) and Hamann et al. (2019). Use of distances from this study would generally lead to modest 0.05 dex reductions in stellar luminosities, albeit with reductions of up to 0.2 dex for relatively distant stars.
- 25 WR stars are found within 2 kpc, compared to 30 WR stars from Conti et al. (1983). Based on the population in GOSC v4.1 (Maíz Apellániz et al. 2013), the WR/O star ratio in this region is 0.09.
- We calculate absolute magnitudes for WR stars, in both the v^{WR} and K_s bands. Of these, 187 stars have an absolute magnitude in either band and were used to generate subtype averages for calibrations. Both WN and WC stars are found to be more diverse in their absolute magnitude ranges than anticipated and therefore we recommend avoiding use of calibrations without accounting for this large intrinsic spread.
- We have applied our new distances to identify 31 potential runaways from the Galactic disk, accounting for the Galactic warp. HII region scale heights define the cut-offs for runaway status. 20 of these WR stars with $|z| > 156$ pc are new detections. The vast majority of the runaway stars are single. However, as both companion supernovae and dynamical ejection from clusters can produce single star runaways, it was not possible for us to determine the dominant runaway production mechanism, which is deferred to Paper II.

The current limitations of our prior are mainly the simplified dust extinction map. With an increased number of observations, the quality of future *Gaia* release data should improve. Therefore, the number of WR stars with negative parallaxes should fall and we thus expect a corresponding

decrease in the number of flagged results. Better parallax to error ratios in the early DR3 release (estimated to improve by a factor 1.2, Brown 2019), will also reduce uncertainties and the effect of our prior when used with small parallaxes. Further improvements to the astrometric modelling and fitting algorithms should also reduce the number of questionable results via a reduction in astrometric excess noise. Finally, there is a possibility that the number of WR stars with distances will increase. 32 objects only had two parameter solutions (fitting positions) from *Gaia* DR2. Future *Gaia* data releases may find satisfactory full five parameter solutions, which would also include parallaxes.

ACKNOWLEDGEMENTS

GR wishes to thank the Science and Technology Facilities Council (STFC), for their financial support through the Doctoral Training Partnership.

We wish to thank the referee Dr Anthony Brown for his helpful comments and suggestions on the submitted manuscript. We also thank Dr Josep Manel Carrasco and Dr Carme Jordi for providing the synthetic photometry in V broadband, *Gaia* $G_{BP} - G_{RP}$ and G filters at different extinctions and for different WR star subtypes, used in Section 3.3.

This work has made use of data from the European Space Agency (ESA) mission *Gaia* (<https://www.cosmos.esa.int/gaia>), processed by the *Gaia* Data Processing and Analysis Consortium (DPAC, <https://www.cosmos.esa.int/web/gaia/dpac/consortium>). Funding for the DPAC has been provided by national institutions, in particular the institutions participating in the *Gaia* Multilateral Agreement.

This publication also makes use of data products from the Two Micron All Sky Survey, which is a joint project of the University of Massachusetts and the Infrared Processing and Analysis Center/California Institute of Technology, funded by the National Aeronautics and Space Administration and the National Science Foundation.

The work in Section 2.1 is based on data products from observations made with ESO Telescopes at the La Silla Paranal Observatory under programme ID 177.D-3023, as part of the VST Photometric H α Survey of the Southern Galactic Plane and Bulge (VPHAS+, www.vphas.eu). Additionally, this paper makes use of data obtained as part of the INT Photometric H α Survey of the Northern Galactic Plane (IPHAS, www.iphas.org) carried out at the Isaac Newton Telescope (INT). The INT is operated on the island of La Palma by the Isaac Newton Group in the Spanish Observatorio del Roque de los Muchachos of the Instituto de Astrofísica de Canarias. All IPHAS data are processed by the Cambridge Astronomical Survey Unit, at the Institute of Astronomy in Cambridge. The bandmerged DR2 catalogue was assembled at the Centre for Astrophysics Research, University of Hertfordshire, supported by STFC grant ST/J001333/1.

In addition to Astropy (Astropy Collaboration et al. 2013), this work would not be possible without the python packages Numpy (Oliphant 2006, Walt et al. 2011), Pandas (McKinney 2010) and Matplotlib (Hunter 2007).

REFERENCES

- Arenou F., et al., 2018, *A&A*, **616**, A17
 Astropy Collaboration et al., 2013, *A&A*, **558**, A33
 Astropy Collaboration et al., 2018, *AJ*, **156**, 123
 Bailer-Jones C. A. L., 2015, *Publications of the Astronomical Society of the Pacific*, **127**, 994
 Bailer-Jones C. A. L., Rybizki J., Fouesneau M., Mantelet G., Andrae R., 2018, *AJ*, **156**, 58
 Barentsen G., et al., 2014, *MNRAS*, **444**, 3230
 Bennett M., Bovy J., 2019, *MNRAS*, **482**, 1417
 Bessell M. S., 1979, *Publications of the Astronomical Society of the Pacific*, **91**, 589
 Blaauw A., 1961, *Bulletin of the Astronomical Institutes of the Netherlands*, **15**, 265
 Bobylev V. V., Bajkova A. T., 2016, *Astronomy Letters*, **42**, 1
 Brown A. G., 2019, The Future of the Gaia Universe, doi:10.5281/zenodo.2637972, <https://doi.org/10.5281/zenodo.2637972>
 Cardelli J. A., Clayton G. C., Mathis J. S., 1989, *ApJ*, **345**, 245
 Chené A. N., et al., 2019, *MNRAS*, **484**, 5834
 Cohen M., van der Hucht K. A., Williams P. M., The P. S., 1991, *ApJ*, **378**, 302
 Conti P. S., Massey P., 1989, *ApJ*, **337**, 251
 Conti P. S., Vacca W. D., 1990, *AJ*, **100**, 431
 Conti P. S., Garmany C. D., De Loore C., Vanbeveren D., 1983, *ApJ*, **274**, 302
 Crowther P. A., 2007, *ARA&A*, **45**, 177
 Crowther P. A., Dessart L., 1998, *MNRAS*, **296**, 622
 Crowther P. A., Smith L. J., 1997, *A&A*, **320**, 500
 Crowther P. A., Smith L. J., Hillier D. J., Schmutz W., 1995, *A&A*, **293**, 427
 Crowther P. A., Dessart L., Hillier D. J., Abbott J. B., Fullerton A. W., 2002, *A&A*, **392**, 653
 Crowther P. A., Hadfield L. J., Clark J. S., Negueruela I., Vacca W. D., 2006, *MNRAS*, **372**, 1407
 De Marco O., Schmutz W., Crowther P. A., Hillier D. J., Dessart L., de Koter A., Schweickhardt J., 2000, *A&A*, **358**, 187
 Drew J. E., et al., 2005, *MNRAS*, **362**, 753
 Drew J. E., et al., 2014, *MNRAS*, **440**, 2036
 Drissen L., Lamontagne R., Moffat A. F. J., Bastien P., Seguin M., 1986, *ApJ*, **304**, 188
 Ducati J. R., Bevilacqua C. M., Rembold S. r. B., Ribeiro D., 2001, *ApJ*, **558**, 309
 Eldridge J. J., Fraser M., Smartt S. J., Maund J. R., Crockett R. M., 2013, *MNRAS*, **436**, 774
 Evans D. W., et al., 2018, *A&A*, **616**, A4
 Fritz T. K., et al., 2011, *ApJ*, **737**, 73
 Gaia Collaboration et al., 2016, *A&A*, **595**, A1
 Gaia Collaboration et al., 2018a, *A&A*, **616**, A1
 Gaia Collaboration et al., 2018b, *A&A*, **616**, A10
 Georgy C., Meynet G., Walder R., Folini D., Maeder A., 2009, *A&A*, **502**, 611
 Göteborg Y., de Mink S. E., Groh J. H., Kupfer T., Crowther P. A., Zapartas E., Renzo M., 2018, *A&A*, **615**, A78
 Graczyk D., et al., 2019, *ApJ*, **872**, 85
 Gravity Collaboration et al., 2018, *A&A*, **615**, L15
 Green G. M., et al., 2015, *ApJ*, **810**, 25
 Hadfield L. J., van Dyk S. D., Morris P. W., Smith J. D., Marston A. P., Peterson D. E., 2007, *MNRAS*, **376**, 248
 Hainich R., et al., 2014, *A&A*, **565**, A27
 Hamann W.-R., Gräfener G., 2004, *A&A*, **427**, 697
 Hamann W. R., Gräfener G., Liermann A., 2006, *A&A*, **457**, 1015
 Hamann W. R., et al., 2019, *A&A*, **625**, A57
 Hambly N., et al., 2018, Technical report, Gaia DR2 documentation Chapter 14: Datamodel description
 Hogg D. W., 2018, preprint, p. arXiv:1804.07766

- Hunter J. D., 2007, *Computing in Science and Engineering*, **9**, 90
- Jordi C., et al., 2010, *A&A*, **523**, A48
- Kippenhahn R., Weigert A., 1967, *zap*, **65**, 251
- Leloudas G., Sollerman J., Levan A. J., Fynbo J. P. U., Malesani D., Maund J. R., 2010, *aap*, **518**, A29
- Li C., Zhao G., Jia Y., Liao S., Yang C., Wang Q., 2019, *ApJ*, **871**, 208
- Lindegren L., et al., 2018a, Gaia DR2 astrometry, <https://www.cosmos.esa.int/web/gaia/dr2-known-issues>
- Lindegren L., et al., 2018b, *A&A*, **616**, A2
- Lundström I., Stenholm B., 1984, *Astronomy and Astrophysics Supplement Series*, **58**, 163
- Luri X., et al., 2018, *A&A*, **616**, A9
- Maíz Apellániz J., Weiler M., 2018, *A&A*, **619**, A180
- Maíz Apellániz J., et al., 2013, in *Massive Stars: From alpha to Omega*. p. 198 ([arXiv:1306.6417](https://arxiv.org/abs/1306.6417))
- Marchenko S. V., Moffat A. F. J., Crowther P. A., 2010, *ApJ*, **724**, L90
- Martins F., Plez B., 2006, *A&A*, **457**, 637
- Mason B. D., Hartkopf W. I., Gies D. R., Henry T. J., Helsel J. W., 2009, *AJ*, **137**, 3358
- Mauerhan J. C., Van Dyk S. D., Morris P. W., 2009, *PASP*, **121**, 591
- McKinney W., 2010, in van der Walt S., Millman J., eds, *Proceedings of the 9th Python in Science Conference*. pp 51 – 56
- Melena N. W., Massey P., Morrell N. I., Zangari A. M., 2008, *AJ*, **135**, 878
- Meynet G., Maeder A., 2005, *A&A*, **429**, 581
- Moffat A. F. J., 1989, *ApJ*, **347**, 373
- Moffat A. F. J., Lamontagne R., Seggewiss W., 1982, *A&A*, **114**, 135
- Munoz M., Moffat A. F. J., Hill G. M., Shenar T., Richardson N. D., Pablo H., St-Louis N., Ramiaramanantsoa T., 2017, *MNRAS*, **467**, 3105
- Oh S., Kroupa P., 2016, *A&A*, **590**, A107
- Oliphant T., 2006, *Guide to NumPy*. Trelgol Publishing
- Paladini R., Burigana C., Davies R. D., Maino D., Bersanelli M., Cappellini B., Platania P., Smoot G., 2003, *A&A*, **397**, 213
- Paladini R., Davies R. D., De Zotti G., 2004, *MNRAS*, **347**, 237
- Poveda A., Ruiz J., Allen C., 1967, *Boletín de los Observatorios Tonantzintla y Tacubaya*, **4**, 86
- Renzo M., et al., 2019, *A&A*, **624**, A66
- Riess A. G., et al., 2018, *ApJ*, **861**, 126
- Romero-Gómez M., Mateu C., Aguilar L., Figueras F., Castro-Ginard A., 2019, *A&A*, **627**, A150
- Rosslowe C. K., Crowther P. A., 2015a, *MNRAS*, **447**, 2322
- Rosslowe C. K., Crowther P. A., 2015b, *MNRAS*, **449**, 2436
- Salgado J., González-Núñez J., Gutiérrez-Sánchez R., Segovia J. C., Durán J., Hernández J. L., Arviset C., 2017, *Astronomy and Computing*, **21**, 22
- Sana H., et al., 2012, *Science*, **337**, 444
- Sander A., Hamann W. R., Todt H., 2012, *A&A*, **540**, A144
- Sander A. A. C., Hamann W. R., Todt H., Hainich R., Shenar T., Ramachandran V., Oskinova L. M., 2019, *A&A*, **621**, A92
- Schnurr O., Moffat A. F. J., St-Louis N., Morrell N. I., Guerrero M. A., 2008, *MNRAS*, **389**, 806
- Schöhrich R., McMillan P., Eyer L., 2019, *MNRAS*, **487**, 3568
- Shara M. M., et al., 2009, *AJ*, **138**, 402
- Shenar T., et al., 2019, *A&A*, **627**, A151
- Skrutskie M. F., et al., 2006, *AJ*, **131**, 1163
- Smith L. F., 1968, *MNRAS*, **140**, 409
- Smith L. F., Shara M. M., Moffat A. F. J., 1990, *ApJ*, **358**, 229
- Smith L. J., Crowther P. A., Prinja R. K., 1994, *A&A*, **281**, 833
- Smith L. F., Shara M. M., Moffat A. F. J., 1996, *MNRAS*, **281**, 163
- Smith N., Li W., Filippenko A. V., Chornock R., 2011, *Monthly Notices of the Royal Astronomical Society*, **412**, 1522
- Smith N., Aghakhanloo M., Murphy J. W., Drout M. R., Stassun K. G., Groh J. H., 2019, *MNRAS*, **488**, 1760
- Stassun K. G., Torres G., 2018, *ApJ*, **862**, 61
- Stead J. J., Hoare M. G., 2009, *MNRAS*, **400**, 731
- Todt H., Sander A., Hainich R., Hamann W.-R., Quade M., Shenar T., 2015, *A&A*, **579**, A75
- Torres-Dodgen A. V., Massey P., 1988, *AJ*, **96**, 1076
- Torres A. V., Conti P. S., Massey P., 1986, *ApJ*, **300**, 379
- Tramper F., et al., 2015, *A&A*, **581**, A110
- Turner D. G., 1982, in *IAU Symp. 99: Wolf-Rayet Stars: Observations, Physics, Evolution*, ed. Ed Loore C.W.H., Willis A.J.D.. Reidel Publishing, pp 57–60
- Vacca W. D., Torres-Dodgen A. V., 1990, *ApJS*, **73**, 685
- Walt S. v. d., Colbert S. C., Varoquaux G., 2011, *Computing in Science & Engineering*, **13**, 22
- Wenger M., et al., 2000, *Astronomy and Astrophysics Supplement Series*, **143**, 9
- Williams P. M., van der Hucht K. A., 2000, *MNRAS*, **314**, 23
- Zhekov S. A., Tomov T., Gawronski M. P., Georgiev L. N., Borissova J., Kurtev R., Gagné M., Hajduk M., 2014, *MNRAS*, **445**, 1663
- Zinn J. C., Pinsonneault M. H., Huber D., Stello D., 2019, *ApJ*, **878**, 136
- van Leeuwen F., 2007, *A&A*, **474**, 653
- van der Hucht K. A., 2001, *New Astronomy Reviews*, **45**, 135

This paper has been typeset from a Te_X/La_TE_X file prepared by the author.

APPENDIX A: ADQL QUERY

```
SELECT TOP 10 DISTANCE(POINT('ICRS', ra,
dec), POINT('ICRS', WRra, WRdec)) AS dist, *
FROM gaiadr2.gaia_source
WHERE CONTAINS(POINT('ICRS', ra, dec), CIRCLE('ICRS', WRra, WRdec, search_radius))=1
ORDER BY dist ASC
```

where WRra and WRdec are the WR RA and DEC search coordinates in decimal format and the search_radius is one arcsecond. The query selects the top ten closest points (arranged in distance order) that are within a 1" circle of the WR search coordinates. All *Gaia* catalogue columns are selected for convenience.

APPENDIX B: INCREASED UNCERTAINTIES

Figure 3 in Section 2.2.1 shows the underestimation of DR2 parallax uncertainties, as compared to the uncertainties of external data (from table 1. in [Arenou et al. 2018](#)). The combined Gaussian and straight line fit to the uncertainties is given by:

$$X = -0.01319G + 1.376 + \frac{1.1}{\sqrt{2\pi}1.35} \exp\left[-\frac{1}{2(1.35)^2}(G - 14.59)^2\right] \quad (\text{B1})$$

where G is the WR *Gaia* G band magnitude and X is the factor by which the error is estimated to increase. The updated parallax (in mas) ω and error σ_ω (also in mas) parallax inputs to the likelihood are therefore given by

$$\omega = \Psi + 0.029 \quad (\text{B2})$$

$$\sigma_\omega = \sigma_\Psi X \quad (\text{B3})$$

where Ψ is the original parallax from the *Gaia* catalogue. This leads to a final likelihood of the form

$$P(\omega|r, \sigma_\omega) = \frac{1}{\sqrt{2\pi}\sigma_\omega} \exp\left[-\frac{1}{2\sigma_\omega^2}\left(\omega - \frac{1}{r}\right)^2\right] \quad (\text{B4})$$

APPENDIX C: PRIOR DETAILS

The prior is a combination of HII region distributions at radio wavelengths (to avoid extinction and get a good spatial sample) and an extinction map.

For the HII region distribution, we chose a Gaussian centred on 3000 pc to best approximate the distribution with distance from the Sun (based on Figure 12 from [Paladini et al. 2004](#)). Over varying Galactic longitudes and latitudes, the number of HII regions and their spread over distance changes. To alter the distribution for different lines of sight, the standard deviation was modified based on the HII region number density at a given latitude and longitude. The standard deviations range from 1-3 kpc, depending on the longitude and latitude of the line of sight. Figure C1 (a) shows the resulting distribution over different longitudes at

different distances and C1 (b) shows the distribution over latitudes.

There is a particularly large excess probability around $l=73-86^\circ$ and $-3 \leq b \leq -4^\circ$ due to the Cygnus X region (as stated in [Paladini et al. 2003](#)). Over these coordinates, the mean of the Gaussian is instead centred on 1400 pc and the standard deviation is correspondingly lower.

The overhead extinction map in Figure C3 was generated using a simple dust disk model (see Figure C2 (a) for the variation in longitude and C2 (b) for the latitude).

Our primary goal was to determine how extinction affected the observable distances along each line of sight. In regions of high extinction, the peak of the prior would have to be shifted towards the Sun, as the probability of seeing a WR star at a greater distance would decrease. The I band (which peaks at $\sim 8000\text{\AA}$) is best suited for this, as it operates towards the extreme red end of the *Gaia* G band (at 10500\AA). Any distance that is too faint to observe in this wavelength range would therefore be very faint in G and have a small or nil probability of hosting a WR star that is visible to *Gaia*. At each distance, the dust was integrated along the line of sight and normalised to the extinction at the Galactic centre. This was chosen to be 15.36 magnitudes, in the I band.

Unfortunately, it was not possible to reliably convert A_I to A_G , as the conversion relationship given in [Evans et al. \(2018\)](#) does not extend to the large values of $V - I_c$ at the Galactic centre.

Galactic centre extinction in the I band was calculated by assuming the V band extinction at the same point is 32 mag (based on averaging optical extinction at 0.55μ from [Fritz et al. 2011](#)) and multiplying by 0.48 [Cardelli et al. \(1989\)](#) to account for the difference in reddening. Figure C3 shows the resulting extinction variation with Galactic longitude.

We then converted the extinction to a factor which could be applied to the probability at each distance, to simulate the reduction of flux from extinction

$$\delta = 2.512^{(-A_I)} \quad (\text{C1})$$

where A_I is the I band extinction at that distance, calculated from $A_I = 0.48AV$ (where AV is the V band extinction).

This conversion factor was then multiplied by the HII region distribution, to give a final distribution. This combines both the radio HII region observations and dust extinction, and so approximates what might be seen by *Gaia*. This final distribution is shown in Figure C4. As compared to Figure C1, the peak of the prior has moved significantly closer to the Sun (within 1-3 kpc, depending on longitude).

APPENDIX D: POSTERIOR

The Bayesian inferred distribution of distances (the posterior $P(r|\Psi, \sigma_\Psi)$) is calculated using

$$P(r|\Psi, \sigma_\Psi) = \frac{1}{Z} P(\Psi|r, \sigma_\Psi) P(r) \quad (\text{D1})$$

([Bailer-Jones 2015](#)), where $P(\Psi|r, \sigma_\Psi)$ is the likelihood (the probability distribution of measured parallaxes, $P(r)$ is

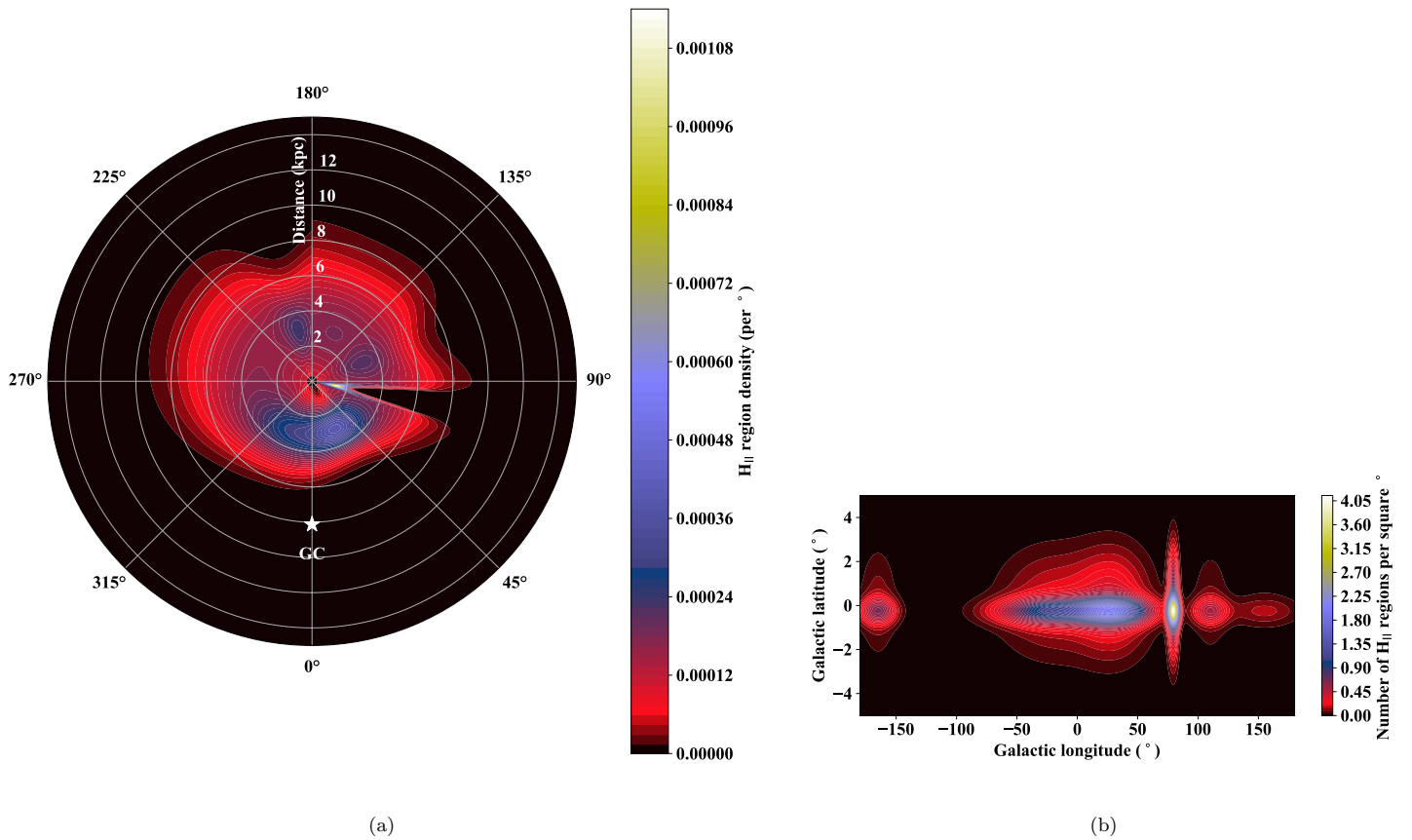


Figure C1. (a) Density of Galactic HII regions over distance and longitude, at zero latitude, before extinction is applied (based on Paladini et al. 2004 and Paladini et al. 2003). The coordinate system is centred on the Sun, with the Galactic Centre at 8.122 kpc. (b) Density of Galactic HII regions across different latitudes, viewed from the Sun and based on Paladini et al. (2003).

the prior (the expected distribution of the distances) and Z is a normalisation constant.

For our likelihood and prior, the resulting posterior distribution is

$$P(\omega|r, \sigma_\omega) = \frac{1}{\sqrt{2\pi}\sigma_\omega\sigma_p} \exp\left[-\frac{1}{2}\left(\frac{\left(\omega - \frac{1}{r}\right)^2}{\sigma_\omega^2} + \frac{(r - \mu_p)^2}{\sigma_p^2}\right)\right] \delta \quad (\text{D2})$$

where σ_p is the standard deviation of the Gaussian from the HII region prior in the direction of the WR and μ_p is the mean. We do not account for errors in the WR position, as these are insignificant compared to the simplifications in the prior (such as the simplification of the dust distribution).

We calculated the credible intervals (uncertainties), by cycling through each of the calculated probabilities, beginning with the maximum. At each probability, the corresponding distances either side of the distribution peak were selected. The area under the curve for this distance range could then be compared to the target area (e.g. 68% for one sigma uncertainties). The process was repeated until the area integrated reached or exceeded the required credible interval. This method could also be applied to the two sigma uncertainties (95%).

Due to the finite nature of the grid, slight deviations from the specified 68% area occurred, the largest of which was for WR11 (which reached 68.5% of the area). However, these deviations led to typical interval changes of a few pc or less, below the reasonable precision of our distance calculation.

APPENDIX E: IMPACT OF UNCERTAINTIES

Figure E1 shows that underestimated parallax errors from *Gaia* have a significant effect on the most probable distance. Beyond ~ 1.4 kpc, the adjusted errors result in systematically closer distances, compared to data with no uncertainty increases. This occurs because the larger parallax to error ratio means the prior has a greater influence on the resulting distance. As the prior accounts for dust extinction, these distances from parallaxes with inflated errors are smaller than those from the original parallaxes.

We can fit a line to determine the typical contribution of modified errors

$$d_e = 0.7724d + 349.25 \quad (\text{E1})$$

where d_e is the distance with extended errors and d contains no error modification. The deviations between this fit and a line $x=y$ indicate a typical contribution of 24% at 10 kpc, decreasing towards zero at 1.5 kpc. Below this distance, the difference begins to increase again because the increased errors have little effect and the fit is no longer accurate. For isolated cases, the maximum deviation was higher, up to $\sim 50\%$.

In most instances, the differences between the distances from the original *Gaia* catalogue parallax error and the distances from the increased parallax error, fall within uncertainties. A major limitation is that the error rescaling used here, may not account for individual errors which are still underestimated.

Overall, the data show that underestimated parallax errors have a significant effect on many distances and that

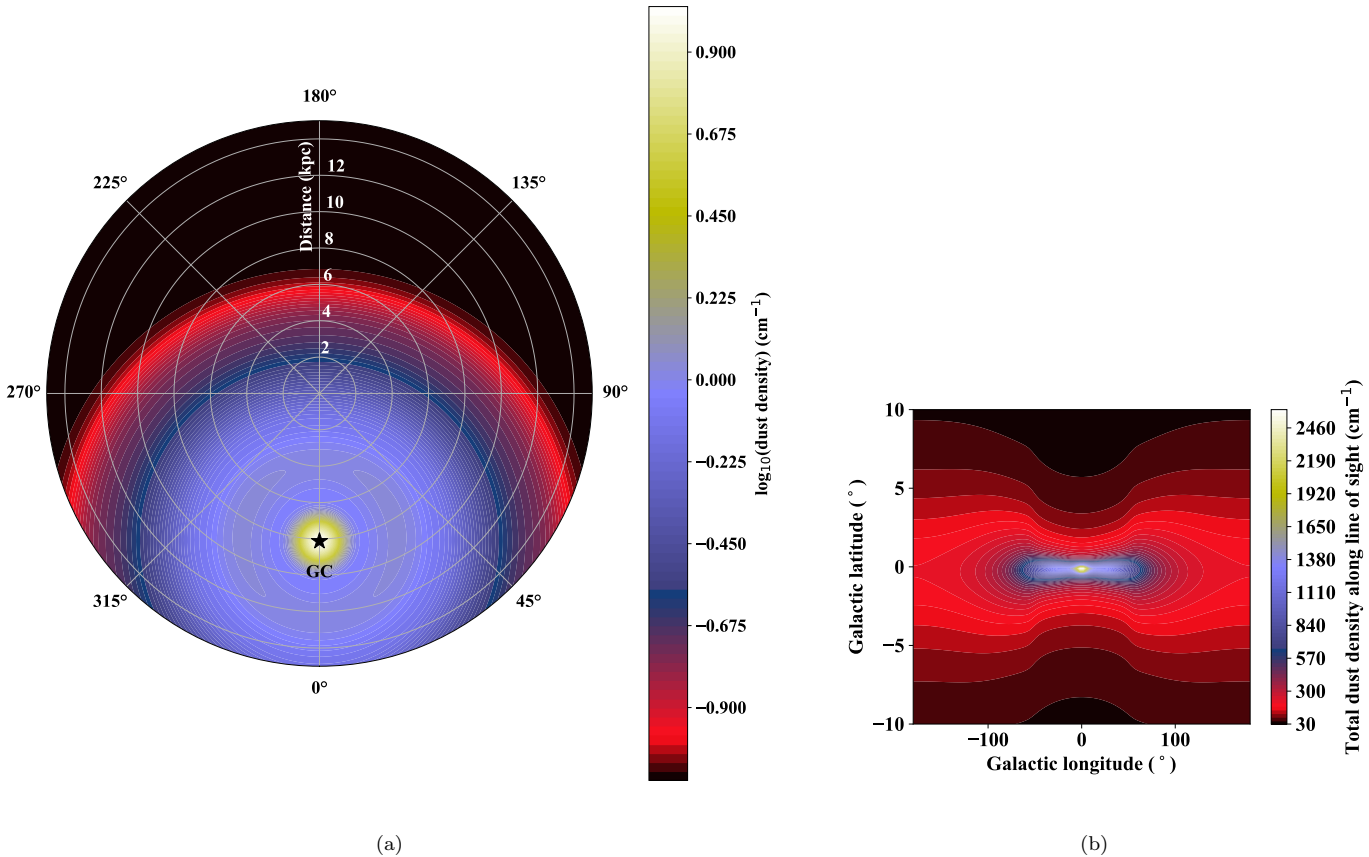


Figure C2. (a) Dust distribution over longitude and distance, at zero latitude, in the simple disk model and (b) the variation of dust integrated along line of sight with latitude, viewed from the Sun. The coordinate system is centred on the Sun, with the Galactic Centre at 8.122 kpc.

these underestimates need to be accounted for in distance calculations.

APPENDIX F: BOOTSTRAPPING AND FITS TO ABSOLUTE MAGNITUDES

For the bootstrapping procedure, we sample 1000 distributions of 20,000 points each (with replacement) from the true distributions of apparent magnitudes (assumed to be a Gaussian with the peak at the measured value and the standard deviation as the uncertainty), distances and extinction. This generated a distribution of absolute magnitudes which could be fitted with a Gaussian if the χ^2 value was below 0.005 (setting the limit below this value made it difficult to fit stars). Alternatively, if the χ^2 value was above 0.005, a Weibull distribution (non symmetric with left or right skew) was fitted instead

$$y = \frac{k}{\lambda} \left(\frac{M_{range}}{\lambda} \right)^{(k-1)} e^{-(M_{range}/\lambda)^k} \quad (\text{F1})$$

where k is the shape parameter, λ is the scale parameter and M_{range} is the range of absolute magnitude values over which the fit is made. As the Weibull distribution is only

valid over a positive interval, we add a constant to transform the negative absolute magnitudes to positive values

$$M_{mod} = M_{range} + M_{max} + 0.1 \quad (\text{F2})$$

where M_{mod} is the transformed range and M_{max} is the maximum value in the fit range.

Both distribution types were fitted using a least squares curve fit in the python SCIPY package. The most likely absolute magnitude was the average of the Gaussian, or the mode M_{mode} of the Weibull distribution, transformed back to negative values

$$M_{mode} = \lambda \left(\frac{k-1}{k} \right)^{(1/k)} - (M_{max} + 0.1) \quad (\text{F3})$$

Credible intervals were again used for 68% uncertainties on individual magnitudes. The typical variation between Monte Carlo runs (due to different data selections), was less than ± 0.05 . In a small number of cases, the distribution fitting failed. In these instances, we calculated the point value of absolute magnitude, using the peaks of the distance, apparent magnitude and extinction probability curves. Due to the non Gaussian nature of the distance distributions, however, there was some offset (usually on the scale of 0.1 mag)

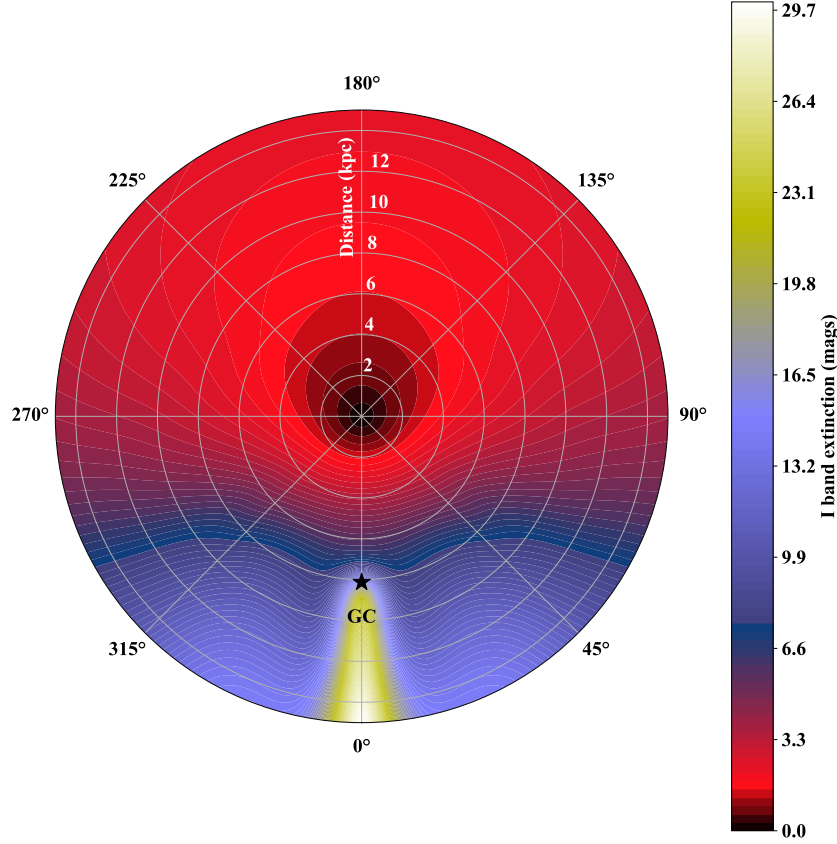


Figure C3. Extinction variation with distance and Galactic longitude, at zero latitude, as calculated using the dust model. The plot is centred on the Sun, with the Galactic Centre at 8.122 kpc.

between the peaks fitted to full distributions and these point values.

REFERENCES

- Arenou F., et al., 2018, [A&A](#), **616**, A17
 Bailer-Jones C. A. L., 2015, [Publications of the Astronomical Society of the Pacific](#), **127**, 994
 Cardelli J. A., Clayton G. C., Mathis J. S., 1989, [ApJ](#), **345**, 245
 Evans D. W., et al., 2018, [A&A](#), **616**, A4
 Fritz T. K., et al., 2011, [ApJ](#), **737**, 73
 Paladini R., Burigana C., Davies R. D., Maino D., Bersanelli M.,
 Cappellini B., Platania P., Smoot G., 2003, [A&A](#), **397**, 213
 Paladini R., Davies R. D., De Zotti G., 2004, [MNRAS](#), **347**, 237

This paper has been typeset from a TeX/LaTeX file prepared by the author.

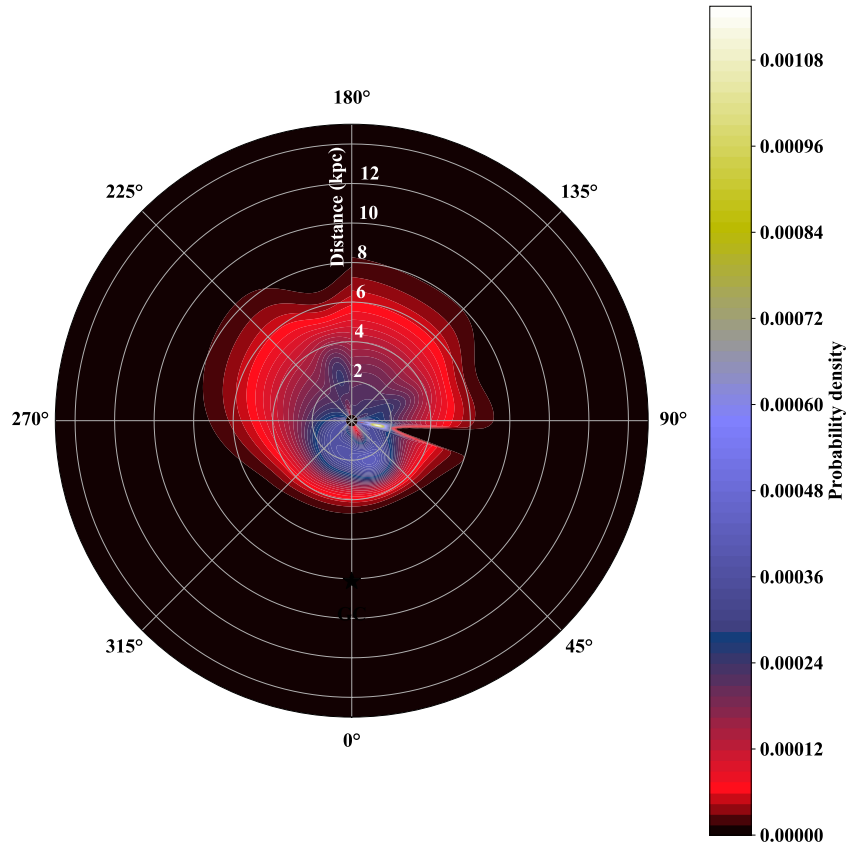


Figure C4. Combined prior, consisting of HII region prior and dust extinction.

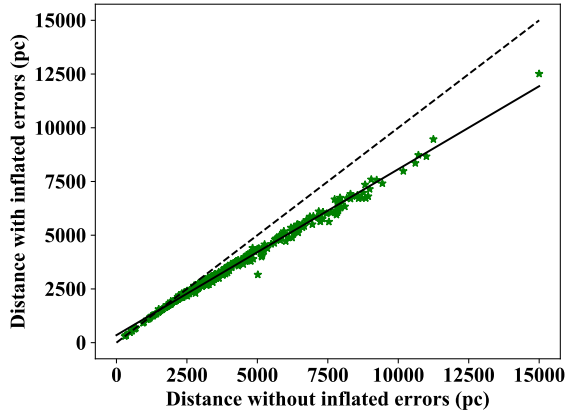


Figure E1. A comparison between distances with and without the modelled error increase. The dashed line denotes where the two distance calculations are the same and the solid line is the fit from equation E1

Table 1: Gaia DR2 astrometric, photometric and parallax properties for 383 Galactic WR stars, including WR11 using a parallax and photometry from Hipparcos (van Leeuwen 2007). The distance for WR11 was calculated in the same manner as WR with *Gaia* results, except the adjustments to calculate ω and σ_ω were not applied. Stellar luminosities, updated from Hamann et al. (2019) and Sander et al. (2019) according to our revised distances, are restricted to sources with no error flags.

WR Number	Spectral Type	Alias	RA J2015	Dec J2015	$\omega \pm \sigma_\omega$ (mas)	d (kpc)	$ z $ (pc)	G (mag)	$G_{BP} - G_{RP}$ (mag)	Excess noise	$\log L/L_\odot$	Flags
WR1	WN4b	HD 4004	00 43 28.39	+64 45 35.4	0.314 ± 0.040	$3.15^{+0.47}_{-0.36}$	125^{+15}_{-12}	9.79	1.05	0.00		g
WR3	WN3ha	HD 9974	01 38 55.62	+58 09 22.6	0.342 ± 0.051	$2.90^{+0.52}_{-0.39}$	188^{+37}_{-27}	10.58	0.18	0.10	5.56	g
WR4	WC5+?	HD 16523	02 41 11.67	+56 43 49.8	0.258 ± 0.051	$3.75^{+0.89}_{-0.62}$	174^{+46}_{-32}	9.68	0.51	0.06	5.72	g
WR5	WC6	HD 17638	02 52 11.66	+56 56 07.1	0.334 ± 0.042	$2.97^{+0.43}_{-0.33}$	90^{+16}_{-12}	10.06	0.94	0.00	5.53	g
WR6	WN4b	EZ CMa	06 54 13.04	-23 55 42.0	0.441 ± 0.065	$2.27^{+0.42}_{-0.31}$	376^{+73}_{-53}	6.57	0.04	0.18	5.78	g
WR7	WN4b	HD 56925	07 18 29.13	-13 13 01.5	0.221 ± 0.051	$4.23^{+1.08}_{-0.74}$	11^{+2}_{-1}	11.17	0.73	0.00	5.33	g
WR8	WN7o/CE	HD 62910	07 44 58.22	-31 54 29.5	0.263 ± 0.038	$3.74^{+0.63}_{-0.48}$	226^{+41}_{-31}	9.92	0.84	0.00		g
WR9	WC5+O7	HD 63099	07 45 50.40	-34 19 48.5	0.212 ± 0.035	$4.57^{+0.84}_{-0.63}$	256^{+70}_{-52}	10.14	1.30	0.00		g
WR10	WN5h	HD 65865	07 59 46.24	-28 44 03.0	0.162 ± 0.040	$5.46^{+1.25}_{-0.91}$	75^{+12}_{-9}	10.94	0.60	0.09	5.78	g
WR11	WC8+O7.5III-V	γ Vel	08 09 31.96	-47 20 11.8	2.920 ± 0.300	$0.34^{+0.04}_{-0.03}$	24^{+5}_{-4}	1.70				
WR12	WN8h	Ve5-5	08 44 47.29	-45 58 55.4	0.154 ± 0.037	$5.71^{+1.34}_{-0.92}$	175^{+42}_{-31}	10.36	1.15	0.00	5.93	g
WR13	WC6	Ve6-15	08 49 52.95	-45 10 24.0	0.189 ± 0.042	$4.80^{+1.09}_{-0.78}$	43^{+14}_{-10}	12.39	1.60	0.00	5.55	g
WR14	WC7+?	HD 76536	08 54 59.16	-47 35 32.6	0.449 ± 0.041	$2.22^{+0.22}_{-0.19}$	42^{+6}_{-5}	8.61	0.73	0.00	5.78	g
WR15	WC6	HD 79573	09 13 11.76	-50 06 25.5	0.334 ± 0.034	$2.96^{+0.34}_{-0.28}$	35^{+6}_{-5}	10.16	1.66	0.00	5.98	g
WR16	WN8h	HD 86161	09 54 52.89	-57 43 38.2	0.378 ± 0.040	$2.63^{+0.32}_{-0.26}$	96^{+14}_{-11}	8.05	0.72	0.00	5.72	g
WR17	WC5	HD 88500	10 10 31.90	-60 38 42.4	0.090 ± 0.051	$6.75^{+1.74}_{-1.33}$	413^{+111}_{-85}	10.42	0.12	0.14	5.56	g
WR17-1	WN5b	SMG09 668-4	10 16 26.21	-57 28 05.7	0.188 ± 0.165	$3.09^{+1.52}_{-0.91}$	13^{+16}_{-10}	16.97		0.79		g
WR18	WN4b	HD 89358	10 17 02.26	-57 54 46.8	0.244 ± 0.049	$3.82^{+0.84}_{-0.60}$	43^{+14}_{-10}	10.34	1.18	0.00	6.07	g
WR19	WC5	LS 3	10 18 04.98	-58 16 26.2	0.219 ± 0.036	$4.33^{+0.78}_{-0.58}$	69^{+16}_{-12}	12.40	1.94	0.00		g
WR19a	WN7:(h)	SMSP 1	10 18 53.38	-58 07 52.9	0.113 ± 0.087	$4.77^{+1.66}_{-1.14}$	63^{+29}_{-20}	12.83	2.87	0.31		g
WR20	WN5o	BS 1	10 19 18.39	-59 09 38.8	0.125 ± 0.025	$6.98^{+1.18}_{-0.93}$	203^{+38}_{-29}	13.54	1.73	0.00	5.77	g
WR20-2	O2If*/WN6	SS215	10 23 23.48	-58 00 20.8	0.147 ± 0.038	$5.53^{+1.15}_{-0.87}$	35^{+11}_{-8}	11.86	1.98	0.00		g
WR20-1	WN7-8	MDM 1	10 23 28.79	-57 46 29.4	0.271 ± 0.164	$2.72^{+1.31}_{-0.77}$	2^{+8}_{-3}	15.90	4.21	0.85		g

WR Number	Spectral Type	Alias	RA J2015	Dec J2015	$\omega \pm \sigma_w$ (mas)	d (kpc)	$ z $ (pc)	G (mag)	$G_{BP} - G_{RP}$ (mag)	Excess noise	$\log L/L_\odot$	Flags
WR20a	O3If*/WN6+O3If*/WN6	SMSP 2	10 23 58.00	-57 45 48.9	0.152±0.049	5.03 ^{+1.18} _{-0.87}	8 ⁺⁶ ₋₃	12.25	2.61	0.00		g
WR20b	WN6ha	SMSP 3	10 24 18.39	-57 48 29.7	0.309±0.057	3.07 ^{+0.64} _{-0.46}	1 ⁺³ ₋₂	12.11	2.74	0.13		g
WR20-3	O2If*/WN6	WR20c	10 25 02.60	-57 21 47.3	0.356±0.128	2.50 ^{+1.04} _{-0.61}	24 ⁺¹ ₋₀	14.85	3.86	0.66		g
WR21a	O2If/WN5	1E 1024.0-5732	10 25 56.49	-57 48 43.5	0.211±0.036	4.38 ^{+0.75} _{-0.57}	2 ⁺³ ₋₂	11.69	2.28	0.00		g
WR21	WN5o+O4-6	HD 90657	10 26 31.40	-58 38 26.1	0.240±0.034	3.99 ^{+0.62} _{-0.48}	42 ⁺⁹ ₋₇	9.49	0.76	0.00		g
WR22	WN7h+O9III-V	HD 92740	10 41 17.50	-59 40 36.8	0.424±0.045	2.33 ^{+0.28} _{-0.22}	13 ⁺⁴ ₋₃	6.23	0.33	0.00	6.25	g
WR23	WC6	HD 92809	10 41 38.31	-58 46 18.7	0.386±0.046	2.55 ^{+0.34} _{-0.27}	19 ⁺⁰ ₋₀	8.87	0.56	0.00	5.60	g
WR24	WN6ha	HD 93131	10 43 52.24	-60 07 04.0	0.269±0.044	3.55 ^{+0.66} _{-0.49}	46 ⁺¹² ₋₉	6.35	0.13	0.11	6.45	g
WR25	O2.5If*/WN6+O	HD 93162	10 44 10.37	-59 43 11.1	0.505±0.042	1.97 ^{+0.18} _{-0.15}	3 ⁺² ₋₁	7.79	0.99	0.00	6.37	g
WR26	WN7b/CE	MS 1	10 44 32.11	-57 50 23.9	0.134±0.023	6.70 ^{+0.95} _{-0.83}	134 ⁺¹⁷ ₋₁₄	13.17	1.33	0.00	5.68	g
WR27	WC6+a	Ls 4	10 44 38.04	-58 48 28.8	0.375±0.042	2.62 ^{+0.33} _{-0.26}	26 ⁺⁰ ₋₀	12.82	2.24	0.00	5.26	g
WR28	WN6(h)+OB?	MS 2	10 48 58.71	-59 03 37.3	0.134±0.039	5.74 ^{+1.18} _{-0.90}	36 ⁺³ ₋₂	12.06	1.72	0.00	5.94	g
WR29	WN7h+O	MS 3	10 50 46.28	-60 28 41.2	0.148±0.038	5.64 ^{+1.21} _{-0.90}	78 ⁺²¹ ₋₁₅	11.90	1.48	0.00		g
WR30	WC6+O6-8	HD 94305	10 51 05.99	-62 17 01.6	0.185±0.034	5.09 ^{+0.99} _{-0.74}	210 ⁺⁴⁵ ₋₃₃	11.16	0.69	0.00		g
WR30a	WO4+O5-5.5	MS 4	10 51 38.89	-60 56 34.9	0.113±0.035	6.72 ^{+1.40} _{-1.09}	140 ⁺³³ ₋₂₆	12.39	1.49	0.00		g
WR31	WN4o+O8V	HD 94546	10 53 44.81	-59 30 46.6	-1.657±0.229	6.11 ^{+1.67} _{-1.37}	22 ⁺⁰ ₋₀	10.39	0.77	0.94		n
WR31a	WN11h	He3-519	10 53 59.57	-60 26 44.3	0.071±0.037	7.35 ^{+1.45} _{-1.18}	82 ⁺²⁰ ₋₁₆	10.27	1.83	0.00		g
WR31b	WN11h	AG Car	10 56 11.57	-60 27 12.8	0.182±0.037	4.85 ^{+0.93} _{-0.70}	38 ⁺¹¹ ₋₈	7.32	0.91	0.00		g
WR31c	WC6	SMSP 4	10 57 42.85	-60 34 00.4	0.083±0.052	6.06 ^{+1.45} _{-1.11}	55 ⁺¹⁸ ₋₁₃	14.06	2.27	0.28		g
WR31-1	O3.5If/WN7	THA 35-II-153	10 59 00.86	-60 08 50.1	0.182±0.046	4.59 ^{+0.96} _{-0.72}	0 ⁺⁴ ₋₃	15.61	1.97	0.07		g
WR32	WC5+OB?	MS 5	10 59 52.91	-59 52 43.4	0.128±0.039	5.77 ^{+1.15} _{-0.88}	22 ⁺⁰ ₋₀	14.52	1.85	0.13		g
WR33	WC6	HD 95435	11 00 00.71	-57 48 59.2	0.072±0.040	7.59 ^{+1.62} _{-1.30}	272 ⁺⁵¹ ₋₄₃	11.47	0.47	0.00	5.43	g
WR34	WN5o	Ls 5	11 00 06.45	-61 26 30.1	0.102±0.029	7.41 ^{+1.37} _{-1.09}	159 ⁺³³ ₋₂₆	13.66	1.66	0.00	5.61	g
WR35	WN6h+OB?	MS 6	11 00 21.84	-61 13 52.4	0.123±0.027	6.86 ^{+1.19} _{-0.94}	121 ⁺²⁴ ₋₁₉	13.13	1.64	0.00	5.60	g
WR35a	WN6h+O8.5V	SMSP 5	11 00 24.33	-59 59 35.6	0.131±0.035	5.84 ^{+1.09} _{-0.85}	14 ⁺¹ ₋₀	12.88	1.80	0.00		g

WR Number	Spectral Type	Alias	RA J2015	Dec J2015	$\omega \pm \sigma_w$ (mas)	d (kpc)	$ z $ (pc)	G (mag)	$G_{BP} - G_{RP}$ (mag)	Excess noise	$\log L/L_\odot$	Flags
WR35b	WN4b	SMSP 6	11 01 02.08	-60 14 01.0	0.156±0.034	5.36 ^{+0.95} _{-0.74}	2 ⁺⁴ ₋₃	13.86	2.01	0.10		g
WR36	WN5-6b+OB?	Ls 6	11 02 32.97	-59 26 20.9	0.156±0.038	5.43 ^{+1.15} _{-0.85}	73 ⁺¹¹ ₋₈	12.69	1.54	0.00	5.21	g
WR37	WN4b	MS 7	11 05 13.89	-61 20 41.1	0.110±0.035	6.71 ^{+1.36} _{-1.06}	102 ⁺²⁵ ₋₁₉	14.14	2.24	0.14		g
WR38	WC4	MS 8	11 05 46.43	-61 13 48.6	0.136±0.033	6.04 ^{+1.18} _{-0.90}	76 ⁺¹⁸ ₋₁₄	14.63	1.44	0.00	5.86	g
WR38a	WN5o	SMSP 7	11 05 48.95	-61 13 41.3	0.163±0.032	5.42 ^{+1.00} _{-0.76}	65 ⁺¹⁵ ₋₁₂	14.44	1.94	0.00	5.08	g
WR40	WN8h	HD 96548	11 06 17.20	-65 30 35.3	0.257±0.038	3.83 ^{+0.67} _{-0.50}	301 ⁺⁵⁶ ₋₄₂	7.46	0.52	0.00	5.88	g
WR38b	WC7	SMSP 8	11 06 18.56	-61 14 13.7	0.195±0.055	4.32 ^{+1.12} _{-0.78}	47 ⁺¹⁷ ₋₁₂	13.74	2.63	0.29		g
WR39	WC7+OB?	MS 9	11 06 18.72	-61 14 18.4	0.008±0.166	3.84 ^{+1.72} _{-1.11}	39 ⁺²⁷ ₋₁₇	12.62	2.49	0.57		e
WR41	WC5+OB?	Ls 7	11 07 54.06	-61 27 40.8	0.146±0.029	6.01 ^{+1.06} _{-0.82}	87 ⁺¹⁹ ₋₁₄	13.79	1.57	0.00		g
WR42	WC7+O7V	HD 97152	11 10 04.07	-60 58 44.9	0.400±0.058	2.44 ^{+0.41} _{-0.31}	0 ⁺³ ₋₂	7.92	0.20	0.00		g
WR42a	WN5b	SMSP 9	11 12 15.73	-61 05 04.8	0.065±0.061	5.63 ^{+1.37} _{-1.05}	26 ⁺¹¹ ₋₈	15.28	2.46	0.23		g
WR42b	WN4b	SMSP 10	11 13 03.61	-62 14 18.4	0.068±0.061	6.33 ^{+1.70} _{-1.31}	147 ⁺⁴⁵ ₋₃₄	14.81	2.70	0.31		g
WR42c	WN5o	SMSP 11	11 14 01.47	-61 03 47.7	0.044±0.046	6.72 ^{+1.35} _{-1.09}	24 ⁺⁹ ₋₇	14.47	2.50	0.21		e
WR42d	WN5b	SMSP 12	11 14 38.63	-61 11 16.3	0.182±0.141	3.20 ^{+1.26} _{-0.83}	5 ⁺¹⁰ ₋₆	13.65	2.54	0.94		g
WR42-1	O3If*/WN6	WR42e	11 14 45.50	-61 15 00.3	0.196±0.048	4.34 ^{+0.94} _{-0.69}	19 ⁺⁸ ₋₆	13.45	2.47	0.28		g
WR43-2	O2If*/WN5	MTT 58	11 15 07.57	-61 16 54.7	0.098±0.042	6.16 ^{+1.27} _{-0.99}	37 ⁺¹² ₋₉	13.77	2.28	0.20		g
WR43-3	O2.5If*/WN6	RFS7	11 15 15.36	-60 51 17.7	0.105±0.032	6.56 ^{+1.13} _{-0.91}	4 ⁺² ₋₂	12.26	1.86	0.00		g
WR43-1	WN4b	SMG09 740_21	11 16 03.52	-61 26 58.3	0.542±0.619	1.34 ^{+1.45} _{-0.59}	5 ⁺¹⁶ ₋₆	18.94		1.77		e a
WR44	WN4o+OB?	LSS 2289	11 16 57.83	-59 26 23.8	0.141±0.034	6.07 ^{+1.22} _{-0.93}	154 ⁺²⁶ ₋₂₀	12.53	0.78	0.00	5.55	g
WR44a	WN5b	SMSP 13	11 18 43.09	-61 26 35.8	0.147±0.047	5.06 ^{+1.12} _{-0.84}	26 ⁺¹⁰ ₋₇	15.20	2.34	0.19		g
WR44-1	WCE	SMG09 740_16	11 19 43.01	-61 27 12.3	-0.339±0.423	2.67 ^{+1.46} _{-0.96}	2 ⁺¹² ₋₈	16.13		1.51		n e a
WR45	WC6	LSS 2423	11 38 05.08	-62 16 01.9	0.228±0.022	4.25 ^{+0.43} _{-0.36}	23 ⁺⁴ ₋₃	13.24	1.92	0.00	5.43	g
WR45-1	WN9-10h	HDM 1	11 42 37.64	-62 41 19.2	0.050±0.093	4.88 ^{+1.58} _{-1.12}	52 ⁺²³ ₋₁₆	15.58	3.32	0.44		e
WR45-2	WN5	SMG09 768_6	11 46 06.64	-62 47 12.7	0.173±0.062	4.39 ^{+1.21} _{-0.84}	44 ⁺¹⁸ ₋₁₂	15.46	2.62	0.31		g
WR45a	WN5o	SMSNPL 1	11 46 18.14	-61 24 41.5	0.197±0.087	3.79 ^{+1.27} _{-0.84}	52 ⁺¹⁰ ₋₇	15.12	2.42	0.47		g

WR Number	Spectral Type	Alias	RA J2015	Dec J2015	$\omega \pm \sigma_w$ (mas)	d (kpc)	$ z $ (pc)	G (mag)	$G_{BP} - G_{RP}$ (mag)	Excess noise	$\log L/L_\odot$	Flags
WR45b	WN4b	SMSNPL 2	11 48 46.02	-62 23 02.6	-0.024±0.068	5.95 ^{+1.34} _{-1.07}	19 ⁺⁹ ₋₇	15.09	2.74	0.33	n e	
WR45-3	WN5b	SMG09 772_17	11 50 04.23	-62 52 15.4	-0.171±0.128	5.21 ^{+1.68} _{-1.26}	54 ⁺²⁴ ₋₁₈	16.82	3.41	0.71	n	
WR45-4	WN6	SMG09 773_3	11 55 52.10	-62 45 02.3	0.020±0.068	5.65 ^{+1.36} _{-1.06}	34 ⁺¹³ ₋₁₀	15.54	3.00	0.35	e	
WR45-5	WN7/Of	VVV CL009-6	11 56 03.75	-63 18 54.4	0.099±0.046	6.27 ^{+1.48} _{-1.13}	100 ⁺²⁸ ₋₂₁	13.60	2.37	0.22	g	
WR45c	WN5o	SMSNPL 3	11 56 04.74	-62 44 05.1	0.130±0.028	6.14 ^{+0.97} _{-0.77}	37 ⁺⁹ ₋₇	14.00	1.93	0.00	g	
WR46	WN3b pec	HD 104994	12 05 18.71	-62 03 10.1	0.379±0.043	2.60 ^{+0.32} _{-0.26}	36 ⁺¹ ₋₁	10.70	0.19	0.08	5.41	g
WR46-1	WN6o	HDM 2	12 06 56.47	-62 38 30.4	0.048±0.083	4.72 ^{+1.18} _{-0.91}	3 ⁺⁴ ₋₃	15.07	2.78	0.42	e	
WR46-18	WC6-7	RC17 E3	12 08 52.47	-62 50 54.6	0.291±0.470	1.81 ^{+1.26} _{-0.71}	8 ⁺⁸ ₋₄	19.38	3.22	2.02	e a	
WR46-7	WC5-7	2MASS J12100795-6244194	12 10 07.95	-62 44 19.4	0.009±0.221	3.06 ^{+1.21} _{-0.86}	7 ⁺⁵ ₋₃	18.26	4.37	0.96	e	
WR46-8	WN6	2MASS J12110256-6257476	12 11 02.55	-62 57 47.6	0.258±0.181	2.59 ^{+1.11} _{-0.71}	0 ⁺⁸ ₋₃	17.43	4.33	0.96	g	
WR46-16	WN9	RMM11 #5	12 11 54.06	-63 17 03.8	0.247±0.214	2.47 ^{+1.26} _{-0.75}	11 ⁺¹⁶ ₋₉	18.34	2.64	0.79	g	
WR46-9	WN5	2MASS J12121681-6246145	12 12 16.80	-62 46 14.6	0.098±0.189	3.05 ^{+1.17} _{-0.82}	8 ⁺⁴ ₋₃	17.49	4.54	0.98	e	
WR46-17	WN9/OIf+	VVV CL011-2	12 12 41.12	-62 42 30.7	-0.034±0.265	2.89 ^{+1.23} _{-0.87}	12 ⁺³ ₋₂	16.47	4.05	1.63	n e a	
WR46a	WN4o	SMSNPL 4	12 13 02.34	-63 42 25.4	0.072±0.048	6.73 ^{+1.56} _{-1.23}	114 ⁺³¹ ₋₂₄	14.88	2.06	0.12	g	
WR46-10	WCE	SMG09 791_12c	12 13 28.27	-62 41 43.0	0.727±0.524	1.25 ^{+1.22} _{-0.50}	17 ⁺³ ₋₁	19.36	3.41	1.77	a	
WR46-2	WN7h	HDM 3	12 13 38.78	-63 08 58.1	0.168±0.088	3.81 ^{+1.12} _{-0.80}	18 ⁺¹¹ ₋₈	14.63	3.29	0.43	g	
WR46-3	O6-7.5If+	KBG2007-4	12 14 31.53	-62 58 54.3	-0.108±0.151	4.07 ^{+1.26} _{-0.96}	8 ⁺⁹ ₋₆	15.30	4.51	0.89	n e	
WR46-4	Ofpe/WN9	KBG2007-3	12 14 31.71	-62 58 52.1	-0.499±0.411	2.81 ^{+1.29} _{-0.92}	0 ⁺⁹ ₋₆	15.81	4.54	2.50	n a	
WR46-5	WN6	KBG2007-2	12 14 33.08	-62 58 51.0	-0.041±0.160	3.73 ^{+1.24} _{-0.92}	5 ⁺⁸ ₋₆	16.53	4.46	0.83	n e	
WR46-6	WN7	KBG2007-1	12 14 33.90	-62 58 48.7	-0.123±0.164	3.93 ^{+1.26} _{-0.96}	7 ⁺⁸ ₋₆	16.86	4.31	0.93	n e	
WR46-15	WN8	MDM 2	12 15 12.48	-62 46 43.9	-1.846±1.211	1.99 ^{+1.32} _{-0.89}	13 ⁺⁴ ₋₃	20.49		4.83	n a	

WR Number	Spectral Type	Alias	RA J2015	Dec J2015	$\omega \pm \sigma_w$ (mas)	d (kpc)	$ z $ (pc)	G (mag)	$G_{BP} - G_{RP}$ (mag)	Excess noise	$\log L/L_\odot$	Flags
WR46-11	WCE	SMG09 808_14	12 28 41.90	-63 25 46.1	-0.130±0.121	4.85 ^{+1.44} _{-1.09}	35 ⁺¹⁶ ₋₁₂	16.97	3.49	0.58		n
WR46-12	WN4b	SMG09 808_23	12 28 50.98	-63 17 00.1	0.093±0.194	3.00 ^{+1.20} _{-0.83}	6 ⁺¹⁰ ₋₇	18.04	3.33	0.66		e
WR46-13	WC7	SMG09 807_16	12 30 03.86	-62 50 17.1	-0.046±0.174	3.58 ^{+1.19} _{-0.90}	16 ⁺¹ ₋₁	17.84	3.61	0.82		n e
WR46-14	WN5b	SMG09 816_10	12 38 18.75	-63 24 19.7	1.538±0.589	0.65 ^{+0.70} _{-0.23}	14 ⁺⁶ ₋₂	17.78	4.00	4.25		a
WR47	WN6o+O5V	HD 311884	12 43 50.99	-63 05 14.8	0.263±0.047	3.49 ^{+0.61} _{-0.47}	6 ⁺² ₋₁	10.29	1.44	0.00		g
WR47a	WN8h	SMSNPL 5	12 45 51.24	-64 09 38.0	0.146±0.064	4.89 ^{+1.46} _{-1.02}	89 ⁺³³ ₋₂₃	13.96	2.75	0.32		g
WR47-1	WN6o	HDM 4	12 46 16.13	-62 57 23.5	0.139±0.123	3.45 ^{+1.06} _{-0.78}	15 ⁺¹ ₋₁	16.49	3.56	0.63		g
WR47b	WN9h	SMSNPL 6	12 48 07.60	-63 38 39.8	-0.075±0.089	5.63 ^{+1.49} _{-1.16}	55 ⁺²⁰ ₋₁₅	14.22	3.34	0.50		n e
WR47-5	WN6(h)	RC17 B13	12 50 48.96	-62 24 39.8	-0.271±0.345	2.96 ^{+1.55} _{-1.01}	44 ⁺¹² ₋₈	19.07	4.33	1.27		n e a
WR47c	WC5	SMSNPL 7	12 52 55.67	-63 46 38.0	0.058±0.044	6.81 ^{+1.43} _{-1.15}	86 ⁺²² ₋₁₈	14.22	2.35	0.19		g
WR47-2	WC5-6	SMG09 832_25	12 55 44.24	-63 35 50.1	0.053±0.158	3.45 ^{+1.30} _{-0.90}	23 ⁺¹⁶ ₋₁₁	17.77	4.48	0.76		e
WR47-3	WC5-6	SMG09 856_13c	13 03 11.06	-63 42 16.4	0.620±0.349	1.41 ^{+1.07} _{-0.48}	0 ⁺¹⁶ ₋₁	18.22	4.11	2.12		a
WR48	WC6(+O9.5/B0Iab) theta Mus		13 08 07.14	-65 18 21.7	0.388±0.128	2.39 ^{+1.23} _{-0.62}	83 ⁺⁵³ ₋₂₆	5.58	0.00	0.45		g
WR48-1	WC7	HDM 5	13 10 12.06	-62 39 06.6	0.250±0.125	2.93 ^{+1.02} _{-0.68}	28 ⁺² ₋₁	15.13	3.58	0.55		g
WR48b	WC9d	SMSNPL 8	13 11 27.69	-63 45 59.9	0.141±0.051	5.12 ^{+1.25} _{-0.92}	66 ⁺²¹ ₋₁₅	14.15	2.50	0.25		g
WR48-6	WN9	MDM11 3	13 12 09.05	-62 43 26.7	0.043±0.210	3.02 ^{+1.16} _{-0.83}	23 ⁺¹ ₋₀	16.32		1.25		e a
WR48-10	WN9h	DCT12 D1-2	13 12 24.97	-62 42 00.2	0.321±0.144	2.52 ^{+0.95} _{-0.61}	24 ⁺¹ ₋₀	14.39	4.40	0.76		g
WR48-7	WN8	MDM11 5	13 12 25.46	-62 44 41.8	0.285±0.154	2.61 ^{+0.99} _{-0.65}	22 ⁺⁰ ₋₀	15.06	4.77	0.83		g
WR48-4	WC6	SMG09 845_35	13 12 27.65	-62 44 22.0	0.255±0.208	2.48 ^{+1.08} _{-0.70}	22 ⁺⁰ ₋₀	18.08	4.39	1.02		a
WR48-8	WN9	MDM11 7	13 12 28.49	-62 41 51.0	0.226±0.103	3.22 ^{+0.97} _{-0.68}	25 ⁺¹ ₋₀	13.98	3.75	0.59		g
WR48-9	WN9h	MDM11 8	13 12 28.55	-62 41 43.8	0.318±0.092	2.78 ^{+0.78} _{-0.53}	24 ⁺¹ ₋₀	12.61	3.68	0.31		g
WR48a	WC8ed+?	D83 1	13 12 39.59	-62 42 55.9	0.374±0.159	2.27 ^{+0.92} _{-0.57}	23 ⁺⁰ ₋₀	13.83	4.62	0.84		g
WR48-5	WN6b	SMG09 847_8	13 12 45.33	-63 05 52.0	0.099±0.456	2.06 ^{+1.16} _{-0.76}	9 ⁺⁶ ₋₄	19.43	4.00	2.03		e a
WR48c	WN3h/C4	SMSNPL 9	13 12 52.36	-63 23 45.9	0.371±0.029	2.67 ^{+0.22} _{-0.19}	8 ⁺² ₋₂	13.71	0.91	0.00		g
WR48-2	WC7-8	MV09 J13125770-6240599	13 12 57.69	-62 40 59.9	0.175±0.127	3.25 ^{+1.07} _{-0.76}	25 ⁺¹ ₋₁	15.05	3.86	0.67		g

WR Number	Spectral Type	Alias	RA J2015	Dec J2015	$\omega \pm \sigma_w$ (mas)	d (kpc)	$ z $ (pc)	G (mag)	$G_{BP} - G_{RP}$ (mag)	Excess noise	$\log L/L_\odot$	Flags
WR49	WN5(h)	LSS 2979	13 13 51.30	-65 18 08.9	0.089±0.025	8.35 ^{+1.44} _{-1.17}	348 ⁺⁶³ ₋₅₁	13.24	1.02	0.00	5.24	g
WR50	WC7+OB	V864 Cen	13 18 01.03	-62 26 04.8	0.273±0.041	3.48 ^{+0.54} _{-0.42}	37 ⁺² ₋₂	11.52	1.34	0.00		g
WR51	WN4o	MR45	13 18 23.35	-62 28 21.2	0.260±0.033	3.67 ^{+0.48} _{-0.39}	35 ⁺² ₋₁	13.61	2.00	0.06	5.07	g
WR52	WC4	HD 115473	13 18 27.99	-58 08 13.7	0.572±0.047	1.75 ^{+0.16} _{-0.13}	159 ⁺¹² ₋₁₀	9.05	0.27	0.00		g
WR52-2	WN6	SMG09 858_26	13 28 15.87	-62 06 23.6	0.284±0.160	2.63 ^{+1.20} _{-0.71}	41 ⁺⁹ ₋₅	17.51	4.31	0.86		g
WR53	WC8d	HD 117297	13 30 53.24	-62 04 51.9	0.221±0.040	4.14 ^{+0.74} _{-0.56}	52 ⁺⁵ ₋₄	10.26	0.97	0.00	5.47	g
WR54	WN5o	MR 48	13 32 43.74	-65 01 27.9	0.128±0.035	6.52 ^{+1.37} _{-1.05}	263 ⁺⁵⁹ ₋₄₅	12.35	1.04	0.00	5.58	g
WR55	WN7o	HD 117688	13 33 30.10	-62 19 01.2	0.315±0.054	3.00 ^{+0.55} _{-0.41}	29 ⁺¹ ₋₁	10.23	0.94	0.00	5.35	g
WR56	WC7	Ls 8	13 33 45.37	-64 07 31.3	0.072±0.026	8.67 ^{+1.46} _{-1.20}	226 ⁺⁴¹ ₋₃₄	13.18	0.91	0.00	5.13	g
WR56a	WN6o	SMSNPL 10	13 41 14.01	-60 53 54.0	0.208±0.055	4.36 ^{+1.20} _{-0.82}	126 ⁺²⁹ ₋₁₉	14.13	2.37	0.22		g
WR57	WC8	HD 119078	13 43 16.35	-67 24 05.1	0.160±0.049	5.50 ^{+1.49} _{-1.06}	461 ⁺¹³¹ ₋₉₃	9.52	0.24	0.12	5.69	g
WR58	WN4b/CE	MR 51	13 49 04.47	-65 41 56.2	0.148±0.041	5.88 ^{+1.42} _{-1.04}	336 ⁺⁸⁶ ₋₆₃	12.53	0.83	0.00	4.89	g
WR59	WC9d	LSS 3164	13 49 32.55	-61 31 42.3	0.262±0.047	3.57 ^{+0.69} _{-0.51}	56 ⁺⁶ ₋₅	12.04	2.59	0.12	5.72	g
WR59-2	WC5-6	SMG09 885_11	13 54 13.43	-61 50 01.9	0.330±0.573	1.65 ^{+1.25} _{-0.68}	24 ⁺³ ₋₁	19.32	3.99	2.02		e a
WR60	WC8	HD 121194	13 55 48.44	-61 09 48.5	0.271±0.045	3.51 ^{+0.65} _{-0.48}	66 ⁺⁸ ₋₆	11.43	2.10	0.12	5.77	g
WR60-7	WC7-8	RC17 B51	14 02 33.42	-61 20 27.4	0.035±0.479	2.06 ^{+1.38} _{-0.80}	33 ⁺⁸ ₋₅	19.33	3.79	2.21		e a
WR60-5	WC7	WR60a	14 06 03.60	-60 27 29.6	0.373±0.125	2.44 ^{+1.13} _{-0.61}	67 ⁺²¹ ₋₁₁	14.62	3.44	0.49		g
WR60-2	WC8	SMG09 903_15c	14 12 36.53	-61 45 32.8	-2.232±1.175	2.09 ^{+1.16} _{-0.85}	6 ⁺⁷ ₋₃	20.26	3.80	6.58		n a
WR61	WN5o	MR 53	14 13 03.51	-65 26 52.8	0.168±0.039	5.49 ^{+1.25} _{-0.91}	353 ⁺⁸⁵ ₋₆₂	12.03	0.67	0.00	4.99	g
WR61-3	WC9	MDM11 13	14 20 30.74	-60 48 22.2	1.015±1.116	0.91 ^{+1.40} _{-0.46}	24 ⁺⁵ ₋₁	20.50	3.11	3.72		e a
WR61-1	WN6	2MASS J14212314-6018041	14 21 23.13	-60 18 04.1	-0.022±0.174	3.88 ^{+1.65} _{-1.12}	64 ⁺¹⁸ ₋₁₂	16.93	5.21	0.91		n e
WR62	WN6b	NS 2	14 31 06.13	-61 20 59.7	0.189±0.049	4.28 ^{+0.89} _{-0.66}	35 ⁺¹¹ ₋₈	12.40	2.62	0.09	5.82	g
WR62a	WN6o	SMSNPL 11	14 32 37.69	-61 29 54.2	0.262±0.050	3.50 ^{+0.70} _{-0.51}	37 ⁺¹¹ ₋₈	12.22	2.02	0.00		g
WR62-2	WN8-9h	VVV CL041-8	14 46 26.37	-59 23 29.2	0.380±0.177	2.20 ^{+0.98} _{-0.58}	31 ⁺⁴ ₋₂	13.07	4.46	0.88		g

WR Number	Spectral Type	Alias	RA J2015	Dec J2015	$\omega \pm \sigma_w$ (mas)	d (kpc)	$ z $ (pc)	G (mag)	$G_{BP} - G_{RP}$ (mag)	Excess noise	$\log L/L_\odot$	Flags
WR62b	WN5o	SMSNPL 12	14 46 40.84	-61 06 57.1	0.108±0.064	5.50 ^{+1.59} _{-1.17}	103 ⁺³⁵ ₋₂₆	15.24	2.58	0.26		g
WR62-1	WN7-8h	AX J144701-5919	14 46 53.56	-59 19 38.3	0.199±0.290	2.30 ^{+1.23} _{-0.75}	33 ⁺⁶ ₋₄	14.65	5.79	1.25		e a
WR64	WC7	BS 3	14 56 55.18	-55 50 58.6	0.062±0.040	7.98 ^{+1.67} _{-1.37}	413 ⁺⁸² ₋₆₇	14.31	1.40	0.00	5.07	g
WR64-3	WN6o	RC17 B87	15 02 46.14	-58 27 06.8	-0.049±0.256	2.90 ^{+1.11} _{-0.83}	28 ⁺² ₋₂	17.68	4.60	1.19		n e a
WR64-4	WN6o+OB	RC17 B88	15 04 11.16	-58 27 21.7	0.613±0.285	1.54 ^{+0.91} _{-0.47}	22 ⁺⁰ ₋₀	17.08	5.22	1.60		a
WR64-5	WN6o	RC17 B91	15 07 31.84	-58 15 09.9	0.361±0.421	1.83 ^{+1.09} _{-0.66}	21 ⁺⁰ ₋₀	19.23	3.69	1.38		e a
WR65	WC9d+OB?	Wra 1297	15 13 41.70	-59 11 45.0	0.292±0.066	3.13 ^{+0.80} _{-0.54}	44 ⁺¹⁶ ₋₁₁	12.18	2.92	0.20	5.82	g
WR66	WN8(h)	HD 134877	15 14 57.71	-59 50 30.2	-21.626±1.436	5.18 ^{+2.08} _{-1.81}	144 ⁺⁶⁶ ₋₅₇	10.91	1.46	2.11		n a
WR67	WN6o	MR 55	15 15 32.62	-59 02 30.7	0.426±0.085	2.23 ^{+0.54} _{-0.37}	25 ⁺¹¹ ₋₇	11.05	1.49	0.00	5.05	g
WR67-3	WN10	G321.0331-0.4274	15 15 39.42	-58 08 16.1	0.261±0.106	2.93 ^{+0.79} _{-0.58}	1 ⁺⁵ ₋₄	13.47	3.44	0.39		g
WR67-1	WN6h	WR67a	15 16 36.95	-58 09 58.8	0.135±0.120	3.36 ^{+0.92} _{-0.70}	9 ⁺⁸ ₋₆	13.45	3.01	0.55		g
WR67-2	WC7	WR67b	15 17 46.29	-57 56 59.3	0.208±0.338	2.17 ^{+1.00} _{-0.69}	5 ⁺⁷ ₋₅	15.41	4.42	1.45		e a
WR68	WC7	BS 4	15 18 20.75	-59 38 17.4	0.188±0.041	4.93 ^{+1.12} _{-0.81}	141 ⁺³⁶ ₋₂₆	12.53	2.00	0.00	5.71	g
WR68-1	WN4b	SMG09 979_11	15 20 35.91	-57 27 12.0	-3.509±2.036	1.88 ^{+1.10} _{-0.85}	14 ⁺³ ₋₂	20.74	2.44	5.36		n a
WR68a	WN6o	SMSNPL 13	15 23 16.60	-57 44 19.9	0.154±0.073	3.97 ^{+0.92} _{-0.70}	22 ⁺¹⁰ ₋₇	12.69	2.69	0.13		g
WR69	WC9d+OB	HD 136488	15 24 11.30	-62 40 37.6	0.285±0.043	3.48 ^{+0.64} _{-0.47}	271 ⁺⁵³ ₋₃₉	9.01	0.74	0.00	5.32	g
WR70	WC9vd+B0I	HD 137603	15 29 44.68	-58 34 51.3	0.326±0.042	3.01 ^{+0.44} _{-0.34}	74 ⁺¹⁴ ₋₁₀	9.20	1.69	0.00		g
WR70-1	WN7	MV09 J15352652-5604123	15 35 26.52	-56 04 12.4	0.128±0.605	1.93 ^{+1.04} _{-0.74}	14 ⁺³ ₋₂	19.93	3.47	2.01		e a
WR70-13	WC8d	RC17 B105	15 37 46.50	-56 08 45.5	-0.365±0.348	2.78 ^{+0.98} _{-0.79}	0 ⁺⁷ ₋₆	18.57	4.24	1.57		n a
WR70-3	WC7	SMG09 1011_24	15 43 04.66	-55 11 12.8	0.337±0.174	2.36 ^{+0.84} _{-0.58}	15 ⁺¹ ₋₁	15.34	4.22	0.83		g
WR70-5	WC9	WM10 11b	15 48 42.10	-55 07 54.3	0.469±0.168	1.95 ^{+0.75} _{-0.47}	1 ⁺⁷ ₋₄	16.44		0.83		g
WR70a	WN6o	SMSNPL 14	15 59 25.28	-54 12 42.8	0.123±0.090	3.99 ^{+1.21} _{-0.84}	38 ⁺¹⁸ ₋₁₂	14.42	2.94	0.35		g
WR70-2	WN5b	2MASS J15595671-5159299	15 59 56.71	-51 59 30.0	-0.131±0.236	3.66 ^{+1.84} _{-1.17}	70 ⁺²⁵ ₋₁₅	16.76	5.82	1.21		n e a

WR Number	Spectral Type	Alias	RA J2015	Dec J2015	$\omega \pm \sigma_w$ (mas)	d (kpc)	$ z $ (pc)	G (mag)	$G_{BP} - G_{RP}$ (mag)	Excess noise	$\log L/L_\odot$	Flags
WR70-11	WN7	1042-25L	16 00 25.26	-52 03 29.6	-0.360±0.233	4.17 ^{+1.77} _{-1.24}	70 ⁺²¹ ₋₁₄	17.82	5.12	1.10	n a	
WR70-16	WC7d+WN WN/Cd+O	or 2XMM J160050.7-514245	16 00 50.49	-51 42 45.3	1.813±0.410	0.55 ^{+0.20} _{-0.12}	29 ⁺³ ₋₁	15.44		1.24	a	
WR71	WN6o	HD 143414	16 03 49.33	-62 41 36.1	0.313±0.052	3.19 ^{+0.67} _{-0.48}	401 ⁺⁸⁸ ₋₆₃	9.89	0.25	0.13	5.07 g	
WR71-1	WN9	1040-B6C	16 04 03.78	-53 10 44.5	-0.094±0.307	2.63 ^{+0.98} _{-0.75}	3 ⁺⁸ ₋₆	18.85	3.44	1.06	n e a	
WR72-5	WN6o	RC17 B132	16 07 01.46	-51 58 18.6	-0.204±0.378	2.57 ^{+1.02} _{-0.79}	24 ⁺¹ ₋₁	18.69	4.43	1.56	n e a	
WR72-1	WC9	HDM6	16 11 39.26	-52 05 45.9	0.211±0.122	3.00 ^{+0.83} _{-0.62}	5 ⁺⁷ ₋₄	14.26	3.89	0.50	g	
WR72-2	WC8	SMG09 1053_27	16 11 43.70	-51 10 16.7	-1.296±0.544	2.79 ^{+1.11} _{-0.87}	28 ⁺³ ₋₂	16.20	6.01	2.92	n a	
WR73	WC9d	NS 3	16 12 37.47	-46 37 36.9	0.051±0.067	6.81 ^{+1.85} _{-1.47}	422 ⁺¹⁰⁹ ₋₈₆	13.58	2.29	0.23	e	
WR74	WN7o	BP 1	16 16 13.79	-51 36 41.8	0.166±0.065	3.98 ^{+0.86} _{-0.66}	23 ⁺⁹ ₋₇	12.60	2.22	0.00	5.41 g	
WR75	WN6b	HD 147419	16 24 26.22	-51 32 06.1	0.282±0.057	3.32 ^{+0.89} _{-0.55}	64 ⁺²⁰ ₋₁₄	10.43	1.23	0.00	5.55 g	
WR75-1	WC8	SMG09 1081_21	16 24 58.87	-48 56 52.5	-0.343±0.598	2.17 ^{+1.19} _{-0.84}	31 ⁺⁵ ₋₃	19.31	4.08	2.27	n e a	
WR75aa	WC9d	HBD 1	16 26 20.14	-45 59 45.8	0.165±0.075	4.88 ^{+1.63} _{-1.14}	205 ⁺⁶¹ ₋₄₂	15.25	2.43	0.21	g	
WR75a	WC9	SMSNPL 15	16 26 37.23	-50 19 23.0	0.215±0.109	3.14 ^{+1.07} _{-0.70}	27 ⁺¹⁶ ₋₁₀	13.62	3.15	0.49	g	
WR75b	WC9	SMSNPL 16	16 28 17.23	-48 17 40.8	0.578±0.121	1.69 ^{+0.45} _{-0.30}	30 ⁺² ₋₁	13.56	3.51	0.53	g	
WR75-21	WC7:	SFZ12 1095-189L	16 33 48.13	-47 52 52.8	0.795±0.041	1.26 ^{+0.07} _{-0.06}	19 ⁺⁰ ₋₀	13.24	2.15	0.13	g	
WR75ab	WN7h	PCG1	16 33 48.73	-49 28 44.1	0.180±0.090	3.79 ^{+1.47} _{-0.88}	54 ⁺²⁹ ₋₁₇	13.56	2.81	0.36	g	
WR75c	WC9	HBD 2	16 34 03.58	-43 40 24.9	0.040±0.061	7.15 ^{+1.78} _{-1.45}	365 ⁺⁸⁶ ₋₆₉	14.20	2.22	0.14	e	
WR75d	WC9	HBD 3	16 34 17.44	-46 08 53.1	0.217±0.111	3.57 ^{+1.61} _{-0.94}	86 ⁺²⁹ ₋₁₇	14.26	3.21	0.46	g	
WR75-23	WC9	SFZ12 1106-31L	16 37 23.98	-46 26 28.8	0.241±0.103	3.17 ^{+1.08} _{-0.70}	46 ⁺⁸ ₋₅	13.80	3.31	0.42	g	
WR76	WC9d	LSS 3693	16 40 05.25	-45 41 12.7	0.122±0.133	3.65 ^{+1.55} _{-0.96}	60 ⁺¹⁶ ₋₁₀	13.06	3.19	0.54	e	
WR77	WC8+OB	He3-1239	16 41 19.25	-48 01 59.2	0.334±0.052	2.85 ^{+0.50} _{-0.37}	33 ⁺⁹ ₋₇	12.36	2.02	0.00	g	
WR77-5	WN6	SFZ12 1115-197L	16 43 40.37	-45 57 57.7	0.395±0.183	2.18 ^{+0.80} _{-0.55}	19 ⁺⁰ ₋₀	14.69	3.77	0.58	g	
WR77-1	WN7b	2MASS J16441069- 4524246	16 44 10.68	-45 24 24.6	0.148±0.211	2.71 ^{+1.08} _{-0.75}	33 ⁺⁵ ₋₃	14.79	4.46	0.75	e	

WR Number	Spectral Type	Alias	RA J2015	Dec J2015	$\omega \pm \sigma_w$ (mas)	d (kpc)	$ z $ (pc)	G (mag)	$G_{BP} - G_{RP}$ (mag)	Excess noise	$\log L/L_\odot$	Flags
WR77aa	WC9d	HBD 4	16 46 46.28	-45 47 58.3	0.274±0.171	2.53 ^{+0.80} _{-0.60}	6 ⁺⁴ ₋₃	14.98	4.52	0.61		g
WR77-2	WN7	2MASS J16465342-4535590	16 46 53.42	-45 35 59.0	0.149±0.209	2.66 ^{+0.84} _{-0.66}	10 ⁺³ ₋₂	16.11	5.31	0.88		e
WR77a	WN6o		16 46 55.53	-45 51 34.5	0.103±0.212	2.72 ^{+0.86} _{-0.67}	2 ⁺⁵ ₋₄	16.82	4.61	0.89		e
WR77b	WC9d		16 46 59.91	-45 55 25.7	-0.250±0.258	3.00 ^{+0.91} _{-0.74}	2 ⁺⁷ ₋₅	15.23		1.11		n e a
WR77c	WN8o		16 47 00.88	-45 51 20.6	0.028±0.196	2.94 ^{+0.87} _{-0.69}	0 ⁺⁶ ₋₄	16.32	5.48	0.88		e
WR77d	WN7o	Wd1-57c	16 47 01.59	-45 51 45.3	0.121±0.216	2.67 ^{+0.86} _{-0.67}	1 ⁺⁶ ₋₄	16.23	4.89	1.00		e
WR77f	WN10-11h	Wd1-5	16 47 02.97	-45 50 19.8	0.268±0.217	2.38 ^{+0.84} _{-0.63}	4 ⁺⁵ ₋₄	14.46	4.64	0.74		g
WR77h	WN8o		16 47 03.80	-45 50 38.8	0.563±0.227	1.72 ^{+0.78} _{-0.46}	8 ⁺⁵ ₋₃	15.80		0.96		g
WR77i	WC9d	Wd1-66	16 47 03.96	-45 51 37.7	0.315±0.217	2.28 ^{+0.84} _{-0.61}	4 ⁺⁶ ₋₄	15.98	5.38	0.98		g
WR77j	WN7o		16 47 04.01	-45 51 25.1	-0.522±0.269	3.21 ^{+0.91} _{-0.75}	2 ⁺⁶ ₋₅	16.75	4.88	1.30		n a
WR77m	WC9d		16 47 04.41	-45 51 03.7	-0.002±0.277	2.62 ^{+0.89} _{-0.71}	2 ⁺⁶ ₋₄	16.80	5.17	1.33		n e a
WR77n	WC9d	Wd1-241	16 47 05.21	-45 52 25.0	0.122±0.204	2.72 ^{+0.86} _{-0.67}	0 ⁺⁶ ₋₄	14.83	4.64	0.86		e
WR77o	WN7o	Wd1-14c	16 47 05.37	-45 51 04.9	-0.065±0.189	3.15 ^{+0.88} _{-0.70}	1 ⁺⁶ ₋₃	16.48	5.75	0.60		n e
WR77p	WC9		16 47 06.06	-45 52 08.3	3.936±0.712	0.30 ^{+0.07} _{-0.00}	18 ⁺⁰ ₋₀	15.01	4.73	3.03		a
WR77q	WN5o		16 47 06.10	-45 50 22.5	0.188±0.324	2.25 ^{+0.90} _{-0.69}	5 ⁺⁶ ₋₄	16.94		0.84		e
WR77r	WN7o		16 47 06.25	-45 51 26.5	-0.583±0.308	3.06 ^{+0.91} _{-0.75}	1 ⁺⁶ ₋₃	17.53	4.25	1.17		n a
WR77s	WN6o	GDTB 1	16 47 06.54	-45 50 39.1	0.473±0.210	1.93 ^{+0.79} _{-0.51}	7 ⁺⁵ ₋₃	16.26	4.88	0.96		g
WR77sa	WN6h	GDTB 3	16 47 07.62	-45 49 22.1	0.023±0.294	2.54 ^{+0.89} _{-0.71}	3 ⁺⁶ ₋₄	18.15	4.91	1.15		e a
WR77sb	WN6o		16 47 07.66	-45 52 36.0	0.228±0.200	2.52 ^{+0.85} _{-0.63}	1 ⁺⁶ ₋₄	16.07	5.07	0.87		g
WR77sc	WN7b	Wd1-72	16 47 08.35	-45 50 45.5	0.095±0.224	2.68 ^{+0.87} _{-0.68}	1 ⁺⁶ ₋₄	15.84	5.44	0.84		e
WR77sd	WN5o	GDTB 2	16 47 14.14	-45 48 32.0	0.547±0.291	1.72 ^{+0.87} _{-0.53}	8 ⁺⁶ ₋₃	18.11	3.87	1.15		a
WR77-3	WN6	MDM11 30	16 47 46.03	-45 59 04.9	-0.019±0.256	2.70 ^{+0.97} _{-0.73}	6 ⁺⁹ ₋₇	16.84	6.02	1.13		n e a
WR77t	WC9d	HBD 5	16 50 57.63	-43 40 27.8	0.234±0.179	2.68 ^{+1.22} _{-0.75}	42 ⁺⁹ ₋₆	15.27	4.50	0.76		g
WR77-6	WN6b	SFZ12 1138-133L	16 51 19.33	-43 26 55.3	-1.068±0.963	1.96 ^{+1.57} _{-0.92}	39 ⁺¹⁵ ₋₈	19.99	3.06	3.11		n a

WR Number	Spectral Type	Alias	RA J2015	Dec J2015	$\omega \pm \sigma_w$ (mas)	d (kpc)	$ z $ (pc)	G (mag)	$G_{BP} - G_{RP}$ (mag)	Excess noise	$\log L/L_\odot$	Flags
WR78	WN7h	HD 151932	16 52 19.25	-41 51 16.3	0.797±0.084	1.25 ^{+0.15} _{-0.12}	52 ⁺³ ₋₃	6.28	0.60	0.00	5.79	g
WR79	WC7+O5-8	HD 152270	16 54 19.70	-41 49 11.6	0.729±0.057	1.37 ^{+0.12} _{-0.10}	48 ⁺² ₋₂	6.54	0.38	0.00		g
WR79a	WN9ha	HD 152408	16 54 58.50	-41 09 03.1	0.475±0.141	2.02 ^{+0.98} _{-1.40}	73 ⁺²⁵ ₋₁₃	5.67	0.36	0.33		g
WR79b	WN9ha	HD 152386	16 55 06.45	-44 59 21.4	-2.210±0.312	5.32 ^{+1.65} _{-1.40}	66 ⁺²⁷ ₋₂₂	7.92	0.85	0.67		n
WR80	WC9d	Wra 1581	16 59 02.19	-45 43 10.1	0.249±0.098	3.50 ^{+1.59} _{-0.90}	97 ⁺⁵³ ₋₃₀	13.27	2.70	0.30	5.16	g
WR81	WC9	He3-1316	17 02 40.38	-45 59 15.5	0.467±0.073	2.11 ^{+0.42} _{-0.30}	74 ⁺¹⁸ ₋₁₃	11.07	2.32	0.12	5.24	g
WR82	WN7(h)	Ls 11	17 04 04.63	-45 12 15.1	0.258±0.055	3.74 ^{+0.98} _{-0.66}	130 ⁺³⁹ ₋₂₆	11.59	1.53	0.00	5.25	g
WR82-2	WC9	1178-66B	17 07 23.95	-39 19 54.5	0.269±0.357	2.02 ^{+1.65} _{-0.79}	46 ⁺²¹ ₋₁₀	18.51	5.03	1.27		e a
WR83	WN5o	He 3-1344	17 10 54.63	-46 36 00.6	0.257±0.059	3.80 ^{+1.10} _{-0.72}	250 ⁺⁷⁸ ₋₅₁	12.07	1.27	0.00		g
WR83-1	WC6:	SFZ12 1179-129L	17 11 00.81	-39 49 31.4	-0.150±1.713	1.75 ^{+1.01} _{-0.88}	17 ⁺² ₋₁	20.46	2.63	4.12		n e a
WR84	WN7o	LS 12	17 11 21.70	-39 53 22.0	0.304±0.056	3.01 ^{+0.51} _{-0.40}	9 ⁺¹ ₋₁	12.13	2.05	0.00	5.28	g
WR84-4	WN7ha	SFZ12 1181-211L	17 11 46.13	-39 20 27.8	0.419±0.184	2.10 ^{+0.81} _{-0.53}	22 ⁺⁹ ₋₀	15.34	4.24	0.58		g
WR84-11	WN9h	1176-B49	17 12 34.87	-40 37 13.7	-0.860±0.335	3.27 ^{+1.43} _{-0.94}	26 ⁺²⁰ ₋₁₃	18.36	4.86	1.16		n a
WR84-9	WN6	VVV CL099-5	17 14 25.40	-38 09 50.5	2.946±1.402	0.35 ^{+1.19} _{-0.05}	22 ⁺⁶ ₋₀	20.38		4.87		a
WR84-10	WC8	VVV CL099-7	17 14 25.65	-38 09 53.8	0.179±0.369	2.13 ^{+1.17} _{-0.75}	32 ⁺⁶ ₋₄	18.47	4.25	1.55		e a
WR85	WN6h	HD 155603B	17 14 27.12	-39 45 47.1	0.495±0.067	1.99 ^{+0.30} _{-0.24}	0 ⁺³ ₋₂	10.03	1.13	0.00	5.38	g
WR88	WC9	The 1	17 18 49.73	-33 57 41.4	0.284±0.058	3.44 ^{+0.88} _{-0.60}	142 ⁺³¹ ₋₂₁	11.75	2.15	0.00	5.47	g
WR87	WN7h+abs	LSS 4064	17 18 52.87	-38 50 03.6	0.305±0.072	2.91 ^{+0.66} _{-0.47}	18 ⁺⁸ ₋₆	10.88	2.40	0.13	6.10	g
WR89	WN8h+abs	LSS 4065	17 19 00.52	-38 48 51.3	0.297±0.079	2.90 ^{+0.72} _{-0.51}	18 ⁺⁹ ₋₆	10.11	2.19	0.00	6.21	g
WR90	WC7	HD 156385	17 19 29.90	-45 38 23.9	0.871±0.073	1.15 ^{+0.11} _{-0.09}	74 ⁺⁸ ₋₇	6.75	0.27	0.06	5.55	g
WR91	WN7b	StSa 1	17 20 22.02	-38 56 48.4	0.155±0.087	4.04 ^{+1.52} _{-0.92}	55 ⁺²⁸ ₋₁₇	13.24	3.03	0.31	5.70	g
WR93	WC7+O7-9	HD 157504	17 25 08.85	-34 11 12.6	0.565±0.053	1.76 ^{+0.19} _{-0.15}	46 ⁺² ₋₂	9.84	2.14	0.00		g
WR92	WC9	HD 157451	17 25 23.28	-43 29 31.5	0.257±0.067	3.78 ^{+1.25} _{-0.79}	270 ⁺⁹⁶ ₋₆₀	10.12	0.62	0.00	4.93	g
WR93a	WN6h	Th3-28	17 30 56.80	-26 59 11.0	0.117±0.177	4.41 ^{+2.15} _{-1.49}	311 ⁺¹⁴¹ ₋₉₈	17.58	2.35	0.24		e
WR93b	WO3	DBU 1	17 32 03.31	-35 04 32.7	0.403±0.099	2.29 ^{+0.61} _{-0.42}	12 ⁺⁸ ₋₆	14.58	2.06	0.24		g

WR Number	Spectral Type	Alias	RA J2015	Dec J2015	$\omega \pm \sigma_w$ (mas)	d (kpc)	$ z $ (pc)	G (mag)	$G_{BP} - G_{RP}$ (mag)	Excess noise	$\log L/L_\odot$	Flags
WR94	WN5o	HD 158860	17 33 07.07	-33 38 23.4	1.052±0.066	0.95 ^{+0.06} _{-0.06}	16 ⁺⁰ ₋₀	9.87	2.31	0.00	5.52	g
WR95	WC9d	He3-1434	17 36 19.89	-33 26 12.3	0.468±0.085	2.07 ^{+0.43} _{-0.31}	4 ⁺⁵ ₋₃	11.98	2.66	0.06	5.19	g
WR96	WC9d	LSS 4265	17 36 24.45	-32 54 31.5	0.342±0.083	2.64 ^{+0.58} _{-0.43}	1 ⁺⁴ ₋₃	12.47	2.48	0.00		g
WR97	WN5b+O7	HDE 320102	17 36 53.62	-34 02 36.8	0.454±0.060	2.15 ^{+0.32} _{-0.25}	21 ⁺⁶ ₋₄	10.39	1.44	0.00		g
WR98	WN8o/C7	HDE 318016	17 37 13.74	-33 27 56.0	0.500±0.070	1.96 ^{+0.31} _{-0.24}	9 ⁺⁴ ₋₃	10.90	2.19	0.00		g
WR98a	WC8-9vd+?	IRAS 17380-3031	17 41 13.04	-30 32 30.4	0.849±0.349	1.26 ^{+0.87} _{-0.41}	20 ⁺⁰ ₋₀	15.46	5.64	1.46		a
WR100	WN7b	HDE 318139	17 42 09.76	-32 33 24.9	0.249±0.064	3.55 ^{+0.06} _{-0.67}	57 ⁺²³ ₋₁₄	11.75	2.21	0.00	5.67	g
WR101	WC8	DA 3	17 45 09.01	-31 50 15.9	0.365±0.153	2.28 ^{+1.26} _{-0.63}	35 ⁺³¹ ₋₁₅	13.19	3.20	0.60		g
WR102	WO2	Sand 4	17 45 47.54	-26 10 26.8	0.376±0.041	2.64 ^{+0.33} _{-0.27}	85 ⁺⁸ ₋₆	13.76	1.47	0.00	5.57	g
WR102-19	WN5	SFZ12 1322-220L	17 55 20.21	-24 07 38.4	0.369±0.131	2.39 ^{+0.96} _{-0.57}	45 ⁺¹⁰ ₋₅	16.13	3.81	0.37		g
WR102-20	WC9	SFZ12 1327-25L	17 59 02.85	-24 20 50.7	0.511±1.356	1.92 ^{+0.92} _{-0.89}	12 ⁺³ ₋₃	20.40		2.98		e a
WR102-25	WN6	KW03-083	17 59 35.60	-30 51 32.5	0.028±0.088	6.42 ^{+1.95} _{-1.55}	380 ⁺¹²¹ ₋₉₆	15.29	1.66	0.16		e
WR102-21	WN6	SFZ12 1342-208L	17 59 48.22	-22 14 52.3	0.358±0.245	2.11 ^{+1.33} _{-0.69}	44 ⁺¹⁵ ₋₇	16.45	4.50	0.75		g
WR102l	WN8o	SMSNPL 17	18 00 34.33	-22 47 39.9	0.192±0.092	3.43 ^{+0.88} _{-0.65}	34 ⁺³ ₋₂	12.62	3.20	0.17		g
WR103	WC9d+?	HD 164270	18 01 43.15	-32 42 55.2	0.283±0.077	3.46 ^{+1.28} _{-0.77}	274 ⁺¹⁰⁸ ₋₆₅	8.57	0.62	0.00	5.46	g
WR104	WC9d+B0.5V (+VB)	Ve2-45	18 02 04.12	-23 37 42.2	0.272±0.124	2.74 ^{+0.72} _{-0.55}	2 ⁺⁶ ₋₄	11.73	2.85	0.34		g
WR105	WN9h	NS 4	18 02 23.46	-23 34 37.5	0.577±0.088	1.73 ^{+0.32} _{-0.23}	4 ⁺² ₋₂	10.60	2.97	0.16	5.89	g
WR105-2	WN8-9	1343-284	18 03 28.36	-22 22 59.0	0.367±0.152	2.38 ^{+0.71} _{-0.53}	14 ⁺¹ ₋₁	14.50	3.58	0.51		g
WR106	WC9d	HDE 313643	18 04 43.66	-21 09 30.6	0.299±0.058	3.07 ^{+0.56} _{-0.43}	31 ⁺¹ ₋₁	11.10	1.95	0.00	5.16	g
WR107	WN8o	DA 1	18 04 46.10	-21 51 27.2	-0.284±0.297	2.87 ^{+0.81} _{-0.69}	12 ⁺² ₋₁	12.37	2.40	0.66		n e
WR107a	WC5-7	SMSNPL 18	18 05 11.49	-22 13 24.7	0.235±0.111	2.95 ^{+0.70} _{-0.55}	0 ⁺⁵ ₋₄	14.46	2.71	0.25		g
WR108	WN9ha	HDE 313846	18 05 25.73	-23 00 20.4	0.342±0.052	2.79 ^{+0.45} _{-0.35}	20 ⁺⁶ ₋₅	9.44	1.37	0.00	5.74	g
WR108-1	WN9	WR1361-1583	18 07 05.16	-20 15 16.7	0.135±0.415	2.22 ^{+0.98} _{-0.75}	26 ⁺² ₋₂	19.44	2.92	0.00		e
WR109	WN5h	NS 3	18 07 50.90	-35 10 25.2	0.072±0.061	6.84 ^{+1.85} _{-1.45}	835 ⁺²³² ₋₁₈₁	14.44	0.32	0.04		g
WR110	WN5-6b	HD 165688	18 07 56.96	-19 23 56.9	0.633±0.053	1.58 ^{+0.15} _{-0.12}	31 ⁺⁰ ₋₀	9.21	1.42	0.00	5.51	g

WR Number	Spectral Type	Alias	RA J2015	Dec J2015	$\omega \pm \sigma_w$ (mas)	d (kpc)	$ z $ (pc)	G (mag)	$G_{BP} - G_{RP}$ (mag)	Excess noise	$\log L/L_\odot$	Flags
WR111	WC5	HD 165763	18 08 28.47	-21 15 11.2	0.612±0.097	1.63 $^{+0.32}_{-0.23}$	3 $^{+3}_{-2}$	7.49	-0.04	0.16	5.37	g
WR111-1	WN6o	HDM7	18 09 45.06	-20 17 10.4	1.733±0.562	0.63 $^{+0.80}_{-0.22}$	16 $^{+5}_{-1}$	18.70	3.56	1.83		a
WR111-9	WC9	1381-19L	18 12 02.42	-18 06 55.3	0.050±0.168	3.17 $^{+0.91}_{-0.48}$	30 $^{+2}_{-2}$	13.63	3.60	0.63		e
WR111-2	WN7b	HDM8	18 13 14.20	-17 53 43.5	0.497±0.179	1.98 $^{+0.73}_{-0.48}$	21 $^{+0}_{-0}$	14.49	4.37	0.69		g
WR111-4	WN7	MDM11 34	18 13 22.49	-17 53 50.3	0.340±0.199	2.37 $^{+0.79}_{-0.60}$	20 $^{+0}_{-0}$	15.18	4.38	0.80		g
WR111-13	WN6b	MCF15 1	18 13 34.82	-18 05 41.5	0.209±0.341	2.36 $^{+0.82}_{-0.69}$	14 $^{+2}_{-1}$	15.39	4.60	1.23		e a
WR111-3	WC8	SMG09 1385-24	18 13 42.47	-17 28 12.3	-0.003±0.392	2.42 $^{+0.94}_{-0.75}$	26 $^{+2}_{-1}$	16.89	5.83	1.76		n e a
WR111-10	WC7	1389-4AB6	18 14 14.11	-17 21 02.8	0.964±0.462	1.23 $^{+1.03}_{-0.46}$	22 $^{+1}_{-0}$	19.49	1.95	0.82		g
WR111-12	WC9	THA 34-30	18 14 32.98	-18 25 14.8	0.406±0.160	2.23 $^{+0.71}_{-0.51}$	1 $^{+6}_{-4}$	13.26	3.20	0.47		g
WR112	WC9d+OB?	GL 2104	18 16 33.49	-18 58 42.4	-1.384±0.483	3.16 $^{+2.06}_{-1.07}$	44 $^{+42}_{-22}$	14.59	4.47	1.34		n a
WR113	WC8d+O8-9IV	HD 168206	18 19 07.36	-11 37 59.2	0.553±0.063	1.80 $^{+0.24}_{-0.19}$	75 $^{+7}_{-5}$	8.78	1.22	0.00		g
WR113-1	WN7o	HDM9	18 19 22.19	-16 03 12.5	0.452±0.192	2.13 $^{+0.73}_{-0.53}$	6 $^{+4}_{-3}$	12.99	3.20	0.66		g
WR113-2	WC5-6	SMG09 1425-47	18 23 03.43	-13 10 00.5	0.517±0.269	1.86 $^{+0.90}_{-0.56}$	26 $^{+2}_{-1}$	14.54	3.20	0.61		g
WR114	WC5+OB?	IC14-17	18 23 16.34	-13 43 26.1	0.479±0.046	2.09 $^{+0.22}_{-0.18}$	16 $^{+0}_{-0}$	11.43	1.73	0.00	5.39	g
WR114-2	WC8	SFZ12 1434-43L	18 23 32.32	-12 03 58.7	-1.121±1.222	1.81 $^{+1.50}_{-0.90}$	39 $^{+15}_{-9}$	20.04	2.92	3.17		n e a
WR114-1	WN6	HDM10	18 25 00.23	-10 33 23.7	0.295±0.242	2.38 $^{+1.65}_{-0.82}$	61 $^{+28}_{-14}$	16.56	4.02	0.61		g
WR115	WN6o	MR 87	18 25 30.01	-14 38 41.0	2.107±0.763	0.48 $^{+0.54}_{-0.17}$	12 $^{+9}_{-3}$	10.90	2.13	2.67		a
WR115-1	WN6o	HDM11	18 25 53.09	-13 28 32.3	0.151±0.119	3.19 $^{+0.77}_{-0.61}$	11 $^{+7}_{-6}$	13.94	3.10	0.41		g
WR115-2	WN8	SFZ12 1431-34L	18 25 53.62	-12 50 03.2	0.472±0.369	2.14 $^{+0.81}_{-0.69}$	10 $^{+3}_{-3}$	17.22	4.68	1.67		a
WR115-3	WN7	MDM11 36	18 26 06.12	-13 04 10.6	0.335±0.089	2.68 $^{+0.58}_{-0.45}$	0 $^{+4}_{-3}$	13.27	2.94	0.36		g
WR116	WN8h	AS 306	18 27 04.29	-12 22 52.7	0.402±0.061	2.44 $^{+0.39}_{-0.30}$	7 $^{+2}_{-1}$	11.50	2.60	0.00	5.41	g
WR116-1	WC9+OBI	2MASS J18281180-1025424	18 28 11.80	-10 25 42.4	0.243±0.196	2.58 $^{+1.00}_{-0.70}$	36 $^{+6}_{-4}$	12.74	3.82	0.35		g
WR116-2	WN5	SMG09 1462-54	18 29 33.84	-08 39 02.2	-0.465±0.764	2.09 $^{+1.82}_{-0.97}$	52 $^{+27}_{-14}$	19.69	3.38	2.16		n e a
WR116-3	WN6ha	MDM11 37	18 30 53.20	-10 19 37.2	0.217±0.138	2.89 $^{+0.68}_{-0.56}$	11 $^{+2}_{-1}$	14.09	3.18	0.42		g

WR Number	Spectral Type	Alias	RA J2015	Dec J2015	$\omega \pm \sigma_w$ (mas)	d (kpc)	$ z $ (pc)	G (mag)	$G_{BP} - G_{RP}$ (mag)	Excess noise	$\log L/L_\odot$	Flags
WR117	WC9d	IC14-22	18 31 02.51	-06 35 49.7	0.236±0.099	$3.66^{+1.45}_{-0.91}$	116^{+37}_{-23}	12.46	2.22	0.00	5.30	g
WR117-1	WN7	XGPS-I J183116-100921	18 31 16.53	-10 09 25.1	0.025±0.128	$3.41^{+0.68}_{-0.59}$	9^{+2}_{-2}	13.12	3.51	0.53		e
WR118	WC9d	GL 2179	18 31 42.21	-09 59 16.8	0.155±0.328	$2.49^{+0.78}_{-0.68}$	11^{+2}_{-2}	15.18	5.93	1.53		e a
WR118-4	WC8	SFZ12 1463-7L	18 33 47.63	-09 23 07.9	0.143±0.460	$2.34^{+0.82}_{-0.73}$	4^{+5}_{-4}	18.63	4.63	2.30		e a
WR118-2	WN9	MDI09 Quartet 2	18 36 16.68	-07 04 59.4	0.109±0.372	$2.41^{+0.91}_{-0.74}$	25^{+1}_{-1}	17.86		1.97		e a
WR118-3	WN9	MDI09 Quartet 1	18 36 17.28	-07 05 07.1	1.725±0.784	$0.70^{+1.33}_{-0.28}$	22^{+2}_{-0}	18.09	5.89	4.61		a
WR118-10	WN6	1485-6C4	18 36 55.53	-06 31 02.1	1.904±0.571	$0.55^{+0.50}_{-0.17}$	23^{+2}_{-0}	17.41	4.55	2.77		a
WR118-5	WC9d	MDM11 40	18 37 51.49	-06 08 41.8	-1.535±0.568	$2.87^{+0.98}_{-0.82}$	31^{+3}_{-2}	19.22	4.67	1.81		n a
WR118-6	WN7:	SFZ12 1483-212L	18 38 27.21	-07 10 45.2	-2.154±1.676	$2.29^{+0.87}_{-0.83}$	4^{+6}_{-3}	20.33	2.92	3.72		n a
WR119	WC9d	The 2	18 39 17.90	-10 05 31.0	0.284±0.086	$3.22^{+1.24}_{-0.73}$	87^{+41}_{-24}	11.57	1.54	0.00	4.63	g
WR119-2	WC8	SFZ12 1493-9L	18 39 34.58	-05 44 23.1	0.393±0.363	$2.19^{+0.86}_{-0.70}$	21^{+9}_{-0}	17.55	4.91	1.52		a
WR119-1	WN7o	HDM12	18 40 08.65	-03 29 31.2	-0.040±0.166	$4.27^{+1.63}_{-1.20}$	88^{+26}_{-19}	15.85	3.87	0.58		n e
WR120	WN7o	MR 89	18 41 00.87	-04 26 14.5	0.666±0.193	$1.50^{+0.64}_{-0.36}$	28^{+3}_{-1}	11.22	1.79	0.25	4.87	g
WR120-16	WC8	1514-AA0	18 41 06.81	-02 56 01.3	0.127±0.429	$2.21^{+1.80}_{-0.91}$	57^{+30}_{-15}	18.72	3.74	1.18		e a
WR120-1	WC9	HDM13	18 41 10.70	-04 51 27.1	0.001±0.221	$2.94^{+0.82}_{-0.69}$	23^{+9}_{-0}	15.26	4.00	0.71		e
WR120-11	WC8	SFZ12 1495-32L	18 41 23.35	-05 40 58.2	-1.716±0.726	$2.66^{+0.80}_{-0.73}$	3^{+5}_{-4}	18.48		2.40		n a
WR120-7	WN7	SFZ12 1503-160L	18 41 34.07	-05 04 01.3	-0.408±0.326	$2.93^{+0.77}_{-0.68}$	14^{+1}_{-1}	15.07	4.62	0.93		n
WR120-3	WN9h	2MASS J18420630-0348224	18 42 06.31	-03 48 22.5	1.046±0.759	$1.08^{+1.29}_{-0.49}$	27^{+7}_{-2}	18.68	4.27	2.44		a
WR120-4	WN9h	2MASS J18420827-0351029	18 42 08.27	-03 51 03.0	-0.283±0.567	$2.33^{+1.09}_{-0.85}$	33^{+5}_{-4}	18.27	3.90	1.67		n e a
WR120-5	WC8	SCB12 2w02	18 42 08.47	-03 49 35.3	-0.054±0.742	$1.98^{+1.14}_{-0.83}$	31^{+6}_{-4}	18.24	4.72	2.05		n e a
WR120-6	WN6	PN G029.0+00.4	18 42 46.92	-03 13 17.3	0.248±0.101	$3.14^{+0.94}_{-0.66}$	45^{+7}_{-5}	16.78	2.68	0.00		g
WR120-15	WC8	SCB12 2w04	18 43 17.23	-03 08 56.7	-0.115±0.265	$3.01^{+1.11}_{-0.84}$	40^{+7}_{-5}	18.20	4.36	1.04		n e a

WR Number	Spectral Type	Alias	RA J2015	Dec J2015	$\omega \pm \sigma_w$ (mas)	d (kpc)	$ z $ (pc)	G (mag)	$G_{BP} - G_{RP}$ (mag)	Excess noise	$\log L/L_\odot$	Flags
WR120-10	WN7	SFZ12 1517-138L	18 43 58.03	-02 45 17.3	0.322±0.135	2.59 ^{+0.90} _{-0.60}	39 ⁺⁶ ₋₄	14.12	3.70	0.49		g
WR121	WC9d	AS 320	18 44 13.15	-03 47 57.8	0.448±0.055	2.23 ^{+0.30} _{-0.24}	15 ⁺⁰ ₋₀	11.08	2.08	0.00	5.16	g
WR121-15	WN4-5	2MASS J18442065-0236510	18 44 20.66	-02 36 51.2	-0.108±0.269	2.98 ^{+1.12} _{-0.85}	40 ⁺⁷ ₋₅	18.03	4.47	1.15		n e a
WR121-12	WN5	1530-8FA	18 46 00.97	-01 14 35.0	-0.027±0.412	2.40 ^{+1.45} _{-0.90}	47 ⁺¹⁶ ₋₁₀	18.33	4.92	1.26		n e a
WR121-1	WN7h	WM10 52	18 49 27.34	-01 04 20.7	0.097±0.143	3.19 ^{+0.73} _{-0.62}	18 ⁺⁰ ₋₀	15.21	3.63	0.54		e
WR121-6	WN5	SFZ12 1536-180L	18 51 10.76	-01 30 03.5	0.288±0.098	2.86 ^{+0.69} _{-0.52}	10 ⁺⁷ ₋₅	13.98	2.95	0.37		g
WR122	WN	NaSt1	18 52 17.55	+00 59 44.3	0.303±0.063	3.03 ^{+0.60} _{-0.45}	34 ⁺² ₋₂	13.18	2.38	0.28		g
WR122-2	WN9	MDM11 51	18 52 43.69	+00 08 41.6	0.227±1.115	2.21 ^{+0.89} _{-0.85}	12 ⁺³ ₋₃	19.63	3.82	2.97		e a
WR122-3	WN6	MDM11 52	18 54 03.12	+01 24 50.8	-0.300±0.593	2.41 ^{+0.93} _{-0.80}	23 ⁺¹ ₋₀	19.48	3.78	1.62		n e a
WR122-1	WC8	IPHAS J190015.86+000517.3	19 00 15.86	+00 05 17.3	0.170±0.077	4.63 ^{+1.55} _{-1.08}	134 ⁺⁵² ₋₃₆	14.90	2.14	0.24		g
WR122-15	WN6	1602-9AF	19 02 42.35	+06 54 44.8	0.262±0.342	2.10 ^{+1.45} _{-0.76}	44 ⁺¹⁶ ₋₈	18.45	4.39	1.42		e a
WR123	WN8o	HD 177230	19 03 59.02	-04 19 02.0	0.164±0.054	5.35 ^{+1.56} _{-1.09}	422 ⁺¹²⁹ ₋₉₀	10.86	0.93	0.00	5.22	g
WR123-1	WN6o	HDM14	19 08 17.97	+08 29 10.5	0.157±0.231	2.67 ^{+0.97} _{-0.73}	27 ⁺² ₋₁	15.59	4.68	0.90		e
WR123-3	WN8	MDM11 55	19 08 38.09	+09 28 20.9	-0.330±0.320	3.18 ^{+1.41} _{-1.01}	50 ⁺¹² ₋₉	18.28	4.18	1.51		n a
WR123-8	WN9h	1629-14D6	19 10 06.40	+09 45 25.4	-0.057±0.888	1.75 ^{+1.29} _{-0.81}	31 ⁺⁷ ₋₄	19.95	4.02	3.37		n e a
WR124	WN8h	209 BAC	19 11 30.87	+16 51 38.1	0.144±0.045	5.87 ^{+1.48} _{-1.09}	359 ⁺⁸⁵ ₋₆₂	10.61	1.56	0.00	5.69	g
WR124-1B	WC8	MDI09 GLIMPSE206	19 12 24.01	+09 57 29.3	1.298±1.160	1.56 ^{+1.05} _{-0.90}	18 ⁺¹ ₋₁	20.01		4.56		a
WR124-1A	WC8	MDI09 GLIMPSE206	19 12 24.13	+09 57 28.8	-0.083±0.516	2.34 ^{+0.97} _{-0.79}	17 ⁺¹ ₋₀	19.17	4.68	1.92		n e a
WR124-3	WC8	SFZ12 1657-51L	19 16 18.38	+12 46 49.3	-0.415±0.255	3.66 ^{+1.30} _{-1.00}	45 ⁺⁸ ₋₆	17.72		1.02		n a
WR124-9	WC6:	SFZ12 1670-57L	19 17 32.80	+14 08 28.0	-0.144±0.392	2.66 ^{+1.73} _{-1.00}	56 ⁺²³ ₋₁₃	18.84	3.91	1.56		n e a
WR124-18	WN9h	1669-3DF	19 18 31.35	+13 43 39.1	-0.608±0.516	2.60 ^{+1.32} _{-0.92}	37 ⁺⁸ ₋₅	19.41	3.65	2.04		n a

WR Number	Spectral Type	Alias	RA J2015	Dec J2015	$\omega \pm \sigma_w$ (mas)	d (kpc)	$ z $ (pc)	G (mag)	$G_{BP} - G_{RP}$ (mag)	Excess noise	$\log L/L_\odot$	Flags
WR124-19	WC6:	1660-1169	19 20 02.47	+12 08 20.2	-1.118±0.733	2.32 $^{+1.18}_{-0.36}$	8 $^{+14}_{-10}$	20.05	2.46	2.34		n a
WR124-2	WC8	SMG09 1671_5	19 20 40.39	+13 50 35.1	-2.755±0.791	2.77 $^{+1.03}_{-0.85}$	18 $^{+9}_{-0}$	20.01	3.08	2.90		n a
WR124-6	WC6	SFZ12 1675-17L	19 22 53.61	+14 08 49.8	-0.694±0.469	2.73 $^{+1.00}_{-0.81}$	2 $^{+6}_{-5}$	18.83	4.64	1.76		n a
WR124-7	WC7	SFZ12 175-10L	19 22 54.45	+14 11 27.9	-1.729±0.585	2.88 $^{+1.00}_{-0.83}$	2 $^{+6}_{-5}$	18.48	4.59	1.48		n a
WR124-11	WN6b	SFZ12 1698-70L	19 24 46.91	+17 14 25.0	0.197±0.272	2.45 $^{+1.53}_{-0.84}$	50 $^{+18}_{-10}$	18.45	4.44	1.17		e a
WR124-20	WC9	1697-38F	19 25 18.14	+17 02 15.5	1.477±0.417	0.68 $^{+0.38}_{-0.18}$	26 $^{+3}_{-1}$	19.23	3.76	1.31		a
WR124-21	WC8	1702-23L	19 26 08.35	+17 46 22.9	-0.353±0.136	5.85 $^{+1.58}_{-1.32}$	87 $^{+17}_{-14}$	15.98	3.75	0.61		n
WR124-22	WC9	1695-2B7	19 27 17.98	+16 05 24.5	0.335±0.476	1.91 $^{+1.07}_{-0.72}$	7 $^{+7}_{-4}$	19.29	4.48	1.83		e a
WR125	WC7ed+O9III	IC14-36	19 28 15.61	+19 33 21.4	0.273±0.070	3.36 $^{+0.99}_{-0.65}$	82 $^{+18}_{-11}$	11.94	2.24	0.00		g
WR125-4	WN7	MDM11 61	19 30 05.31	+17 46 01.0	-1.173±0.484	2.96 $^{+1.05}_{-0.86}$	11 $^{+3}_{-2}$	19.17	3.63	1.72		n a
WR125-3	WN7ha	Mercer 23 #2	19 30 13.56	+18 32 02.4	-0.190±0.304	2.93 $^{+1.18}_{-0.88}$	29 $^{+3}_{-2}$	12.81	3.41	0.92		n e
WR125-2	WN8-9	IPHAS J193038.84+183909.8	19 30 38.84	+18 39 09.7	0.222±0.099	3.28 $^{+0.93}_{-0.67}$	28 $^{+2}_{-1}$	12.44	3.68	0.28		g
WR125-1	WC8	HDM15	19 33 44.01	+19 22 47.4	0.121±0.051	4.80 $^{+0.85}_{-0.70}$	7 $^{+7}_{-1}$	13.33	2.69	0.25		g
WR126	WC5/WN	ST 2	19 39 56.19	+26 34 42.4	0.091±0.033	7.57 $^{+1.49}_{-1.39}$	299 $^{+55}_{-43}$	12.42	1.21	0.00	5.90	g
WR127	WN3b+O9.5V	HD 186943	19 46 15.94	+28 16 19.0	0.321±0.032	3.09 $^{+0.35}_{-0.29}$	114 $^{+10}_{-8}$	10.00	0.57	0.00		g
WR129	WN4o	MR 96	19 48 18.26	+30 26 52.6	0.165±0.039	5.47 $^{+1.22}_{-0.90}$	254 $^{+52}_{-38}$	12.71	1.14	0.00		g
WR128	WN4(h)	HD 187282	19 48 32.20	+18 12 03.6	0.342±0.052	2.90 $^{+0.54}_{-0.39}$	170 $^{+35}_{-26}$	10.35	0.21	0.09	5.22	g
WR130	WN8(h)	LS 16	19 59 12.59	+31 27 08.9	-0.474±0.145	6.67 $^{+1.89}_{-1.57}$	131 $^{+31}_{-26}$	11.23	2.17	0.52		n
WR131	WN7h+abs	MR 97	20 00 19.12	+33 15 51.0	0.113±0.033	6.92 $^{+1.40}_{-1.09}$	227 $^{+41}_{-32}$	11.52	1.53	0.00	6.02	g
WR132	WC6+?	HD 190002	20 01 39.73	+32 34 17.9	0.232±0.035	4.15 $^{+0.68}_{-0.52}$	100 $^{+13}_{-10}$	12.12	1.43	0.00	5.32	g
WR133	WN5o+O9I	HD 190918	20 05 57.32	+35 47 18.0	0.541±0.042	1.85 $^{+0.16}_{-0.14}$	87 $^{+5}_{-4}$	6.73	0.26	0.05		g
WR134	WN6b	HD 191765	20 10 14.19	+36 10 34.9	0.571±0.039	1.75 $^{+0.13}_{-0.11}$	67 $^{+3}_{-3}$	7.74	0.57	0.00	5.62	g
WR135	WC8	HD 192103	20 11 53.52	+36 11 50.4	0.504±0.041	1.98 $^{+0.18}_{-0.15}$	64 $^{+3}_{-3}$	7.88	0.40	0.00	5.39	g
WR136	WN6b(h)	HD 192163	20 12 06.53	+38 21 17.7	0.515±0.043	1.93 $^{+0.18}_{-0.15}$	102 $^{+7}_{-6}$	7.18	0.59	0.00	5.79	g
WR137	WC7pd+O9	HD 192641	20 14 31.76	+36 39 39.5	0.473±0.038	2.10 $^{+0.18}_{-0.16}$	60 $^{+3}_{-2}$	7.75	0.54	0.00		g

WR Number	Spectral Type	Alias	RA J2015	Dec J2015	$\omega \pm \sigma_w$ (mas)	d (kpc)	$ z $ (pc)	G (mag)	$G_{BP} - G_{RP}$ (mag)	Excess noise	$\log L/L_\odot$	Flags
WR138	WN6o	HD 193077	20 17 00.02	+37 25 23.7	0.397±0.055	2.47 $^{+0.40}_{-0.31}$	68 $^{+7}_{-5}$	7.92	0.62	0.00		g
WR138-1	WN8-9h	HBHA 4202-22	20 17 08.11	+41 07 26.9	-0.015±0.072	12.51 $^{+2.49}_{-2.71}$	709 $^{+136}_{-149}$	13.82	2.89	0.40		n e
WR139	WN5o+O6III-V	HD 193576	20 19 32.42	+38 43 53.9	0.765±0.037	1.31 $^{+0.07}_{-0.06}$	53 $^{+1}_{-1}$	7.75	0.82	0.00		g
WR140	WC7pd+O4-5	HD 193793	20 20 27.97	+43 51 16.3	0.611±0.037	1.64 $^{+0.11}_{-0.09}$	140 $^{+7}_{-6}$	6.62	0.72	0.00		g
WR141	WN5o+O5V-III	HD 193928	20 21 31.73	+36 55 12.7	0.516±0.036	1.92 $^{+0.14}_{-0.12}$	23 $^{+0}_{-0}$	9.33	1.46	0.00		g
WR142	WO2	Sand 5	20 21 44.34	+37 22 30.4	0.605±0.036	1.65 $^{+0.11}_{-0.09}$	29 $^{+0}_{-0}$	12.23	1.96	0.00		g
WR142a	WC8	PCG02 1	20 24 06.19	+41 25 33.8	0.536±0.124	1.81 $^{+0.61}_{-0.37}$	91 $^{+24}_{-14}$	13.77	3.90	0.64		g
WR142-1	WN6o	HBHalpha 4203-27	20 28 14.55	+43 39 25.4	0.561±0.062	1.77 $^{+0.23}_{-0.18}$	110 $^{+11}_{-9}$	12.80	3.25	0.24		g
WR143	WC4+OB?	HD 195177	20 28 22.66	+38 37 18.9	0.417±0.039	2.22 $^{+0.18}_{-0.16}$	19 $^{+0}_{-0}$	10.80	1.73	0.00		g
WR144	WC4	HM19-1	20 32 03.02	+41 15 20.4	0.565±0.069	1.75 $^{+0.24}_{-0.19}$	49 $^{+3}_{-3}$	12.87	2.65	0.28	5.19	g
WR145	WN7o/CE+?	AS 422	20 32 06.27	+40 48 29.5	0.684±0.051	1.46 $^{+0.12}_{-0.10}$	37 $^{+1}_{-1}$	10.63	2.64	0.11	5.61	g
WR146	WC6+O8	MR 112	20 35 47.08	+41 22 44.6	0.863±0.456	1.10 $^{+0.67}_{-0.36}$	29 $^{+5}_{-2}$	11.05	3.32	2.04		a
WR147	WN8(h)+B0.5V	AS 431	20 36 43.63	+40 21 07.4	-1.244±0.390	1.79 $^{+0.28}_{-0.26}$	10 $^{+1}_{-1}$	10.82	4.21	1.81		n a
WR148	WN8h+	HD 197406	20 41 21.54	+52 35 15.1	0.028±0.035	9.47 $^{+1.77}_{-1.49}$	1087 $^{+199}_{-168}$	10.15	0.92	0.00		e
WR149	WN5o	St 4	21 07 11.69	+48 25 36.2	0.194±0.031	4.89 $^{+0.83}_{-0.63}$	76 $^{+9}_{-7}$	13.35	2.01	0.07	5.41	g
WR150	WC5	ST 5	21 50 05.57	+50 42 24.7	0.053±0.033	8.73 $^{+1.70}_{-1.38}$	357 $^{+73}_{-59}$	12.26	0.98	0.00	5.75	g
WR151	WN4o+O5V	CX Cep	22 09 33.44	+57 44 30.5	0.158±0.046	5.38 $^{+1.31}_{-0.96}$	151 $^{+31}_{-23}$	11.71	1.34	0.00		g
WR152	WN3(h)	HD 211564	22 16 24.03	+55 37 36.7	0.205±0.054	4.36 $^{+1.12}_{-0.79}$	46 $^{+17}_{-12}$	11.40	0.51	0.00	5.64	g
WR153	WN6o/CE+O6I	HD 211853	22 18 45.60	+56 07 33.9	0.236±0.037	4.06 $^{+0.68}_{-0.52}$	25 $^{+7}_{-5}$	8.81	0.70	0.00	5.88	g
WR154	WC6	HD 213049	22 27 17.81	+56 15 11.7	0.162±0.041	5.38 $^{+1.20}_{-0.89}$	90 $^{+24}_{-18}$	10.67	0.90	0.00		g
WR155	WN6o+O9II-Ib	CQ Cep	22 36 53.95	+56 54 20.9	0.330±0.043	2.99 $^{+0.45}_{-0.35}$	46 $^{+10}_{-9}$	8.71	0.74	0.00		g
WR156	WN8h	MR 119	23 00 10.12	+60 55 38.4	0.238±0.031	4.10 $^{+0.60}_{-0.47}$	86 $^{+9}_{-7}$	10.30	1.70	0.00	6.00	g
WR157	WN5o(+B1II)	HD 219460	23 15 12.39	+60 27 01.8	0.387±0.043	2.57 $^{+0.32}_{-0.26}$	10 $^{+1}_{-1}$	10.26	0.93	0.00		g
WR158	WN7h	MR 112	23 43 30.59	+61 55 48.1	0.184±0.032	5.00 $^{+0.83}_{-0.65}$	29 $^{+1}_{-1}$	10.71	1.53	0.00	6.02	g
WR159	WN4	BCC 1	23 47 20.38	+63 13 14.2	0.542±0.122	1.82 $^{+0.60}_{-0.37}$	60 $^{+13}_{-7}$	10.53	1.55	0.37		g

Columns are: (1) WR Number, (2) Spectral type, (3) Alternative name, (4) *Gaia* Right Ascension, (5) *Gaia* Declination, (6) Zero point corrected parallax ω and inflated error σ_ω , (7) Distance from the Sun, (8) Distance from the midplane, (9) *Gaia* G band apparent magnitude, (10) *Gaia* colour index, (11) Astrometric excess noise, (12) Stellar luminosity, (13) Error flags, a = astrometric excess noise > 1 mas; e = large parallax uncertainty $|\sigma_\omega/\omega|>1$; n = negative parallax $\omega<0$, g = good astrometry.

Table 6: Absolute K_s -band magnitudes for Galactic WR stars.

WR Num- ber	Spectral type	K_s (mag)	μ (mag)	$J-K_s$ (mag)	$H-K_s$ (mag)	A_{K_s} (mag)	$M_{K_s}^{\text{Sys}}$ (mag)	$F_{\text{WR}}^{K_s}/F_{\text{Sys}}^{K_s}$	$M_{K_s}^{\text{WR}}$ (mag)	Flags
WR1	WN4b	7.48	12.49	0.73	0.38	0.30 ± 0.08			$-5.4_{-0.3}^{+0.3}$	b:
WR3	WN3ha	10.01	12.31	0.23	0.12	0.11 ± 0.08			$-2.5_{-0.4}^{+0.3}$	b:
WR4	WC5+?	7.88	12.87	0.87	0.69	0.18 ± 0.11			$-5.2_{-0.5}^{+0.4}$	b
WR5	WC6	7.65	12.36	0.98	0.69	0.30 ± 0.11			$-5.1_{-0.3}^{+0.3}$	g
WR6	WN4b	5.89	11.78	0.46	0.34	0.05 ± 0.08			$-6.0_{-0.4}^{+0.3}$	b
WR7	WN4b	9.27	13.13	0.70	0.40	0.24 ± 0.08			$-4.2_{-0.5}^{+0.4}$	g
WR8	WN7o/CE	7.93	12.87	0.64	0.39	0.31 ± 0.08			$-5.3_{-0.3}^{+0.3}$	b:
WR9	WC5+O7	7.54	13.3	0.91	0.57	0.45 ± 0.08	$-6.3_{-0.4}^{+0.3}$	0.60 ± 0.24	$-5.7_{-0.7}^{+0.9}$	b
WR10	WN5h	9.61	13.69	0.44	0.28	0.24 ± 0.17			$-4.4_{-0.5}^{+0.5}$	g
WR11	WC8+O7.5III-V	2.10	7.67	0.05	0.15	-0.00 ± 0.11	$-5.6_{-0.4}^{+0.4}$	0.45 ± 0.02	$-4.8_{-0.4}^{+0.4}$	b:
WR12	WN8h	7.87	13.78	0.75	0.39	0.25 ± 0.08			$-6.3_{-0.4}^{+0.4}$	g
WR13	WC6	8.86	13.41	1.27	0.77	0.45 ± 0.11			$-5.1_{-0.4}^{+0.4}$	g
WR14	WC7+?	6.61	11.73	0.88	0.64	0.15 ± 0.11			$-5.3_{-0.2}^{+0.2}$	g
WR15	WC6	6.60	12.36	1.25	0.74	0.41 ± 0.11			$-6.2_{-0.3}^{+0.3}$	b
WR16	WN8h	6.38	12.1	0.59	0.33	0.20 ± 0.08			$-6.0_{-0.2}^{+0.2}$	g
WR17	WC5	9.17	14.15	0.76	0.57	0.15 ± 0.11			$-5.2_{-0.3}^{+0.5}$	b
WR17-1	WN5b	9.53	12.45	2.20	0.85	0.85 ± 0.20			$-4.1_{-0.8}^{+0.8}$	g
WR18	WN4b	7.68	12.91	0.89	0.53	0.32 ± 0.08			$-5.6_{-0.5}^{+0.4}$	b:
WR19	WC5	8.53	13.18	1.22	0.60	0.56 ± 0.11			$-5.3_{-0.4}^{+0.3}$	b
WR19a	WN7:(h)	7.50	13.39	1.57	0.63	0.82 ± 0.08			$-6.9_{-0.6}^{+0.6}$	b
WR20	WN5o	9.93	14.22	1.07	0.50	0.51 ± 0.08			$-4.9_{-0.3}^{+0.3}$	b:
WR20-2	O2If*/WN6	8.38	13.72	0.90	0.35	0.53 ± 0.13			$-6.0_{-0.4}^{+0.4}$	b
WR20-1	WN7-8	8.34	12.17	2.26	0.86	1.03 ± 0.23			$-5.2_{-0.8}^{+0.8}$	b:
WR20a	O3If*/WN6+ O3If*/WN6	7.59	13.51	1.27	0.49	0.76 ± 0.08	$-6.8_{-0.4}^{+0.4}$	0.50 ± 0.00	$-6.0_{-0.4}^{+0.4}$	g

WR	Num- ber	Spectral type	K_s (mag)	μ (mag)	$J-K_s$ (mag)	$H-K_s$ (mag)	A_{K_s} (mag)	$M_{K_s}^{\text{Sys}}$ (mag)	$F_{\text{WR}}^{K_s}/F_{\text{Sys}}^{K_s}$	$M_{K_s}^{\text{WR}}$ (mag)	Flags
WR20b		WN6ha	7.18	12.44	1.47	0.62	0.89 ± 0.08		$-6.2_{-0.4}^{+0.3}$		g
WR20-3		O2If*/WN6	9.04	11.99	1.47	0.53	0.80 ± 0.18		$-3.9_{-0.8}^{+0.6}$		b
WR21a		O2If/WN5	7.83	13.21	0.98	0.37	0.57 ± 0.14		$-6.0_{-0.4}^{+0.3}$		g
WR21		WN5o+O4-6	8.03	13.0	0.38	0.19	0.25 ± 0.08	$-5.3_{-0.3}^{+0.3}$	0.92 ± 0.22	$-5.2_{-0.4}^{+0.6}$	b
WR22		WN7h+O9III-V	5.39	11.84	0.32	0.19	0.18 ± 0.08		$-6.7_{-0.2}^{+0.2}$		b:
WR23		WC6	7.05	12.03	0.84	0.55	0.07 ± 0.11		$-5.1_{-0.3}^{+0.3}$		g
WR24		WN6ha	5.82	12.75	0.28	0.19	0.13 ± 0.08		$-7.1_{-0.4}^{+0.3}$		b
WR25		O2.5If*/WN6+O	5.72	11.47	0.54	0.25	0.34 ± 0.11		$-6.1_{-0.2}^{+0.2}$		b:
WR26		WN7b/CE	9.68	14.13	1.16	0.59	0.51 ± 0.08		$-5.0_{-0.3}^{+0.3}$		g
WR27		WC6+a	8.29	12.09	1.59	0.88	0.66 ± 0.11		$-4.5_{-0.3}^{+0.3}$		g
WR28		WN6(h)+OB?	8.73	13.79	0.98	0.43	0.48 ± 0.08		$-5.6_{-0.4}^{+0.4}$		b
WR29		WN7h+O	9.12	13.76	0.79	0.34	0.40 ± 0.14	$-5.1_{-0.4}^{+0.4}$	0.32 ± 0.89	$-3.9_{-1.6}^{+1.6}$	b
WR30		WC6+O6-8	9.21	13.54	0.84	0.55	0.23 ± 0.08	$-4.6_{-0.4}^{+0.4}$	0.72 ± 0.29	$-4.3_{-0.7}^{+0.9}$	b:
WR30a		WO4+O5-5.5	9.56	14.14	0.69	0.27	0.48 ± 0.07	$-5.2_{-0.4}^{+0.4}$	0.22 ± 0.02	$-3.5_{-0.5}^{+0.5}$	g
WR31		WN4o+O8V	8.69	13.93	0.48	0.27	0.26 ± 0.08		$-5.6_{-0.5}^{+0.5}$		b
WR31a		WN11h	6.10	14.33	1.22	0.62	0.60 ± 0.14		$-8.9_{-0.4}^{+0.4}$		g
WR31b		WN11h	4.53	13.43	0.89	0.55	0.47 ± 0.11		$-9.5_{-0.4}^{+0.4}$		g
WR31c		WC6	9.49	13.91	1.55	0.85	0.51 ± 0.11		$-5.0_{-0.5}^{+0.5}$		g
WR31-1		O3.5If/WN7		13.31							u
WR32		WC5+OB?	10.23	13.8	1.49	0.81	0.68 ± 0.08	$-4.3_{-0.4}^{+0.4}$	0.72 ± 0.31	$-4.0_{-0.7}^{+1.0}$	g
WR33		WC6	9.69	14.4	0.93	0.66	0.16 ± 0.11		$-5.0_{-0.4}^{+0.4}$		g
WR34		WN5o	10.04	14.35	1.16	0.55	0.46 ± 0.08		$-4.8_{-0.4}^{+0.4}$		b:
WR35		WN6h+OB?	9.62	14.18	1.08	0.47	0.39 ± 0.24	$-5.0_{-0.4}^{+0.4}$	0.56 ± 1.27	$-4.4_{-1.0}^{+1.0}$	g
WR35a		WN6h+O8.5V	9.65	13.83	0.82	0.32	0.51 ± 0.08	$-4.8_{-0.4}^{+0.4}$	0.12 ± 0.01	$-2.4_{-0.5}^{+0.5}$	b
WR35b		WN4b	9.76	13.65	1.19	0.59	0.64 ± 0.08		$-4.6_{-0.3}^{+0.3}$		g

WR	Num- ber	Spectral type	K_s (mag)	μ (mag)	$J-K_s$ (mag)	$H-K_s$ (mag)	A_{K_s} (mag)	$M_{K_s}^{\text{Sys}}$ (mag)	$F_{\text{WR}}^{K_s}/F_{\text{Sys}}^{K_s}$	$M_{K_s}^{\text{WR}}$ (mag)	Flags
WR36		WN5-6b+OB?	9.40	13.67	1.00	0.51	0.40 ± 0.09	$-4.8_{-0.4}^{+0.4}$	0.83 ± 0.48	$-4.6_{-0.6}^{+1.4}$	g
WR37		WN4b	9.67	14.13	1.36	0.67	0.62 ± 0.08			$-5.2_{-0.4}^{+0.4}$	g
WR38		WC4	10.79	13.91	1.20	0.71	0.50 ± 0.11			$-3.7_{-0.4}^{+0.4}$	b
WR38a		WN5o	10.71	13.67	0.82	0.50	0.49 ± 0.08			$-3.5_{-0.4}^{+0.4}$	g
WR40		WN8h	6.11	12.92	0.51	0.30	0.15 ± 0.08			$-7.0_{-0.4}^{+0.3}$	b:
WR38b		WC7	8.61	13.18	1.78	0.67	0.75 ± 0.11			$-5.4_{-0.5}^{+0.4}$	b:
WR39		WC7+OB?	8.21	12.92	1.30	0.53	0.68 ± 0.08	$-5.7_{-0.7}^{+0.7}$	0.53 ± 0.27	$-5.0_{-1.5}^{+1.5}$	g
WR41		WC5+OB?	10.12	13.89	1.41	0.86	0.46 ± 0.10	$-4.3_{-0.3}^{+0.3}$	0.87 ± 0.35	$-4.2_{-0.5}^{+0.9}$	g
WR42		WC7+O7V	7.08	11.93	0.51	0.44	0.14 ± 0.08	$-5.1_{-0.3}^{+0.3}$	0.66 ± 0.33	$-4.6_{-0.8}^{+1.1}$	g
WR42a		WN5b	10.81	13.75	1.27	0.50	0.72 ± 0.08			$-3.8_{-0.5}^{+0.5}$	b:
WR42b		WN4b	9.90	14.01	1.45	0.62	1.15 ± 0.08			$-5.4_{-0.5}^{+0.5}$	b
WR42c		WN5o	9.90	14.14	1.25	0.57	0.72 ± 0.08			$-5.0_{-0.4}^{+0.4}$	b
WR42d		WN5b	8.91	12.53	1.29	0.61	0.67 ± 0.08			$-4.5_{-0.7}^{+0.7}$	g
WR42-1		O3If*/WN6	9.04	13.19	1.14	0.43	0.65 ± 0.15			$-4.9_{-0.4}^{+0.4}$	b
WR43-2		O2If*/WN5	9.24	13.95	1.23	0.44	0.68 ± 0.16			$-5.5_{-0.4}^{+0.4}$	b
WR43-3		O2.5If*/WN6	9.12	14.08	0.73	0.27	0.44 ± 0.12			$-5.5_{-0.4}^{+0.4}$	b
WR43-1		WN4b	10.47	10.63	2.69	1.10	1.13 ± 0.25			$-2.1_{-1.3}^{+1.3}$	b
WR44		WN4o+OB?	10.47	13.92	0.69	0.42	0.30 ± 0.07	$-3.8_{-0.4}^{+0.4}$	0.15 ± 0.09	$-1.8_{-0.9}^{+1.3}$	b
WR44a		WN5b	10.82	13.52	1.25	0.52	0.76 ± 0.08			$-3.6_{-0.4}^{+0.4}$	b:
WR45		WC6	9.20	13.14	1.40	0.79	0.58 ± 0.11			$-4.6_{-0.2}^{+0.2}$	g
WR45-1		WN9-10h	9.81	13.44	1.69	0.73	0.80 ± 0.18			$-4.6_{-0.6}^{+0.6}$	b:
WR45-2		WN5	10.78	13.21	1.37	0.58	0.58 ± 0.15			$-3.2_{-0.5}^{+0.5}$	b:
WR45a		WN5o	10.73	12.89	1.17	0.51	0.65 ± 0.08			$-3.0_{-0.6}^{+0.6}$	b:
WR45b		WN4b	9.92	13.87	1.53	0.69	0.70 ± 0.08			$-4.7_{-0.4}^{+0.4}$	g
WR45-3		WN5b	10.94	13.58	1.63	0.63	0.56 ± 0.15			$-3.4_{-0.6}^{+0.6}$	b

WR	Num- ber	Spectral type	K_s (mag)	μ (mag)	$J-K_s$ (mag)	$H-K_s$ (mag)	A_{K_s} (mag)	$M_{K_s}^{\text{Sys}}$ (mag)	$F_{\text{WR}}^{K_s}/F_{\text{Sys}}^{K_s}$	$M_{K_s}^{\text{WR}}$ (mag)	Flags
WR45-4		WN6	10.14	13.76	1.51	0.62	0.64 ± 0.16		$-4.4_{-0.3}^{+0.5}$	g	
WR45c		WN5o	10.32	13.94	1.03	0.47	0.52 ± 0.08		$-4.2_{-0.3}^{+0.3}$	g	
WR46		WN3b pec	9.83	12.07	0.37	0.25	0.07 ± 0.08		$-2.3_{-0.3}^{+0.3}$	b:	
WR46-1		WN6o	10.22	13.37	1.33	0.60	0.58 ± 0.14		$-3.8_{-0.5}^{+0.5}$	g	
WR46-18		WC6-7	10.47	11.29	2.87	1.20	0.97 ± 0.27		$-2.3_{-1.1}^{+1.0}$	b	
WR46-7		WC5-7	9.74	12.43	3.01	1.34	1.11 ± 0.28		$-4.0_{-0.7}^{+0.7}$	g	
WR46-8		WN6	9.85	12.06	2.17	0.85	0.97 ± 0.22		$-3.5_{-0.7}^{+0.7}$	g	
WR46-16		WN9	11.54	11.96	1.90	0.51	0.71 ± 0.19		$-1.5_{-0.8}^{+0.8}$	b	
WR46-9		WN5	9.88	12.42	2.19	0.84	0.96 ± 0.22		$-3.7_{-0.7}^{+0.7}$	g	
WR46-17		WN9/OIf+		12.3						u	
WR46a		WN4o	10.92	14.14	1.16	0.50	0.60 ± 0.08		$-3.9_{-0.4}^{+0.4}$	b:	
WR46-2		WN7h	9.03	12.91	1.53	0.61	0.69 ± 0.16		$-4.7_{-0.5}^{+0.5}$	g	
WR46-3		O6-7.5IIf+		13.05						u	
WR46-4		Ofpe/WN9		12.24						u	
WR46-5		WN6	9.67	12.86	1.85	0.58	0.69 ± 0.19		$-4.1_{-0.6}^{+0.6}$	b	
WR46-6		WN7	9.64	12.97	2.02	0.66	0.84 ± 0.21		$-4.3_{-0.6}^{+0.6}$	b:	
WR46-15		WN8	9.84	11.5	3.29	1.19	1.51 ± 0.33		$-3.5_{-1.2}^{+1.0}$	b	
WR46-12		WN4b	11.84	12.39	1.72	0.71	0.64 ± 0.16		$-1.4_{-0.7}^{+0.7}$	b	
WR46-13		WC7	11.09	12.77	2.07	0.96	0.61 ± 0.21		$-2.5_{-0.6}^{+0.6}$	b	
WR46-14		WN5b	10.96	9.06	1.97	0.80	0.75 ± 0.18		$0.5_{-1.3}^{+1.1}$	b	
WR47		WN6o+O5V	7.55	12.72	0.77	0.37	0.46 ± 0.22	$-5.7_{-0.4}^{+0.4}$	0.53 ± 1.20	$-5.0_{-1.1}^{+1.1}$	b
WR47a		WN8h	9.06	13.45	1.38	0.62	0.83 ± 0.08		$-5.4_{-0.5}^{+0.5}$	g	
WR47-1		WN6o	10.55	12.69	1.63	0.67	0.70 ± 0.17		$-3.0_{-0.6}^{+0.6}$	b:	
WR47b		WN9h	8.84	13.75	1.45	0.60	0.92 ± 0.08		$-6.0_{-0.5}^{+0.5}$	g	
WR47-5		WN6(h)	11.09	12.36	2.23	0.83	0.96 ± 0.22		$-2.6_{-0.9}^{+0.9}$	b	

WR	Num- ber	Spectral type	K_s (mag)	μ (mag)	$J-K_s$ (mag)	$H-K_s$ (mag)	A_{K_s} (mag)	$M_{K_s}^{\text{Sys}}$ (mag)	$F_{\text{WR}}^{K_s}/F_{\text{Sys}}^{K_s}$	$M_{K_s}^{\text{WR}}$ (mag)	Flags
WR47c		WC5	9.89	14.16	1.35	0.59	0.71 ± 0.11			$-5.1_{-0.4}^{+0.4}$	b:
WR47-2		WC5-6	10.22	12.69	2.26	0.90	0.62 ± 0.22			$-3.3_{-0.7}^{+0.7}$	b
WR47-3		WC5-6	11.05	10.74	2.08	0.87	0.55 ± 0.21			$-0.7_{-1.1}^{+0.9}$	b
WR48		WC6(+O9.5/B0Iab)	5.43	11.9	0.14	0.14	0.08 ± 0.08	$-6.8_{-0.8}^{+0.7}$	0.99 ± 0.44	$-6.8_{-0.8}^{+1.3}$	b
WR48-1		WC7	9.31	12.34	1.74	0.78	0.40 ± 0.19			$-3.6_{-0.6}^{+0.6}$	b
WR48b		WC9d	8.58	13.55	2.41	1.20	0.61 ± 0.08			$-5.7_{-0.5}^{+0.5}$	b:
WR48-6		WN9	7.58	12.4	2.63	0.99	1.22 ± 0.27			$-6.3_{-0.7}^{+0.7}$	g
WR48-10		WN9h	7.48	12.01	1.94	0.67	0.83 ± 0.20			$-5.6_{-0.7}^{+0.7}$	g
WR48-7		WN8	7.65	12.09	2.16	0.83	0.99 ± 0.22			$-5.7_{-0.7}^{+0.7}$	g
WR48-4		WC6	10.71	11.97	2.45	1.11	0.81 ± 0.24			$-2.4_{-0.8}^{+0.8}$	b
WR48-8		WN9	8.15	12.54	1.66	0.68	0.77 ± 0.18			$-5.3_{-0.6}^{+0.6}$	g
WR48-9		WN9h	6.61	12.22	1.65	0.66	0.75 ± 0.17			$-6.5_{-0.5}^{+0.5}$	b:
WR48a		WC8ed+?	5.08	11.78	3.66	1.72	0.89 ± 0.08	$-7.8_{-0.7}^{+0.6}$	0.30 ± 0.17	$-6.5_{-1.2}^{+1.6}$	b
WR48-5		WN6b	10.26	11.57	2.80	1.08	1.15 ± 0.26			$-2.8_{-1.0}^{+0.9}$	b
WR48c		WN3h/C4	11.16	12.13	0.70	0.36	0.27 ± 0.08			$-1.3_{-0.2}^{+0.2}$	b
WR48-2		WC7-8	8.98	12.56	1.84	0.85	0.48 ± 0.20			$-4.2_{-0.6}^{+0.6}$	b
WR49		WN5(h)	11.21	14.61	0.68	0.36	0.27 ± 0.08			$-3.7_{-0.3}^{+0.3}$	g
WR50		WC7+OB	8.81	12.7	0.94	0.57	0.34 ± 0.10	$-4.3_{-0.3}^{+0.3}$	0.84 ± 0.42	$-4.1_{-0.5}^{+1.1}$	b:
WR51		WN4o	13.46	12.82	0.67	0.17	0.60 ± 0.08			$-0.0_{-0.3}^{+0.3}$	b
WR52		WC4	7.55	11.21	0.86	0.66	0.22 ± 0.11			$-3.9_{-0.2}^{+0.2}$	b:
WR52-2		WN6	10.68	12.1	1.85	0.72	0.79 ± 0.19			$-2.5_{-0.8}^{+0.7}$	b
WR53		WC8d	6.83	13.08	1.91	1.09	0.35 ± 0.08			$-6.7_{-0.3}^{+0.3}$	b
WR54		WN5o	10.09	14.07	0.76	0.39	0.33 ± 0.08			$-4.4_{-0.4}^{+0.4}$	g
WR55		WN7o	8.01	12.38	0.76	0.48	0.24 ± 0.08			$-4.7_{-0.4}^{+0.3}$	g
WR56		WC7	10.77	14.69	1.07	0.71	0.28 ± 0.11			$-4.3_{-0.3}^{+0.3}$	b:

WR	Num- ber	Spectral type	K_s (mag)	μ (mag)	$J-K_s$ (mag)	$H-K_s$ (mag)	A_{K_s} (mag)	$M_{K_s}^{\text{Sys}}$ (mag)	$F_{\text{WR}}^{K_s}/F_{\text{Sys}}^{K_s}$	$M_{K_s}^{\text{WR}}$ (mag)	Flags
WR56a		WN6o	9.73	13.2	1.17	0.55	0.71 ± 0.08		$-4.3_{-0.5}^{+0.5}$		g
WR57		WC8	8.01	13.7	1.08	0.74	0.21 ± 0.08		$-6.0_{-0.5}^{+0.5}$		b:
WR58		WN4b/CE	10.54	13.85	0.76	0.44	0.35 ± 0.08		$-3.8_{-0.4}^{+0.4}$		b:
WR59		WC9d	6.61	12.77	2.18	1.10	0.69 ± 0.08		$-6.9_{-0.4}^{+0.3}$		g
WR59-2		WC5-6	10.86	11.08	2.74	1.21	0.94 ± 0.26		$-1.7_{-1.2}^{+1.0}$		b
WR60		WC8	7.70	12.73	1.21	0.67	0.62 ± 0.08		$-5.7_{-0.4}^{+0.3}$		g
WR60-7		WC7-8	10.28	11.57	3.00	1.29	1.07 ± 0.28		$-2.8_{-1.0}^{+1.0}$		b
WR60-5		WC7	9.39	11.94	1.45	0.73	0.30 ± 0.17		$-3.1_{-0.8}^{+0.6}$		b
WR60-2		WC8	9.71	11.6	3.87	1.62	1.69 ± 0.36		$-3.8_{-1.1}^{+1.0}$		b
WR61		WN5o	10.35	13.7	0.61	0.32	0.28 ± 0.08		$-3.7_{-0.4}^{+0.4}$		g
WR61-3		WC9	10.38	9.8	3.24	1.25	1.41 ± 0.31		$-2.1_{-1.5}^{+1.4}$		b
WR61-1		WN6	9.62	12.95	2.06	0.81	0.90 ± 0.21		$-4.5_{-0.7}^{+0.7}$		b
WR62		WN6b	7.75	13.15	1.36	0.60	0.78 ± 0.08		$-6.3_{-0.4}^{+0.4}$		b
WR62a		WN6o	9.06	12.72	0.73	0.30	0.67 ± 0.08		$-4.4_{-0.4}^{+0.3}$		g
WR62-2		WN8-9h	6.87	11.71	1.54	0.55	0.65 ± 0.16		$-5.7_{-0.8}^{+0.7}$		b
WR62b		WN5o	10.97	13.7	1.04	0.47	0.90 ± 0.08		$-3.8_{-0.5}^{+0.5}$		g
WR62-1		WN7-8h	6.82	11.81	2.11	0.78	0.95 ± 0.22		$-6.3_{-0.9}^{+0.9}$		b
WR64		WC7	11.33	14.51	1.17	0.70	0.16 ± 0.11		$-3.4_{-0.4}^{+0.4}$		b
WR64-3		WN6o	10.18	12.31	2.21	0.86	0.98 ± 0.22		$-3.3_{-0.7}^{+0.7}$		b:
WR64-4		WN6o+OB	9.10	10.93	2.25	0.91	1.14 ± 0.24	$-3.3_{-1.0}^{+0.8}$	0.63 ± 0.42	$-2.8_{-1.5}^{+2.0}$	b
WR64-5		WN6o	10.80	11.31	2.31	0.86	1.00 ± 0.24		$-1.9_{-1.0}^{+0.9}$		b
WR65		WC9d+OB?	6.17	12.48	2.29	1.11	0.76 ± 0.08	$-7.1_{-0.5}^{+0.4}$	0.34 ± 0.22	$-6.0_{-1.0}^{+1.5}$	g
WR66		WN8(h)	8.15	13.57	0.78	0.33	0.39 ± 0.08		$-5.9_{-0.8}^{+0.7}$		g
WR67		WN6o	8.45	11.75	0.83	0.41	0.51 ± 0.08		$-3.9_{-0.5}^{+0.4}$		g
WR67-3		WN10	7.74	12.34	1.63	0.72	0.77 ± 0.17		$-5.5_{-0.5}^{+0.5}$		b

WR	Num- ber	Spectral type	K_s (mag)	μ (mag)	$J-K_s$ (mag)	$H-K_s$ (mag)	A_{K_s} (mag)	$M_{K_s}^{\text{Sys}}$ (mag)	$F_{\text{WR}}^{K_s}/F_{\text{Sys}}^{K_s}$	$M_{K_s}^{\text{WR}}$ (mag)	Flags
WR67-1		WN6h	8.82	12.63	1.04	0.36	0.34 ± 0.12			$-4.3_{-0.5}^{+0.5}$	b
WR67-2		WC7	8.46	11.68	1.88	0.80	0.46 ± 0.20			$-3.9_{-0.8}^{+0.8}$	b
WR68		WC7	8.75	13.46	1.15	0.63	0.52 ± 0.11			$-5.3_{-0.4}^{+0.4}$	g
WR68-1		WN4b	11.06	11.37	2.82	1.09	1.16 ± 0.26			$-1.7_{-1.1}^{+1.0}$	b
WR68a		WN6o	8.62	12.99	0.97	0.40	0.77 ± 0.08			$-5.2_{-0.4}^{+0.4}$	b
WR69		WC9d+OB	6.40	12.71	1.56	0.88	0.20 ± 0.08	$-6.5_{-0.4}^{+0.3}$	0.47 ± 0.30	$-5.7_{-0.9}^{+1.4}$	b:
WR70		WC9vd+B0I	5.74	12.39	1.33	0.82	0.56 ± 0.08	$-7.3_{-0.3}^{+0.3}$	0.11 ± 0.07	$-4.9_{-0.8}^{+1.4}$	b
WR70-1		WN7	11.46	11.42	2.38	0.93	1.11 ± 0.24			$-1.3_{-1.0}^{+0.9}$	b
WR70-13		WC8d		12.22							u
WR70-3		WC7	9.06	11.87	1.90	0.88	0.52 ± 0.20			$-3.5_{-0.6}^{+0.6}$	b
WR70-5		WC9	8.49	11.45	2.70	1.22	1.26 ± 0.26			$-4.4_{-0.7}^{+0.7}$	g
WR70a		WN6o	9.76	13.01	1.18	0.48	0.67 ± 0.08			$-4.1_{-0.5}^{+0.5}$	g
WR70-2		WN5b	8.66	12.82	2.22	0.86	0.86 ± 0.20			$-5.3_{-0.9}^{+0.8}$	b:
WR70-11		WN7	9.88	13.1	2.14	0.77	0.94 ± 0.22			$-4.4_{-0.8}^{+0.8}$	b:
WR70-16		WC7d+WN WN/Cd+O	or	8.7							u
WR71		WN6o	9.09	12.52	0.39	0.22	0.10 ± 0.08			$-3.6_{-0.4}^{+0.3}$	g
WR71-1		WN9	11.17	12.1	1.96	0.73	0.87 ± 0.20			$-2.0_{-0.7}^{+0.7}$	b
WR72-5		WN6o	10.27	12.05	2.29	0.87	1.00 ± 0.23			$-3.0_{-0.8}^{+0.7}$	b:
WR72-1		WC9	8.46	12.38	1.70	0.79	0.72 ± 0.17			$-4.8_{-0.5}^{+0.5}$	g
WR72-2		WC8	8.10	12.23	2.16	0.87	0.76 ± 0.19			$-5.0_{-0.8}^{+0.7}$	g
WR73		WC9d	7.47	14.17	2.85	1.32	0.68 ± 0.08			$-7.5_{-0.5}^{+0.5}$	b:
WR74		WN7o	8.80	13.0	0.93	0.42	0.76 ± 0.08			$-5.1_{-0.4}^{+0.4}$	g
WR75		WN6b	7.84	12.6	0.76	0.40	0.39 ± 0.08			$-5.2_{-0.5}^{+0.4}$	g
WR75-1		WC8	10.73	11.68	2.55	1.03	0.96 ± 0.23			$-2.2_{-1.0}^{+0.9}$	b
WR75aa		WC9d		13.44							u

WR	Num- ber	Spectral type	K_s (mag)	μ (mag)	$J-K_s$ (mag)	$H-K_s$ (mag)	A_{K_s} (mag)	$M_{K_s}^{\text{Sys}}$ (mag)	$F_{\text{WR}}^{K_s}/F_{\text{Sys}}^{K_s}$	$M_{K_s}^{\text{WR}}$ (mag)	Flags
WR75a		WC9	8.50	12.49	1.46	0.68	0.82 ± 0.08		$-4.9_{-0.6}^{+0.5}$		g
WR75b		WC9	8.36	11.14	1.40	0.64	0.89 ± 0.08		$-3.7_{-0.5}^{+0.4}$		b
WR75-21		WC7:	9.35	10.5	1.08	0.27	-0.11 ± 0.16		$-1.1_{-0.2}^{+0.2}$		b
WR75ab		WN7h	8.91	12.9	1.31	0.38	0.47 ± 0.15		$-4.6_{-0.7}^{+0.6}$		g
WR75c		WC9	10.52	14.27	1.10	0.60	0.45 ± 0.12		$-4.3_{-0.5}^{+0.5}$		b:
WR75d		WC9	9.12	12.76	1.56	0.76	0.67 ± 0.16		$-4.6_{-0.8}^{+0.7}$		g
WR75-23		WC9	8.93	12.5	1.34	0.66	0.55 ± 0.14		$-4.3_{-0.6}^{+0.5}$		b
WR76		WC9d	4.88	12.81	3.58	1.63	0.63 ± 0.08		$-8.8_{-0.7}^{+0.7}$		b
WR77		WC8+OB	8.53	12.27	1.33	0.74	0.42 ± 0.10	$-4.2_{-0.4}^{+0.3}$	0.76 ± 0.45	$-3.9_{-0.7}^{+1.3}$	b
WR77-5		WN6	9.14	11.69	1.42	0.57	0.58 ± 0.15		$-3.4_{-0.7}^{+0.7}$		b
WR77-1		WN7b	8.29	12.16	1.77	0.71	0.64 ± 0.16		$-4.8_{-0.7}^{+0.7}$		b
WR77aa		WC9d		12.01							u
WR77-2		WN7	8.73	12.13	2.02	0.80	0.93 ± 0.21		$-4.5_{-0.6}^{+0.6}$		b
WR77a		WN6o	10.00	12.17	1.72	0.67	0.73 ± 0.20		$-3.0_{-0.6}^{+0.6}$		b
WR77b		WC9d		12.38							u
WR77c		WN8o	8.86	12.34	2.03	0.71	0.87 ± 0.23		$-4.5_{-0.6}^{+0.6}$		b
WR77d		WN7o	9.26	12.13	1.80	0.57	0.72 ± 0.21		$-3.7_{-0.6}^{+0.6}$		b
WR77f		WN10-11h	8.29	11.89	1.52	0.51	0.59 ± 0.19		$-4.4_{-0.7}^{+0.7}$		b
WR77h		WN8o	8.76	11.17	1.99	0.66	0.83 ± 0.23		$-3.5_{-0.8}^{+0.8}$		b
WR77i		WC9d		11.79							u
WR77j		WN7o	9.28	12.53	2.08	0.69	0.87 ± 0.24		$-4.2_{-0.6}^{+0.6}$		b:
WR77m		WC9d		12.09							u
WR77n		WC9d		12.17							u
WR77o		WN7o	9.18	12.49	1.73	0.61	0.73 ± 0.21		$-4.2_{-0.6}^{+0.6}$		b
WR77p		WC9	8.29	7.39	1.83	0.80	0.76 ± 0.21		$-0.1_{-0.4}^{+0.3}$		b

WR	Num- ber	Spectral type	K_s (mag)	μ (mag)	$J-K_s$ (mag)	$H-K_s$ (mag)	A_{K_s} (mag)	$M_{K_s}^{\text{Sys}}$ (mag)	$F_{\text{WR}}^{K_s}/F_{\text{Sys}}^{K_s}$	$M_{K_s}^{\text{WR}}$ (mag)	Flags
WR77q		WN5o	9.18	11.76	1.73	0.61	0.69 ± 0.20			$-3.5_{-0.8}^{+0.7}$	g
WR77r		WN7o	10.26	12.43	1.66	0.58	0.70 ± 0.20			$-3.0_{-0.6}^{+0.6}$	b
WR77s		WN6o	6.17	11.43	0.43	0.87	0.56 ± 0.13			$-6.1_{-0.7}^{+0.7}$	b
WR77sa		WN6h	10.17	12.02	2.06	0.25	0.52 ± 7.04			$-2.5_{-7.1}^{+7.0}$	b
WR77sb		WN6o	8.33	12.0	1.65	0.48	0.58 ± 0.27			$-4.4_{-0.7}^{+0.7}$	b
WR77sc		WN7b	6.33	12.14	1.69	0.59	0.54 ± 0.15			$-6.5_{-0.6}^{+0.6}$	b
WR77sd		WN5o	10.25	11.18	2.11	0.83	0.93 ± 0.21			$-2.2_{-0.8}^{+0.8}$	b
WR77-3		WN6	9.10	12.16	2.02	0.74	0.85 ± 0.20			$-4.1_{-0.7}^{+0.7}$	g
WR77t		WC9d		12.14							u
WR77-6		WN6b	10.95	11.46	2.61	0.98	1.04 ± 0.24			$-2.1_{-1.2}^{+1.1}$	b
WR78		WN7h	4.98	10.48	0.46	0.29	0.16 ± 0.08			$-5.7_{-0.2}^{+0.2}$	b
WR79		WC7+O5-8	5.39	10.68	0.57	0.42	0.11 ± 0.09	$-5.4_{-0.2}^{+0.2}$	0.80 ± 0.41	$-5.2_{-0.4}^{+1.0}$	g
WR79a		WN9ha	4.90	11.52	0.25	0.19	0.21 ± 0.08			$-7.1_{-0.8}^{+0.6}$	g
WR79b		WN9ha	6.47	13.63	0.29	0.15	0.38 ± 0.08			$-7.6_{-0.7}^{+0.6}$	b
WR80		WC9d	6.31	12.72	3.15	1.46	0.85 ± 0.08			$-7.5_{-0.8}^{+0.6}$	b:
WR81		WC9	7.12	11.62	1.17	0.64	0.63 ± 0.08			$-5.2_{-0.4}^{+0.3}$	g
WR82		WN7(h)	8.69	12.87	0.78	0.35	0.44 ± 0.08			$-4.7_{-0.5}^{+0.4}$	g
WR82-2		WC9	10.26	11.53	2.23	0.86	0.90 ± 0.22			$-2.7_{-1.2}^{+1.0}$	b
WR83		WN5o	15.17	12.9	0.87	0.02	0.47 ± 0.08			$1.7_{-0.6}^{+0.5}$	b
WR83-1		WC6:	12.81	11.21	2.45	1.08	0.79 ± 0.25			$0.6_{-1.2}^{+1.0}$	b
WR84		WN7o	8.50	12.39	1.08	0.46	0.53 ± 0.08			$-4.5_{-0.3}^{+0.3}$	g
WR84-4		WN7ha	9.49	11.62	1.39	0.51	0.69 ± 0.16			$-3.1_{-0.7}^{+0.7}$	b
WR84-11		WN9h	10.41	12.57	2.25	0.81	1.00 ± 0.23			$-3.4_{-0.8}^{+0.8}$	b:
WR84-9		WN6	10.64	7.7	2.79	1.06	1.26 ± 0.29			$-0.5_{-1.8}^{+1.7}$	b
WR84-10		WC8	9.26	11.64	2.41	0.80	0.77 ± 0.24			$-3.5_{-0.9}^{+0.9}$	b

WR	Num- ber	Spectral type	K_s (mag)	μ (mag)	$J-K_s$ (mag)	$H-K_s$ (mag)	A_{K_s} (mag)	$M_{K_s}^{\text{Sys}}$ (mag)	$F_{\text{WR}}^{K_s}/F_{\text{Sys}}^{K_s}$	$M_{K_s}^{\text{WR}}$ (mag)	Flags
WR85		WN6h	7.47	11.49	0.73	0.47	0.37 ± 0.08			$-4.5_{-0.3}^{+0.3}$	g
WR88		WC9	8.05	12.68	0.98	0.51	0.58 ± 0.08			$-5.3_{-0.5}^{+0.4}$	g
WR87		WN7h+abs	7.08	12.32	0.90	0.37	0.84 ± 0.08			$-6.1_{-0.5}^{+0.4}$	g
WR89		WN8h+abs	6.58	12.31	0.80	0.38	0.68 ± 0.08			$-6.5_{-0.5}^{+0.4}$	g
WR90		WC7	5.52	10.3	0.73	0.57	0.04 ± 0.11			$-4.8_{-0.2}^{+0.2}$	g
WR91		WN7b	8.20	13.03	1.33	0.57	0.74 ± 0.08			$-5.8_{-0.7}^{+0.6}$	b
WR93		WC7+O7-9	5.87	11.23	1.17	0.66	0.61 ± 0.08	$-6.0_{-0.2}^{+0.2}$	0.71 ± 0.36	$-5.6_{-0.6}^{+1.0}$	b:
WR92		WC9	8.82	12.89	0.68	0.40	0.17 ± 0.08			$-4.4_{-0.6}^{+0.5}$	b:
WR93a		WN6h	12.72	13.22	1.16	0.50	0.12 ± 0.08			$-0.9_{-0.9}^{+0.8}$	b
WR93b		WO3	10.17	11.8	1.16	0.38	0.52 ± 0.14			$-2.2_{-0.5}^{+0.4}$	b:
WR94		WN5o	5.91	9.9	1.18	0.28	0.45 ± 0.08			$-4.4_{-0.2}^{+0.2}$	g
WR95		WC9d	5.27	11.57	3.02	1.40	0.71 ± 0.08			$-7.1_{-0.4}^{+0.4}$	g
WR96		WC9d	6.20	12.11	2.84	1.32	0.59 ± 0.08			$-6.6_{-0.4}^{+0.4}$	g
WR97		WN5b+O7	8.01	11.66	0.49	0.20	0.43 ± 0.08	$-4.1_{-0.3}^{+0.3}$	0.17 ± 0.10	$-2.2_{-0.8}^{+1.2}$	b
WR98		WN8o/C7	7.04	11.46	1.05	0.51	0.58 ± 0.08			$-5.1_{-0.3}^{+0.3}$	b:
WR98a		WC8-9vd+?	4.33	10.5	4.81	2.17	0.13 ± 0.08	$-6.8_{-1.0}^{+0.9}$	0.35 ± 0.22	$-5.6_{-1.5}^{+2.0}$	g
WR100		WN7b	7.71	12.75	1.14	0.56	0.60 ± 0.08			$-5.7_{-0.6}^{+0.5}$	b
WR101		WC8	7.89	11.79	1.73	0.89	0.82 ± 0.08			$-5.0_{-0.9}^{+0.7}$	g
WR102		WO2	11.29	12.11	0.63	0.42	0.50 ± 0.08			$-1.4_{-0.3}^{+0.3}$	b
WR102-19		WN5	10.32	11.89	1.52	0.63	0.65 ± 0.16			$-2.4_{-0.7}^{+0.6}$	b
WR102-20		WC9	10.89	11.42	2.89	1.49	1.50 ± 0.29			$-2.1_{-1.1}^{+1.0}$	b
WR102-25		WN6	12.83	14.04	0.89	0.45	0.37 ± 0.13			$-1.7_{-0.6}^{+0.6}$	b
WR102-21		WN6	9.47	11.62	1.93	0.82	0.88 ± 0.19			$-3.4_{-1.0}^{+0.9}$	b:
WR102l		WN8o	7.57	12.67	1.26	0.53	0.86 ± 0.08			$-6.1_{-0.5}^{+0.5}$	g
WR103		WC9d+?	6.37	12.7	1.38	0.84	0.15 ± 0.09	$-6.6_{-0.7}^{+0.5}$	0.71 ± 0.45	$-6.3_{-1.0}^{+1.6}$	g

WR	Num- ber	Spectral type	K_s (mag)	μ (mag)	$J-K_s$ (mag)	$H-K_s$ (mag)	A_{K_s} (mag)	$M_{K_s}^{\text{Sys}}$ (mag)	$F_{\text{WR}}^{K_s}/F_{\text{Sys}}^{K_s}$	$M_{K_s}^{\text{WR}}$ (mag)	Flags
WR104		WC9d+B0.5V (+VB)	2.42	12.19	4.25	1.92	0.71 ± 0.07	$-10.6_{-0.6}^{+0.6}$	0.72 ± 0.14	$-10.2_{-0.8}^{+0.8}$	b
WR105		WN9h	5.73	11.19	1.31	0.52	0.88 ± 0.08		$-6.4_{-0.4}^{+0.3}$		g
WR105-2		WN8-9	9.02	11.88	1.45	0.58	0.65 ± 0.16		$-3.7_{-0.6}^{+0.6}$		b
WR106		WC9d	4.82	12.43	3.12	1.46	0.49 ± 0.08		$-8.2_{-0.4}^{+0.4}$		b:
WR107		WN8o	8.19	12.29	1.19	0.50	0.65 ± 0.08		$-4.8_{-0.6}^{+0.5}$		b:
WR107a		WC5-7	9.38	12.35	1.79	0.93	0.67 ± 0.11		$-3.7_{-0.5}^{+0.5}$		b
WR108		WN9ha	7.10	12.22	0.57	0.24	0.49 ± 0.08		$-5.7_{-0.3}^{+0.3}$		b
WR108-1		WN9	11.16	11.73	3.71	1.51	1.84 ± 0.37		$-2.6_{-0.9}^{+0.9}$		b
WR109		WN5h	13.27	14.18	0.25	0.52	0.12 ± 0.08		$-1.2_{-0.5}^{+0.5}$		b
WR110		WN5-6b	6.22	10.99	0.90	0.50	0.41 ± 0.08		$-5.2_{-0.2}^{+0.2}$		g
WR111		WC5	6.51	11.06	0.77	0.63	0.08 ± 0.11		$-4.7_{-0.4}^{+0.3}$		g
WR111-1		WN6o	10.13	9.01	2.45	0.93	1.08 ± 0.24		$-0.8_{-1.3}^{+1.2}$		b
WR111-9		WC9	7.79	12.5	1.87	0.83	0.79 ± 0.18		$-5.6_{-0.6}^{+0.6}$		b:
WR111-2		WN7b	7.94	11.48	1.68	0.66	0.59 ± 0.15		$-4.4_{-0.6}^{+0.6}$		b
WR111-4		WN7	8.66	11.87	1.64	0.61	0.71 ± 0.17		$-4.1_{-0.6}^{+0.6}$		b
WR111-13		WN6b	8.02	11.87	2.15	0.87	0.84 ± 0.20		$-4.8_{-0.8}^{+0.7}$		g
WR111-3		WC8	8.57	11.91	2.64	1.13	1.05 ± 0.24		$-4.5_{-0.8}^{+0.7}$		b:
WR111-10		WC7	12.24	10.44	3.89	2.02	1.80 ± 0.37		$-0.6_{-1.2}^{+1.0}$		b
WR111-12		WC9	5.76	11.74	3.28	1.49	1.59 ± 0.32		$-7.7_{-0.7}^{+0.7}$		b
WR112		WC9d+OB?	4.25	12.5	4.43	2.01	0.71 ± 0.08	$-9.4_{-1.0}^{+0.9}$	0.18 ± 0.11	$-7.5_{-1.5}^{+2.0}$	b:
WR113		WC8d+O8-9IV	5.49	11.28	1.53	0.79	0.34 ± 0.08	$-6.2_{-0.3}^{+0.3}$	0.48 ± 0.28	$-5.4_{-0.8}^{+1.2}$	g
WR113-1		WN7o	7.76	11.64	1.33	0.54	0.59 ± 0.15		$-4.7_{-0.6}^{+0.6}$		g
WR113-2		WC5-6	8.27	11.34	2.07	1.01	0.65 ± 0.21		$-4.1_{-0.8}^{+0.8}$		g
WR114		WC5+OB?	7.61	11.6	1.37	0.82	0.49 ± 0.11		$-4.5_{-0.2}^{+0.2}$		g
WR114-2		WC8	11.69	11.29	2.76	1.21	1.14 ± 0.25		$-1.3_{-1.3}^{+1.2}$		b

WR	Num- ber	Spectral type	K_s (mag)	μ (mag)	$J-K_s$ (mag)	$H-K_s$ (mag)	A_{K_s} (mag)	$M_{K_s}^{\text{Sys}}$ (mag)	$F_{\text{WR}}^{K_s}/F_{\text{Sys}}^{K_s}$	$M_{K_s}^{\text{WR}}$ (mag)	Flags
WR114-1		WN6	10.61	11.89	1.60	0.63	0.67 ± 0.17			$-2.4_{-1.0}^{+0.9}$	b
WR115		WN6o	6.95	8.39	1.04	0.47	0.61 ± 0.08			$-2.7_{-1.3}^{+1.1}$	b
WR115-1		WN6o	8.96	12.52	1.36	0.56	0.56 ± 0.14			$-4.2_{-0.5}^{+0.5}$	g
WR115-2		WN8	9.28	11.65	2.25	0.85	1.02 ± 0.23			$-3.5_{-0.8}^{+0.7}$	b
WR115-3		WN7	8.30	12.14	1.29	0.52	0.57 ± 0.14			$-4.5_{-0.4}^{+0.4}$	g
WR116		WN8h	6.96	11.94	1.25	0.61	0.25 ± 0.08			$-5.3_{-0.3}^{+0.3}$	b
WR116-1		WC9+OBI	5.63	12.06	2.73	1.30	1.65 ± 0.30	$-8.3_{-0.7}^{+0.7}$	0.10 ± 0.07	$-5.9_{-1.3}^{+1.8}$	b
WR116-2		WN5	11.93	11.6	2.14	0.82	0.94 ± 0.21			$-1.2_{-1.2}^{+1.1}$	b
WR116-3		WN6ha	9.43	12.3	1.25	0.48	0.62 ± 0.15			$-3.6_{-0.5}^{+0.5}$	b
WR117		WC9d	7.36	12.81	2.31	1.13	0.65 ± 0.08			$-6.3_{-0.7}^{+0.6}$	g
WR117-1		WN7	7.63	12.66	1.46	0.66	0.70 ± 0.16			$-5.8_{-0.4}^{+0.4}$	b
WR118		WC9d	3.65	11.98	4.45	1.76	1.46 ± 0.08			$-9.8_{-0.7}^{+0.6}$	b
WR118-4		WC8	9.36	11.85	2.82	1.16	1.12 ± 0.25			$-3.7_{-0.8}^{+0.7}$	b
WR118-2		WN9	7.58	11.91	2.99	1.08	1.36 ± 0.30			$-5.8_{-0.8}^{+0.7}$	g
WR118-3		WN9	7.38	9.22	2.96	1.02	1.31 ± 0.30			$-4.7_{-1.3}^{+1.4}$	b:
WR118-10		WN6	10.02	8.68	2.02	0.79	0.88 ± 0.20			$-0.1_{-1.2}^{+1.0}$	b
WR118-5		WC9d		12.29							u
WR118-6		WN7:	10.59	11.8	3.05	1.14	1.42 ± 0.31			$-2.7_{-0.9}^{+0.8}$	b
WR119		WC9d	7.26	12.54	2.24	1.17	0.42 ± 0.08			$-5.9_{-0.7}^{+0.6}$	g
WR119-2		WC8	9.56	11.7	2.27	0.93	0.83 ± 0.20			$-3.1_{-0.8}^{+0.7}$	b
WR119-1		WN7o	10.29	13.15	1.48	0.57	0.64 ± 0.16			$-3.7_{-0.7}^{+0.7}$	b
WR120		WN7o	8.01	10.89	0.89	0.40	0.52 ± 0.08			$-3.6_{-0.7}^{+0.6}$	b
WR120-16		WC8	10.54	11.72	2.38	0.70	0.70 ± 0.21			$-2.5_{-1.2}^{+1.1}$	b
WR120-1		WC9	9.45	12.34	1.60	0.72	0.65 ± 0.16			$-3.7_{-0.6}^{+0.6}$	b
WR120-11		WC8	10.25	12.12	2.10	0.90	0.76 ± 0.19			$-2.7_{-0.7}^{+0.6}$	b

WR	Num- ber	Spectral type	K_s (mag)	μ (mag)	$J-K_s$ (mag)	$H-K_s$ (mag)	A_{K_s} (mag)	$M_{K_s}^{\text{Sys}}$ (mag)	$F_{\text{WR}}^{K_s}/F_{\text{Sys}}^{K_s}$	$M_{K_s}^{\text{WR}}$ (mag)	Flags
WR120-7		WN7	8.51	12.33	1.71	0.70	0.79 ± 0.18		$-4.7_{-0.6}^{+0.5}$	b	
WR120-3		WN9h	9.16	10.16	2.79	1.06	1.30 ± 0.28		$-3.2_{-1.4}^{+1.3}$	b	
WR120-4		WN9h	9.27	11.83	2.58	0.99	1.20 ± 0.26		$-3.9_{-0.9}^{+0.8}$	b:	
WR120-5		WC8		11.49						u	
WR120-6		WN6	12.32	12.48	1.19	0.51	0.48 ± 0.13		$-0.8_{-0.5}^{+0.5}$	b	
WR120-15		WC8	10.66	12.39	2.03	0.71	0.62 ± 0.18		$-2.5_{-0.7}^{+0.7}$	b	
WR120-10		WN7	8.53	12.06	1.47	0.63	0.68 ± 0.16		$-4.4_{-0.6}^{+0.6}$	b:	
WR121		WC9d	5.77	11.74	2.52	1.29	0.57 ± 0.08		$-6.6_{-0.3}^{+0.3}$	g	
WR121-15		WN4-5	10.72	12.37	2.02	0.85	1.13 ± 0.23		$-3.0_{-0.7}^{+0.7}$	g	
WR121-12		WN5	10.64	11.9	2.12	0.79	0.90 ± 0.21		$-2.6_{-1.0}^{+0.9}$	b	
WR121-1		WN7h	9.47	12.52	1.47	0.60	0.66 ± 0.16		$-3.8_{-0.5}^{+0.5}$	b	
WR121-6		WN5	9.34	12.28	1.08	0.42	0.39 ± 0.12		$-3.4_{-0.5}^{+0.5}$	b	
WR122-2		WN9	9.61	11.72	2.88	1.07	1.33 ± 0.29		$-3.5_{-0.9}^{+0.8}$	b:	
WR122-3		WN6	9.99	11.91	2.82	1.07	1.27 ± 0.28		$-3.3_{-0.9}^{+0.8}$	b:	
WR122-1		WC8	10.30	13.33	1.88	1.00	0.78 ± 0.17		$-4.0_{-0.6}^{+0.6}$	b	
WR122-15		WN6	11.05	11.61	2.06	0.57	0.74 ± 0.21		$-1.8_{-1.0}^{+1.0}$	b	
WR123		WN8o	8.92	13.64	0.60	0.36	0.26 ± 0.08		$-5.1_{-0.5}^{+0.5}$	b:	
WR123-1		WN6o	8.71	12.13	1.88	0.76	0.83 ± 0.19		$-4.4_{-0.7}^{+0.7}$	b	
WR123-3		WN8	9.94	12.51	2.28	0.87	1.05 ± 0.23		$-3.9_{-0.8}^{+0.8}$	b	
WR123-8		WN9h	12.62	11.21	2.11	0.82	0.97 ± 0.22		$-0.0_{-1.2}^{+1.1}$	b	
WR124		WN8h	7.73	13.84	0.85	0.45	0.42 ± 0.08		$-6.7_{-0.5}^{+0.5}$	g	
WR124-1B		WC8	9.19	10.96	2.85	1.19	1.15 ± 0.26		$-3.3_{-1.3}^{+1.2}$	b	
WR124-1A		WC8	9.19	11.85	2.85	1.19	1.15 ± 0.26		$-3.9_{-0.9}^{+0.8}$	b	
WR124-3		WC8	10.77	12.82	2.19	1.05	0.89 ± 0.20		$-3.1_{-0.7}^{+0.7}$	b	
WR124-9		WC6:	11.67	12.12	2.23	1.05	0.72 ± 0.22		$-1.6_{-1.0}^{+0.9}$	b	

WR	Num- ber	Spectral type	K_s (mag)	μ (mag)	$J-K_s$ (mag)	$H-K_s$ (mag)	A_{K_s} (mag)	$M_{K_s}^{\text{Sys}}$ (mag)	$F_{\text{WR}}^{K_s}/F_{\text{Sys}}^{K_s}$	$M_{K_s}^{\text{WR}}$ (mag)	Flags
WR124-18		WN9h	9.97	12.07	2.82	1.07	1.32 ± 0.28			$-3.7_{-0.9}^{+0.9}$	b:
WR124-19		WC6:	12.08	11.83	2.57	1.21	0.91 ± 0.25			$-0.9_{-1.0}^{+0.9}$	b
WR124-2		WC8	10.76	12.21	2.81	1.04	1.03 ± 0.25			$-2.6_{-0.8}^{+0.7}$	b
WR124-6		WC6	9.68	12.18	2.99	1.23	1.03 ± 0.28			$-3.7_{-0.8}^{+0.7}$	b
WR124-7		WC7	9.58	12.3	3.25	1.44	1.23 ± 0.31			$-4.0_{-0.8}^{+0.7}$	b
WR124-11		WN6b	10.25	11.95	2.40	0.94	0.95 ± 0.22			$-3.1_{-1.0}^{+0.9}$	b
WR124-20		WC9	9.92	9.15	3.05	1.26	1.37 ± 0.30			$-0.9_{-0.9}^{+0.7}$	b
WR124-21		WC8	10.21	13.83	1.65	0.76	0.56 ± 0.15			$-4.3_{-0.5}^{+0.5}$	b
WR124-22		WC9	9.64	11.41	3.37	1.45	1.58 ± 0.33			$-3.6_{-1.0}^{+0.9}$	b
WR125		WC7ed+O9III	8.21	12.63	1.09	0.53	0.69 ± 0.09	$-5.2_{-0.6}^{+0.5}$	0.76 ± 0.39	$-4.9_{-0.9}^{+1.2}$	g
WR125-4		WN7	10.12	12.35	2.59	0.95	1.18 ± 0.26			$-3.5_{-0.7}^{+0.7}$	b
WR125-3		WN7ha	7.33	12.34	1.32	0.50	0.67 ± 0.16			$-5.9_{-0.7}^{+0.7}$	g
WR125-2		WN8-9	6.60	12.58	1.61	0.68	0.75 ± 0.17			$-6.9_{-0.5}^{+0.5}$	b:
WR125-1		WC8	9.07	13.4	1.13	0.54	0.27 ± 0.10			$-4.7_{-0.4}^{+0.4}$	b
WR126		WC5/WN	10.09	14.4	0.61	0.31	0.40 ± 0.11			$-4.8_{-0.4}^{+0.4}$	b:
WR127		WN3b+O9.5V	8.76	12.45	0.42	0.26	0.19 ± 0.07	$-3.9_{-0.2}^{+0.2}$	0.40 ± 0.23	$-2.9_{-0.7}^{+1.2}$	g
WR129		WN4o	10.40	13.69	0.68	0.32	0.38 ± 0.08			$-3.8_{-0.4}^{+0.4}$	b:
WR128		WN4(h)	9.62	12.31	0.35	0.22	0.14 ± 0.08			$-2.9_{-0.4}^{+0.3}$	g
WR130		WN8(h)	7.45	14.12	1.00	0.42	0.59 ± 0.08			$-7.4_{-0.6}^{+0.5}$	b
WR131		WN7h+abs	8.86	14.2	0.66	0.29	0.47 ± 0.08			$-5.9_{-0.4}^{+0.4}$	g
WR132		WC6+?	9.05	13.09	1.13	0.71	0.40 ± 0.11			$-4.5_{-0.3}^{+0.3}$	g
WR133		WN5o+O9I	6.25	11.33	0.07	0.07	0.13 ± 0.07	$-5.2_{-0.2}^{+0.2}$	0.23 ± 0.14	$-3.7_{-0.7}^{+1.1}$	g
WR134		WN6b	6.16	11.21	0.55	0.36	0.17 ± 0.08			$-5.2_{-0.2}^{+0.2}$	g
WR135		WC8	6.66	11.48	0.57	0.45	0.15 ± 0.08			$-5.0_{-0.2}^{+0.2}$	g
WR136		WN6b(h)	5.56	11.43	0.57	0.34	0.18 ± 0.08			$-6.1_{-0.2}^{+0.2}$	b

WR	Num- ber	Spectral type	K_s (mag)	μ (mag)	$J-K_s$ (mag)	$H-K_s$ (mag)	A_{K_s} (mag)	$M_{K_s}^{\text{Sys}}$ (mag)	$F_{\text{WR}}^{K_s}/F_{\text{Sys}}^{K_s}$	$M_{K_s}^{\text{WR}}$ (mag)	Flags
WR137		WC7pd+O9	6.18	11.61	0.80	0.59	0.18 ± 0.08	$-5.6_{-0.2}^{+0.2}$	0.56 ± 0.28	$-5.0_{-0.6}^{+1.0}$	g
WR138		WN6o	6.58	11.96	0.38	0.22	0.22 ± 0.08			$-5.7_{-0.3}^{+0.3}$	b
WR138-1		WN8-9h	8.65	15.49	1.50	0.62	0.68 ± 0.16			$-7.3_{-0.6}^{+0.5}$	b
WR139		WN5o+O6III-V	6.33	10.58	0.37	0.19	0.30 ± 0.09	$-4.6_{-0.1}^{+0.1}$	0.62 ± 0.36	$-4.0_{-0.6}^{+1.1}$	g
WR140		WC7pd+O4-5	5.04	11.07	0.51	0.39	0.24 ± 0.08	$-6.3_{-0.2}^{+0.2}$	0.62 ± 0.31	$-5.8_{-0.6}^{+0.9}$	b
WR141		WN5o+O5V-III	6.54	11.42	0.80	0.39	0.44 ± 0.08			$-5.3_{-0.2}^{+0.2}$	b
WR142		WO2	8.60	11.08	0.94	0.29	0.78 ± 0.08			$-3.3_{-0.2}^{+0.2}$	g
WR142a		WC8	7.12	11.29	2.15	0.97	0.83 ± 0.19			$-5.1_{-0.5}^{+0.5}$	g
WR142-1		WN6o	7.19	11.24	1.58	0.67	0.69 ± 0.16			$-4.8_{-0.3}^{+0.3}$	b:
WR143		WC4+OB?	7.46	11.73	1.12	0.64	0.65 ± 0.08	$-4.9_{-0.2}^{+0.2}$	0.67 ± 0.26	$-4.5_{-0.5}^{+0.7}$	g
WR144		WC4	7.71	11.21	1.70	0.88	0.47 ± 0.19			$-4.0_{-0.3}^{+0.3}$	g
WR145		WN7o/CE+?	6.24	10.81	1.13	0.47	0.83 ± 0.14	$-5.4_{-0.2}^{+0.2}$	0.86 ± 0.75	$-5.3_{-0.4}^{+2.4}$	b:
WR146		WC6+O8	5.49	10.21	1.58	0.75	1.16 ± 0.08	$-6.3_{-0.9}^{+0.8}$	0.71 ± 0.31	$-5.9_{-1.3}^{+1.4}$	b
WR147		WN8(h)+B0.5V	4.11	11.26	1.90	0.75	1.01 ± 0.08			$-8.2_{-0.3}^{+0.3}$	b
WR148		WN8h+	8.32	14.88	0.44	0.21	0.22 ± 0.08			$-6.9_{-0.4}^{+0.4}$	b:
WR149		WN5o	9.61	13.45	1.01	0.45	0.65 ± 0.08			$-4.6_{-0.3}^{+0.3}$	b:
WR150		WC5	9.60	14.71	1.12	0.71	0.32 ± 0.11			$-5.5_{-0.4}^{+0.4}$	b
WR151		WN4o+O5V	9.01	13.65	0.75	0.35	0.43 ± 0.11	$-5.2_{-0.5}^{+0.5}$	0.83 ± 0.49	$-5.0_{-0.7}^{+1.4}$	b
WR152		WN3(h)	10.04	13.2	0.45	0.28	0.22 ± 0.08			$-3.5_{-0.5}^{+0.4}$	g
WR153		WN6o/CE+O6I	7.41	13.04	0.37	0.19	0.23 ± 0.10	$-5.9_{-0.3}^{+0.3}$	0.81 ± 0.47	$-5.7_{-0.6}^{+1.3}$	b
WR154		WC6	8.29	13.65	1.01	0.72	0.25 ± 0.11			$-5.7_{-0.4}^{+0.4}$	b:
WR155		WN6o+O9II-Ib	7.16	12.38	0.32	0.18	0.25 ± 0.11	$-5.5_{-0.3}^{+0.3}$	0.24 ± 0.54	$-4.0_{-1.6}^{+1.9}$	g
WR156		WN8h	7.03	13.07	0.91	0.41	0.43 ± 0.08			$-6.5_{-0.3}^{+0.3}$	g
WR157		WN5o(+B1II)	7.73	12.05	0.49	0.21	0.33 ± 0.08	$-4.7_{-0.3}^{+0.3}$	0.38 ± 0.22	$-3.6_{-0.8}^{+1.2}$	g
WR158		WN7h	7.81	13.49	0.83	0.39	0.40 ± 0.08	$-6.1_{-0.3}^{+0.3}$	0.37 ± 1.00	$-5.1_{-1.4}^{+1.4}$	g

WR	Num- ber	Spectral type	K_s (mag)	μ (mag)	$J-K_s$ (mag)	$H-K_s$ (mag)	A_{K_s} (mag)	$M_{K_s}^{Sys}$ (mag)	$F_{WR}^{K_s}/F_{Sys}^{K_s}$	$M_{K_s}^{WR}$ (mag)	Flags
WR159		WN4	5.53	11.3	0.57	0.23	0.34 ± 0.10		$-6.2^{+0.5}_{-0.6}$		b

Columns: (1) WR Number, (2) Spectral type, (3) K_s apparent magnitude, (4) Distance modulus μ , (5) $J-K_s$ colour, (6) $H-K_s$ colour, (7) K_s band extinction A_{K_s} , (8) Absolute magnitude of binary system (including companion), (9) Fraction of light contributed to the binary system by the WR component, (10) Absolute magnitude of WR star, (11) Error flags, where $M > upper_{initial}$ or $M < lower_{initial} = b$, $M > upper_{final}$ or $M < lower_{final} = b$: (_{initial} denotes the averages calculated before sigma clipping, _{final} are the final absolute magnitude boundaries) and g are results with no issues.

This paper has been typeset from a TeX/LaTeX file prepared by the author.

Table 7: Absolute v^{WR} -band magnitudes for Galactic WR stars.

WR Number	Spectral type	$v^{WR} \pm 0.1$ (mag)	μ (mag)	$(b - v)^{WR}$ (mag)	A_v^{WR} (mag)	$M_{V^{sys}}$ (mag)	$F_{V^{sys}}^{WR} / F_{V^{sys}}$	M_v^{WR} (mag)	Flags
WR1	WN4b	10.51	12.49	0.51	2.84 ± 0.71			$-4.9_{-0.8}^{+0.8}$	g
WR3	WN3ha	10.70	12.31	-0.06	1.07 ± 0.71			$-2.8_{-0.8}^{+0.8}$	b:
WR4	WC5+?	10.53	12.87	0.20	1.65 ± 1.01			$-4.2_{-1.1}^{+1.1}$	g
WR5	WC6	11.02	12.36	0.47	2.76 ± 1.01			$-4.2_{-1.1}^{+1.1}$	g
WR6	WN4b	6.94	11.78	-0.07	0.45 ± 0.71			$-5.4_{-0.8}^{+0.8}$	b:
WR7	WN4b	11.75	13.13	0.36	2.22 ± 0.71			$-3.8_{-0.9}^{+0.9}$	b:
WR8	WN7o/CE	10.48	12.87	0.47	2.88 ± 0.71			$-5.4_{-0.8}^{+0.8}$	b:
WR9	WC5+O7	10.93	13.3	0.74	4.16 ± 0.72	$-6.6_{-0.8}^{+0.8}$	0.29 ± 0.12	$-5.3_{-1.2}^{+1.4}$	b
WR10	WN5h	11.08	13.69	0.22	2.26 ± 1.61			$-5.0_{-1.7}^{+1.7}$	b:
WR11	WC8+O7.5III-V	1.74	7.67	-0.32	-0.02 ± 1.03	$-6.0_{-1.1}^{+1.1}$	0.24 ± 0.03	$-4.4_{-1.2}^{+1.2}$	g
WR12	WN8h	10.99	13.78	0.42	2.35 ± 0.71			$-5.3_{-0.8}^{+0.8}$	g
WR13	WC6	13.78	13.41	0.82	4.20 ± 1.01			$-4.0_{-1.1}^{+1.1}$	g
WR14	WC7+?	9.40	11.73	0.14	1.40 ± 1.01			$-3.8_{-1.0}^{+1.0}$	g
WR15	WC6	11.72	12.36	0.72	3.79 ± 1.01			$-4.5_{-1.0}^{+1.0}$	b:
WR16	WN8h	8.44	12.1	0.30	1.85 ± 0.71			$-5.6_{-0.8}^{+0.8}$	g
WR17	WC5	11.03	14.15	0.14	1.40 ± 1.01			$-4.6_{-1.1}^{+1.1}$	g
WR17-1	WN5b		12.45						u
WR18	WN4b	11.11	12.91	0.55	3.01 ± 0.71			$-5.0_{-0.8}^{+0.8}$	g
WR19	WC5	13.75	13.18	1.06	5.19 ± 1.01			$-4.7_{-1.1}^{+1.1}$	b:
WR19a	WN7:(h)	17.45	13.39	1.71	7.66 ± 0.71			$-3.8_{-0.9}^{+0.9}$	b:
WR20	WN5o	14.45	14.22	0.88	4.78 ± 0.71			$-4.6_{-0.8}^{+0.8}$	g
WR20-2	O2If*/WN6		13.72						u
WR20-1	WN7-8		12.17						u
WR20a	O3If*/WN6+ O3If*/WN6	14.14	13.51	1.38	7.09 ± 0.71	$-6.6_{-0.8}^{+0.8}$	0.50 ± 0.00	$-5.8_{-0.8}^{+0.8}$	g

WR Number	Spectral type	$v^{WR} \pm 0.1$ (mag)	μ (mag)	$(b - v)^{WR}$ (mag)	A_v^{WR} (mag)	$M_{V^S}^{S_V}$ (mag)	$F_{V^S}^{WR} / F_{V^S}^{S_V}$	M_v^{WR} (mag)	Flags
WR20b	WN6ha	15.40	12.44	1.69	8.32 ± 0.71			$-5.5_{-0.8}^{+0.8}$	b
WR20-3	O2If*/WN6			11.99					u
WR21a	O2If/WN5	12.80	13.21						u
WR21	WN5o+O4-6	9.76	13.0	0.27	2.32 ± 0.76	$-5.6_{-0.8}^{+0.8}$	0.86 ± 0.20	$-5.5_{-1.0}^{+1.1}$	b
WR22	WN7h+O9III-V	7.16	11.84	0.08	1.69 ± 0.71			$-6.4_{-0.8}^{+0.8}$	g
WR23	WC6	9.67	12.03	-0.05	0.62 ± 1.01			$-3.0_{-1.0}^{+1.0}$	b
WR24	WN6ha	7.20	12.75	-0.04	1.19 ± 0.71			$-6.9_{-0.8}^{+0.8}$	b:
WR25	O2.5If*/WN6+O	8.84	11.47	0.17	3.16 ± 1.07			$-5.8_{-1.1}^{+1.1}$	b
WR26	WN7b/CE	14.61	14.13	0.92	4.74 ± 0.71			$-4.3_{-0.8}^{+0.8}$	g
WR27	WC6+a	14.96	12.09	1.29	6.14 ± 1.01			$-3.3_{-1.0}^{+1.0}$	b:
WR28	WN6(h)+OB?	13.00	13.79	0.77	4.53 ± 0.71			$-5.4_{-0.8}^{+0.8}$	b
WR29	WN7h+O	12.65	13.76	0.65	3.76 ± 1.32	$-5.0_{-1.4}^{+1.4}$	0.26 ± 0.82	$-3.5_{-2.9}^{+2.9}$	b
WR30	WC6+O6-8	11.73	13.54	0.27	2.18 ± 0.77	$-4.1_{-0.9}^{+0.9}$	0.44 ± 0.18	$-3.2_{-1.2}^{+1.4}$	b:
WR30a	WO4+O5-5.5	13.33	14.14	0.79	4.52 ± 0.70	$-5.4_{-0.8}^{+0.8}$	0.10 ± 0.05	$-2.9_{-1.2}^{+1.6}$	g
WR31	WN4o+O8V	10.69	13.93	0.28	2.47 ± 0.71			$-5.8_{-0.9}^{+0.9}$	b
WR31a	WN11h		14.33						u
WR31b	WN11h		13.43						u
WR31c	WC6	16.37	13.91	0.96	4.78 ± 1.01			$-2.4_{-1.1}^{+1.1}$	b
WR31-1	O3.5If/WN7		13.31						u
WR32	WC5+OB?	15.90	13.8	1.29	6.37 ± 0.77	$-4.4_{-0.9}^{+0.9}$	0.44 ± 0.18	$-3.5_{-1.2}^{+1.4}$	g
WR33	WC6	12.35	14.4	0.16	1.48 ± 1.01			$-3.6_{-1.1}^{+1.1}$	g
WR34	WN5o	14.50	14.35	0.76	4.28 ± 0.71			$-4.2_{-0.8}^{+0.8}$	g
WR35	WN6h+OB?	13.90	14.18	0.59	3.63 ± 2.21	$-4.0_{-0.2}^{+2.2}$	0.48 ± 1.25	$-3.2_{-3.0}^{+3.0}$	b:
WR35a	WN6h+O8.5V	13.92	13.83	0.86	4.77 ± 0.71	$-4.8_{-0.8}^{+0.8}$	0.09 ± 0.09	$-2.1_{-1.5}^{+5.3}$	b
WR35b	WN4b	14.49	13.65	1.27	5.97 ± 0.71			$-5.2_{-0.8}^{+0.8}$	b:

WR Number	Spectral type	$v^{WR} \pm 0.1$ (mag)	μ (mag)	$(b - v)^{WR}$ (mag)	A_v^{WR} (mag)	$M_{\text{V}}^{\text{Sys}}$ (mag)	$F_{\text{V}}^{\text{WR}} / F_{\text{V}}^{\text{Sys}}$	M_{V}^{WR} (mag)	Flags
WR36	WN5-6b+OB?	13.70	13.67	0.68	3.75 ± 0.82	$-3.8_{-0.9}^{+0.9}$	0.59 ± 0.34	$-3.3_{-1.4}^{+1.9}$	b:
WR37	WN4b	15.77	14.13	1.23	5.81 ± 0.71			$-4.3_{-0.8}^{+0.8}$	g
WR38	WC4	15.40	13.91	0.93	4.66 ± 1.01			$-3.3_{-1.1}^{+1.1}$	b:
WR38a	WN5o	16.21	13.67	0.83	4.57 ± 0.71			$-2.1_{-0.8}^{+0.8}$	b
WR40	WN8h	7.60	12.92	0.19	1.40 ± 0.71			$-6.8_{-0.8}^{+0.8}$	b
WR38b	WC7	16.21	13.18	1.50	7.00 ± 1.01			$-4.1_{-1.1}^{+1.1}$	g
WR39	WC7+OB?	14.50	12.92	1.26	6.32 ± 0.72	$-5.0_{-1.0}^{+1.0}$	0.25 ± 0.13	$-3.5_{-1.5}^{+1.8}$	g
WR41	WC5+OB?	14.80	13.89	0.80	4.26 ± 0.90	$-3.4_{-1.0}^{+1.0}$	0.66 ± 0.27	$-3.0_{-1.3}^{+1.5}$	b
WR42	WC7+O7V	8.25	11.93	0.06	1.33 ± 0.76	$-5.1_{-0.8}^{+0.8}$	0.37 ± 0.19	$-4.0_{-1.3}^{+1.6}$	g
WR42a	WN5b	17.61	13.75	1.46	6.76 ± 0.71			$-3.0_{-0.8}^{+0.8}$	b
WR42b	WN4b	16.96	14.01	2.43	10.75 ± 0.71			$-7.9_{-0.9}^{+0.9}$	b
WR42c	WN5o	16.56	14.14	1.36	6.76 ± 0.71			$-4.4_{-0.8}^{+0.8}$	g
WR42d	WN5b	15.28	12.53	1.33	6.22 ± 0.71			$-3.7_{-1.0}^{+1.0}$	b:
WR42-1	O3If*/WN6		13.19						u
WR43-2	O2If*/WN5		13.95						u
WR43-3	O2.5If*/WN6		14.08						u
WR43-1	WN4b		10.63						u
WR44	WN4o+OB?	12.96	13.92	0.37	2.77 ± 0.70	$-3.8_{-0.8}^{+0.8}$	0.10 ± 0.06	$-1.4_{-1.3}^{+1.8}$	b
WR44a	WN5b	16.20	13.52	1.55	7.13 ± 0.71			$-4.6_{-0.8}^{+0.8}$	g
WR45	WC6	14.80	13.14	1.12	5.44 ± 1.01			$-3.8_{-1.0}^{+1.0}$	g
WR45-1	WN9-10h		13.44						u
WR45-2	WN5		13.21						u
WR45a	WN5o	16.69	12.89	1.19	6.06 ± 0.71			$-2.5_{-0.9}^{+0.9}$	b
WR45b	WN4b	18.08	13.87	1.40	6.51 ± 0.71			$-2.4_{-0.8}^{+0.8}$	b
WR45-3	WN5b		13.58						u

WR Number	Spectral type	$v^{WR} \pm 0.1$ (mag)	μ (mag)	$(b - v)^{WR}$ (mag)	A_v^{WR} (mag)	$M_{V^S}^{S_V}$ (mag)	$F_{V^S}^{WR} / F_{V^S}^{S_V}$	M_v^{WR} (mag)	Flags
WR45-4	WN6		13.76						u
WR45c	WN5o	15.44	13.94	0.91	4.90 \pm 0.71			-3.5 $^{+0.8}_{-0.8}$	b:
WR46	WN3b pec	10.87	12.07	-0.03	0.62 \pm 0.71			-1.9 $^{+0.8}_{-0.8}$	b
WR46-1	WN6o		13.37						u
WR46-18	WC6-7		11.29						u
WR46-7	WC5-7		12.43						u
WR46-8	WN6		12.06						u
WR46-16	WN9		11.96						u
WR46-9	WN5		12.42						u
WR46-17	WN9/OIf+		12.3						u
WR46a	WN4o	16.00	14.14	1.04	5.60 \pm 0.71			-3.8 $^{+0.8}_{-0.8}$	g
WR46-2	WN7h		12.91						u
WR46-3	O6-7.5If+		13.05						u
WR46-4	Ofpe/WN9		12.24						u
WR46-5	WN6		12.86						u
WR46-6	WN7		12.97						u
WR46-15	WN8		11.5						u
WR46-12	WN4b		12.39						u
WR46-13	WC7		12.77						u
WR46-14	WN5b		9.06						u
WR47	WN6o+O5V	11.08	12.72	0.76	4.33 \pm 2.08	-6.1 $^{+2.1}_{-2.1}$	0.45 \pm 1.17	-5.2 $^{+3.0}_{-3.0}$	b:
WR47a	WN8h	15.98	13.45	1.73	7.75 \pm 0.71			-5.4 $^{+0.9}_{-0.9}$	g
WR47-1	WN6o		12.69						u
WR47b	WN9h	17.05	13.75	1.93	8.57 \pm 0.71			-5.4 $^{+0.9}_{-0.9}$	g
WR47-5	WN6(h)		12.36						u

WR Number	Spectral type	$v^{WR} \pm 0.1$ (mag)	μ (mag)	$(b - v)^{WR}$ (mag)	A_v^{WR} (mag)	$M_{V^S}^{S_V}$ (mag)	$F_{V^S}^{WR} / F_{V^S}^{S_V}$	M_v^{WR} (mag)	Flags
WR47c	WC5	16.09	14.16	1.40	6.59 ± 1.01			$-4.8_{-1.1}^{+1.1}$	b:
WR47-2	WC5-6			12.69					u
WR47-3	WC5-6			10.74					u
WR48	WC6(+O9.5/B0Iab)	5.88	11.9	-0.12	0.72 ± 0.70	$-7.2_{-1.0}^{+1.0}$	0.96 ± 0.42	$-7.1_{-1.1}^{+1.7}$	b
WR48-1	WC7			12.34					u
WR48b	WC9d	15.96	13.55	1.07	5.73 ± 0.71			$-3.5_{-0.8}^{+0.8}$	b
WR48-6	WN9			12.4					u
WR48-10	WN9h			12.01					u
WR48-7	WN8			12.09					u
WR48-4	WC6			11.97					u
WR48-8	WN9			12.54					u
WR48-9	WN9h			12.22					u
WR48a	WC8ed+?	16.80	11.78	1.70	8.28 ± 0.70	$-3.5_{-1.0}^{+1.0}$	0.12 ± 0.07	$-1.3_{-1.5}^{+1.9}$	b
WR48-5	WN6b			11.57					u
WR48c	WN3h/C4	13.98	12.13	0.39	2.55 ± 0.71			$-0.7_{-0.7}^{+0.7}$	b
WR48-2	WC7-8			12.56					u
WR49	WN5(h)	13.84	14.61	0.34	2.55 ± 0.71			$-3.4_{-0.8}^{+0.8}$	b:
WR50	WC7+OB	12.49	12.7	0.54	3.21 ± 0.91	$-3.5_{-1.0}^{+1.0}$	0.60 ± 0.31	$-3.0_{-1.4}^{+1.8}$	b
WR51	WN4o	14.64	12.82	1.04	5.60 ± 0.71			$-3.9_{-0.8}^{+0.8}$	g
WR52	WC4	9.86	11.21	0.29	2.02 ± 1.01			$-3.4_{-1.0}^{+1.0}$	b:
WR52-2	WN6			12.1					u
WR53	WC8d	10.88	13.08	0.42	3.25 ± 0.71			$-5.6_{-0.8}^{+0.8}$	b:
WR54	WN5o	12.99	14.07	0.46	3.05 ± 0.71			$-4.2_{-0.8}^{+0.8}$	g
WR55	WN7o	10.87	12.38	0.40	2.27 ± 0.71			$-3.9_{-0.8}^{+0.8}$	b:
WR56	WC7	13.87	14.69	0.44	2.64 ± 1.01			$-3.5_{-1.1}^{+1.1}$	g

WR Number	Spectral type	$v^{WR} \pm 0.1$ (mag)	μ (mag)	$(b - v)^{WR}$ (mag)	A_v^{WR} (mag)	$M_{V^S}^{S_V}$ (mag)	$F_{V^S}^{WR} / F_{V^S}^{S_V}$	M_v^{WR} (mag)	Flags
WR56a	WN6o	15.91	13.2	1.32	6.59 \pm 0.71			-4.1 $^{+0.9}_{-0.9}$	g
WR57	WC8	10.02	13.7	0.10	1.94 \pm 0.71			-5.8 $^{+0.9}_{-0.9}$	b
WR58	WN4b/CE	13.05	13.85	0.57	3.30 \pm 0.71			-4.2 $^{+0.8}_{-0.8}$	g
WR59	WC9d	13.90	12.77	1.24	6.43 \pm 0.71			-5.4 $^{+0.8}_{-0.8}$	b
WR59-2	WC5-6		11.08						u
WR60	WC8	13.25	12.73	1.04	5.81 \pm 0.71			-5.4 $^{+0.8}_{-0.8}$	b:
WR60-7	WC7-8		11.57						u
WR60-5	WC7		11.94						u
WR60-2	WC8		11.6						u
WR61	WN5o	12.41	13.7	0.36	2.64 \pm 0.71			-4.1 $^{+0.8}_{-0.8}$	g
WR61-3	WC9		9.8						u
WR61-1	WN6		12.95						u
WR62	WN6b	14.22	13.15	1.60	7.33 \pm 0.71			-6.4 $^{+0.8}_{-0.8}$	b
WR62a	WN6o	13.80	12.72	1.24	6.26 \pm 0.71			-5.3 $^{+0.8}_{-0.8}$	b:
WR62-2	WN8-9h		11.71						u
WR62b	WN5o	17.26	13.7	1.77	8.45 \pm 0.71			-5.0 $^{+0.9}_{-0.9}$	b:
WR62-1	WN7-8h		11.81						u
WR64	WC7	15.57	14.51	0.16	1.48 \pm 1.01			-0.5 $^{+1.1}_{-1.1}$	b
WR64-3	WN6o		12.31						u
WR64-4	WN6o+OB		10.93						u
WR64-5	WN6o		11.31						u
WR65	WC9d+OB?	14.50	12.48	1.41	7.06 \pm 0.71	-5.2 $^{+0.9}_{-0.9}$	0.17 \pm 0.11	-3.3 $^{+2.0}_{-1.4}$	b
WR66	WN8(h)	11.66	13.57	0.73	3.63 \pm 0.71			-5.7 $^{+1.1}_{-1.1}$	g
WR67	WN6o	12.12	11.75	0.87	4.74 \pm 0.71			-4.5 $^{+0.8}_{-0.8}$	g
WR67-3	WN10		12.34						u

WR Number	Spectral type	$v^{WR} \pm 0.1$ (mag)	μ (mag)	$(b - v)^{WR}$ (mag)	A_v^{WR} (mag)	$M_{\text{V}}^{\text{Svs}}$ (mag)	$F_{\text{V}}^{\text{WR}} / F_{\text{V}}^{\text{Svs}}$	M_{V}^{WR} (mag)	Flags
WR67-1	WN6h		12.63						u
WR67-2	WC7		11.68						u
WR68	WC7	14.09	13.46	0.97	4.82 ± 1.01			$-4.3^{+1.1}_{-1.1}$	b:
WR68-1	WN4b		11.37						u
WR68a	WN6o	14.41	12.99	1.46	7.17 ± 0.71			$-5.9^{+0.8}_{-0.8}$	b
WR69	WC9d+OB	9.43	12.71	0.14	1.83 ± 0.73	$-5.2^{+0.8}_{-0.8}$	0.25 ± 0.16	$-3.7^{+1.9}_{-1.3}$	b:
WR70	WC9vd+B0I	10.10	12.39	0.96	5.20 ± 0.71	$-7.6^{+0.8}_{-0.8}$	0.05 ± 0.03	$-4.3^{+2.0}_{-1.3}$	g
WR70-1	WN7		11.42						u
WR70-13	WC8d		12.22						u
WR70-3	WC7		11.87						u
WR70-5	WC9		11.45						u
WR70a	WN6o	16.90	13.01	1.23	6.22 ± 0.71			$-2.5^{+0.9}_{-0.9}$	b
WR70-2	WN5b		12.82						u
WR70-11	WN7		13.1						u
WR70-16	WC7d+WN WN/Cd+O	or	8.7						u
WR71	WN6o	10.23	12.52	-0.05	0.95 ± 0.71			$-3.4^{+0.8}_{-0.8}$	b:
WR71-1	WN9		12.1						u
WR72-5	WN6o		12.05						u
WR72-1	WC9		12.38						u
WR72-2	WC8		12.23						u
WR73	WC9d	15.20	14.17	1.23	6.39 ± 0.71			$-5.5^{+0.9}_{-0.9}$	b
WR74	WN7o	13.98	13.0	1.58	7.13 ± 0.71			$-6.3^{+0.8}_{-0.8}$	b
WR75	WN6b	11.23	12.6	0.71	3.67 ± 0.71			$-5.2^{+0.8}_{-0.8}$	b:
WR75-1	WC8		11.68						u
WR75aa	WC9d		13.44						u

WR Number	Spectral type	$v^{WR} \pm 0.1$ (mag)	μ (mag)	$(b - v)^{WR}$ (mag)	A_v^{WR} (mag)	$M_{V^s}^{S_V}$ (mag)	$F_{V^s}^{WR} / F_{V^s}^{S_V}$	$M_{V^s}^{WR}$ (mag)	Flags
WR75a	WC9	14.51	12.49	1.53	7.62 ± 0.71			$-5.8_{-0.9}^{+0.9}$	b
WR75b	WC9	16.09	11.14	1.71	8.36 ± 0.71			$-3.6_{-0.9}^{+0.9}$	b
WR75-21	WC7:		10.5						u
WR75ab	WN7h		12.9						u
WR75c	WC9		14.27						u
WR75d	WC9		12.76						u
WR75-23	WC9		12.5						u
WR76	WC9d	15.46	12.81	1.12	5.93 ± 0.71			$-3.6_{-1.0}^{+1.0}$	b
WR77	WC8+OB	13.00	12.27	0.61	3.90 ± 0.90	$-3.3_{-1.0}^{+1.0}$	0.52 ± 0.32	$-2.6_{-1.5}^{+2.0}$	b
WR77-5	WN6		11.69						u
WR77-1	WN7b		12.16						u
WR77aa	WC9d		12.01						u
WR77-2	WN7		12.13						u
WR77a	WN6o		12.17						u
WR77b	WC9d		12.38						u
WR77c	WN8o		12.34						u
WR77d	WN7o		12.13						u
WR77f	WN10-11h		11.89						u
WR77h	WN8o		11.17						u
WR77i	WC9d		11.79						u
WR77j	WN7o		12.53						u
WR77m	WC9d		12.09						u
WR77n	WC9d		12.17						u
WR77o	WN7o		12.49						u
WR77p	WC9		7.39						u

WR Number	Spectral type	$v^{WR} \pm 0.1$ (mag)	μ (mag)	$(b - v)^{WR}$ (mag)	A_v^{WR} (mag)	$M_{V^S}^{S_V}$ (mag)	$F_v^{WR} / F_v^{S_V}$	M_v^{WR} (mag)	Flags
WR77q	WN5o		11.76						u
WR77r	WN7o		12.43						u
WR77s	WN6o		11.43						u
WR77sa	WN6h		12.02						u
WR77sb	WN6o		12.0						u
WR77sc	WN7b		12.14						u
WR77sd	WN5o		11.18						u
WR77-3	WN6		12.16						u
WR77t	WC9d		12.14						u
WR77-6	WN6b		11.46						u
WR78	WN7h	6.61	10.48	0.21	1.48 \pm 0.71			-5.4 $^{+0.8}_{-0.8}$	b:
WR79	WC7+O5-8	6.95	10.68	0.01	1.05 \pm 0.87	-4.8 $^{+0.9}_{-0.9}$	0.54 \pm 0.29	-4.2 $^{+1.7}_{-1.4}$	g
WR79a	WN9ha	5.29	11.52	0.15	1.94 \pm 0.71			-8.6 $^{+1.0}_{-1.0}$	b
WR79b	WN9ha	8.32	13.63	0.55	3.58 \pm 0.71			-9.0 $^{+0.9}_{-0.9}$	b
WR80	WC9d	14.63	12.72	1.60	7.91 \pm 0.71			-6.3 $^{+1.0}_{-1.0}$	b
WR81	WC9	12.71	11.62	1.10	5.85 \pm 0.71			-4.9 $^{+0.8}_{-0.8}$	g
WR82	WN7(h)	12.41	12.87	0.85	4.12 \pm 0.71			-4.8 $^{+0.9}_{-0.9}$	g
WR82-2	WC9		11.53						u
WR83	WN5o	12.80	12.9	0.79	4.41 \pm 0.71			-4.7 $^{+0.9}_{-0.9}$	g
WR83-1	WC6:		11.21						u
WR84	WN7o	13.60	12.39	1.06	4.99 \pm 0.71			-3.9 $^{+0.8}_{-0.8}$	b:
WR84-4	WN7ha		11.62						u
WR84-11	WN9h		12.57						u
WR84-9	WN6		7.7						u
WR84-10	WC8		11.64						u

WR Number	Spectral type	$v^{WR} \pm 0.1$ (mag)	μ (mag)	$(b - v)^{WR}$ (mag)	A_v^{WR} (mag)	$M_{V^S}^{S_V}$ (mag)	$F_{V^S}^{WR} / F_{V^S}^{S_V}$	M_v^{WR} (mag)	Flags
WR85	WN6h	10.60	11.49	0.57	3.50 \pm 0.71			-4.5 $^{+0.8}_{-0.8}$	g
WR88	WC9	13.25	12.68	1.00	5.44 \pm 0.71			-5.1 $^{+0.9}_{-0.9}$	b:
WR87	WN7h+abs	12.50	12.32	1.58	7.87 \pm 0.71			-7.8 $^{+0.8}_{-0.8}$	b
WR89	WN8h+abs	11.50	12.31	1.22	6.34 \pm 0.71			-7.3 $^{+0.8}_{-0.8}$	g
WR90	WC7	7.45	10.3	-0.12	0.33 \pm 1.01			-3.2 $^{+1.0}_{-1.0}$	b:
WR91	WN7b	15.76	13.03	1.50	6.92 \pm 0.71			-4.5 $^{+0.9}_{-0.9}$	g
WR93	WC7+O7-9	11.46	11.23	1.12	5.68 \pm 0.79	-5.5 $^{+0.8}_{-0.8}$	0.42 \pm 0.22	-4.6 $^{+1.6}_{-1.3}$	b:
WR92	WC9	10.43	12.89	0.07	1.61 \pm 0.71			-4.3 $^{+0.9}_{-0.9}$	g
WR93a	WN6h	13.90	13.22	0.00	1.15 \pm 0.71			-0.8 $^{+1.1}_{-1.1}$	b
WR93b	WO3		11.8						u
WR94	WN5o	12.27	9.9	0.74	4.20 \pm 0.71			-1.8 $^{+0.7}_{-0.7}$	b
WR95	WC9d	14.00	11.57	1.29	6.63 \pm 0.71			-4.3 $^{+0.8}_{-0.8}$	g
WR96	WC9d	14.14	12.11	1.01	5.48 \pm 0.71			-3.6 $^{+0.8}_{-0.8}$	b
WR97	WN5b+O7	11.14	11.66	0.68	4.01 \pm 0.70	-4.6 $^{+0.8}_{-0.8}$	0.06 \pm 0.03	-1.5 $^{+1.7}_{-1.3}$	b
WR98	WN8o/C7	12.51	11.46	1.08	5.40 \pm 0.71			-4.4 $^{+0.8}_{-0.8}$	b
WR98a	WC8-9vd+?	19.70	10.5	0.00	1.25 \pm 0.71	7.4 $^{+1.1}_{-1.2}$	0.17 \pm 0.11	9.3 $^{+2.2}_{-1.7}$	b
WR100	WN7b	13.44	12.75	1.17	5.56 \pm 0.71			-5.1 $^{+0.9}_{-0.9}$	g
WR101	WC8	16.40	11.79	1.50	7.70 \pm 0.71			-3.5 $^{+1.1}_{-1.1}$	b:
WR102	WO2	15.10	12.11	0.77	4.70 \pm 0.71			-1.8 $^{+0.8}_{-0.8}$	g
WR102-19	WN5		11.89						u
WR102-20	WC9		11.42						u
WR102-25	WN6		14.04						u
WR102-21	WN6		11.62						u
WR102I	WN8o	15.53	12.67	1.80	8.03 \pm 0.71			-5.3 $^{+0.9}_{-0.9}$	g
WR103	WC9d+?	9.01	12.7	0.03	1.40 \pm 0.88	-5.4 $^{+1.1}_{-1.1}$	0.48 \pm 0.32	-4.6 $^{+2.3}_{-1.6}$	g

WR Number	Spectral type	$v^{WR} \pm 0.1$ (mag)	μ (mag)	$(b - v)^{WR}$ (mag)	A_v^{WR} (mag)	$M_{V^S}^{S_V}$ (mag)	$F_{V^S}^{WR} / F_{V^S}^{S_V}$	M_v^{WR} (mag)	Flags
WR104	WC9d+B0.5V (+VB)	13.54	12.19	1.31	6.67 ± 0.68	$-5.5_{-0.8}^{+0.8}$	0.50 ± 0.10	$-4.7_{-1.0}^{+1.1}$	g
WR105	WN9h	12.92	11.19	1.84	8.20 ± 0.71			$-6.6_{-0.8}^{+0.8}$	g
WR105-2	WN8-9		11.88						u
WR106	WC9d	12.33	12.43	0.80	4.61 ± 0.71			$-4.8_{-0.8}^{+0.8}$	g
WR107	WN8o	14.10	12.29	1.32	6.06 ± 0.71			$-4.3_{-0.9}^{+0.9}$	b
WR107a	WC5-7	16.43	12.35	1.32	6.26 ± 1.01			$-2.3_{-1.1}^{+1.1}$	b
WR108	WN9ha	10.16	12.22	0.80	4.61 ± 0.71			$-6.8_{-0.8}^{+0.8}$	g
WR108-1	WN9		11.73						u
WR109	WN5h	14.48	14.18	0.00	1.15 ± 0.71			$-1.0_{-0.9}^{+0.9}$	b
WR110	WN5-6b	10.30	10.99	0.75	3.83 ± 0.71			$-4.6_{-0.7}^{+0.7}$	g
WR111	WC5	8.23	11.06	-0.02	0.74 ± 1.01			$-3.7_{-1.1}^{+1.1}$	g
WR111-1	WN6o		9.01						u
WR111-9	WC9		12.5						u
WR111-2	WN7b		11.48						u
WR111-4	WN7		11.87						u
WR111-13	WN6b		11.87						u
WR111-3	WC8		11.91						u
WR111-10	WC7		10.44						u
WR111-12	WC9		11.74						u
WR112	WC9d+OB?	18.80	12.5	1.30	6.60 ± 0.70	$-0.8_{-1.1}^{+1.1}$	0.08 ± 0.05	$2.0_{-1.7}^{+2.3}$	b
WR113	WC8d+O8-9IV	9.43	11.28	0.46	3.20 ± 0.73	$-5.1_{-0.8}^{+0.8}$	0.24 ± 0.15	$-3.6_{-1.3}^{+1.8}$	b:
WR113-1	WN7o		11.64						u
WR113-2	WC5-6		11.34						u
WR114	WC5+OB?	12.95	11.6	0.91	4.57 ± 1.01			$-3.3_{-1.0}^{+1.0}$	b:
WR114-2	WC8		11.29						u

WR Number	Spectral type	$v^{WR} \pm 0.1$ (mag)	μ (mag)	$(b - v)^{WR}$ (mag)	A_v^{WR} (mag)	$M_{V^S}^{S_V}$ (mag)	$F_{V^S}^{WR} / F_{V^S}^{S_V}$	M_v^{WR} (mag)	Flags
WR114-1	WN6		11.89						u
WR115	WN6o	12.32	8.39	1.10	5.69 ± 0.71			$-2.5_{-1.5}^{+1.3}$	b
WR115-1	WN6o		12.52						u
WR115-2	WN8		11.65						u
WR115-3	WN7		12.14						u
WR116	WN8h	13.38	11.94	0.41	2.31 ± 0.71			$-0.9_{-0.8}^{+0.8}$	b
WR116-1	WC9+OBI		12.06			0.04 ± 0.03			u
WR116-2	WN5		11.6						u
WR116-3	WN6ha		12.3						u
WR117	WC9d	14.19	12.81	1.15	6.06 ± 0.71			$-5.0_{-1.0}^{+1.0}$	b:
WR117-1	WN7		12.66						u
WR118	WC9d	22.00	11.98	3.00	13.68 ± 0.71			$-3.7_{-0.9}^{+0.9}$	b:
WR118-4	WC8		11.85						u
WR118-2	WN9		11.91						u
WR118-3	WN9		9.22						u
WR118-10	WN6		8.68						u
WR118-5	WC9d		12.29						u
WR118-6	WN7:		11.8						u
WR119	WC9d	12.41	12.54	0.63	3.91 ± 0.71			$-4.3_{-0.9}^{+0.9}$	g
WR119-2	WC8		11.7						u
WR119-1	WN7o		13.15						u
WR120	WN7o	12.30	10.89	1.02	4.82 ± 0.71			$-3.7_{-1.0}^{+1.0}$	b
WR120-16	WC8		11.72						u
WR120-1	WC9		12.34						u
WR120-11	WC8		12.12						u

WR Number	Spectral type	$v^{WR} \pm 0.1$ (mag)	μ (mag)	$(b - v)^{WR}$ (mag)	A_v^{WR} (mag)	$M_{\text{V}}^{\text{Sys}}$ (mag)	$F_{\text{V}}^{\text{WR}} / F_{\text{V}}^{\text{Sys}}$	M_{V}^{WR} (mag)	Flags
WR120-7	WN7		12.33						u
WR120-3	WN9h		10.16						u
WR120-4	WN9h		11.83						u
WR120-5	WC8		11.49						u
WR120-6	WN6		12.48						u
WR120-15	WC8		12.39						u
WR120-10	WN7		12.06						u
WR121	WC9d	12.41	11.74	0.97	5.31±0.71		-4.7 ^{+0.8} _{-0.8}		g
WR121-15	WN4-5		12.37						u
WR121-12	WN5		11.9						u
WR121-1	WN7h		12.52						u
WR121-6	WN5		12.28						u
WR122-2	WN9		11.72						u
WR122-3	WN6		11.91						u
WR122-1	WC8		13.33						u
WR122-15	WN6		11.61						u
WR123	WN8o	11.26	13.64	0.43	2.39±0.71		-5.0 ^{+0.9} _{-0.9}		b:
WR123-1	WN6o		12.13						u
WR123-3	WN8		12.51						u
WR123-8	WN9h		11.21						u
WR124	WN8h	11.58	13.84	0.81	3.96±0.71		-6.4 ^{+0.9} _{-0.9}		b:
WR124-1B	WC8		10.96						u
WR124-1A	WC8		11.85						u
WR124-3	WC8		12.82						u
WR124-9	WC6:		12.12						u

WR Number	Spectral type	$v^{WR} \pm 0.1$ (mag)	μ (mag)	$(b - v)^{WR}$ (mag)	A_v^{WR} (mag)	$M_{V^S}^{S_V}$ (mag)	$F_{V^S}^{WR} / F_{V^S}^{S_V}$	M_v^{WR} (mag)	Flags
WR124-18	WN9h		12.07						u
WR124-19	WC6:		11.83						u
WR124-2	WC8		12.21						u
WR124-6	WC6		12.18						u
WR124-7	WC7		12.3						u
WR124-11	WN6b		11.95						u
WR124-20	WC9		9.15						u
WR124-21	WC8		13.83						u
WR124-22	WC9		11.41						u
WR125	WC7ed+O9III	13.52	12.63	1.32	6.48 ± 0.83	$-5.8_{-1.0}^{+1.0}$	0.48 ± 0.26	$-5.0_{-1.4}^{+1.8}$	b
WR125-4	WN7		12.35						u
WR125-3	WN7ha		12.34						u
WR125-2	WN8-9		12.58						u
WR125-1	WC8		13.4						u
WR126	WC5/WN	13.29	14.4	0.70	3.71 ± 1.01			$-4.9_{-1.1}^{+1.1}$	b
WR127	WN3b+O9.5V	10.33	12.45	0.15	1.77 ± 0.69	$-3.9_{-0.7}^{+0.7}$	0.17 ± 0.10	$-2.0_{-1.2}^{+1.7}$	b
WR129	WN4o	13.27	13.69	0.55	3.58 ± 0.71			$-4.1_{-0.8}^{+0.8}$	b:
WR128	WN4(h)	10.54	12.31	-0.01	1.28 ± 0.71			$-3.2_{-0.8}^{+0.8}$	g
WR130	WN8(h)	12.60	14.12	1.18	5.48 ± 0.71			$-7.1_{-0.9}^{+0.9}$	b
WR131	WN7h+abs	12.36	14.2	0.73	4.37 ± 0.71			$-6.3_{-0.8}^{+0.8}$	g
WR132	WC6+?	13.49	13.09	0.70	3.71 ± 1.01			$-3.4_{-1.1}^{+1.1}$	b:
WR133	WN5o+O9I	6.70	11.33	0.00	1.22 ± 0.70	$-5.9_{-0.7}^{+0.7}$	0.16 ± 0.09	$-3.9_{-1.2}^{+1.7}$	g
WR134	WN6b	8.23	11.21	0.20	1.57 ± 0.71			$-4.6_{-0.7}^{+0.7}$	g
WR135	WC8	8.36	11.48	-0.03	1.40 ± 0.71			$-4.6_{-0.7}^{+0.7}$	g
WR136	WN6b(h)	7.65	11.43	0.23	1.69 ± 0.71			$-5.5_{-0.7}^{+0.7}$	b

WR Number	Spectral type	$v^{WR} \pm 0.1$ (mag)	μ (mag)	$(b - v)^{WR}$ (mag)	A_v^{WR} (mag)	$M_{V^S}^{S_V}$ (mag)	$F_{V^S}^{WR} / F_{V^S}^{S_V}$	M_v^{WR} (mag)	Flags
WR137	WC7pd+O9	8.15	11.61	0.14	1.70 ± 0.73	$-5.2_{-0.8}^{+0.8}$	0.28 ± 0.15	$-3.8_{-1.2}^{+1.6}$	g
WR138	WN6o	8.10	11.96	0.22	2.06 ± 0.71			$-6.0_{-0.8}^{+0.8}$	b
WR138-1	WN8-9h		15.49						u
WR139	WN5o+O6III-V	8.10	10.58	0.38	2.76 ± 0.83	$-5.3_{-0.8}^{+0.8}$	0.51 ± 0.30	$-4.5_{-1.3}^{+1.8}$	g
WR140	WC7pd+O4-5	7.07	11.07	0.27	2.21 ± 0.74	$-6.2_{-0.8}^{+0.8}$	0.33 ± 0.17	$-5.0_{-1.2}^{+1.5}$	b
WR141	WN5o+O5V-III	10.14	11.42	0.71	4.08 ± 0.71			$-5.4_{-0.7}^{+0.7}$	b
WR142	WO2	13.82	11.08	1.39	7.25 ± 0.71			$-4.5_{-0.7}^{+0.7}$	b
WR142a	WC8		11.29						u
WR142-1	WN6o		11.24						u
WR143	WC4+OB?	11.95	11.73	1.21	6.07 ± 0.74	$-5.9_{-0.8}^{+0.8}$	0.36 ± 0.15	$-4.8_{-1.1}^{+1.3}$	b:
WR144	WC4	15.49	11.21						u
WR145	WN7o/CE+?	12.55	10.81	1.63	7.76 ± 1.31	$-6.1_{-1.3}^{+1.3}$	0.65 ± 0.64	$-5.6_{-1.8}^{+6.3}$	b
WR146	WC6+O8	13.91	10.21	2.38	10.87 ± 0.77	$-7.6_{-1.2}^{+1.2}$	0.43 ± 0.19	$-6.7_{-1.6}^{+1.8}$	b
WR147	WN8(h)+B0.5V	14.89	11.26	2.15	9.48 ± 0.71			$-5.9_{-0.8}^{+0.8}$	g
WR148	WN8h+	10.46	14.88	0.36	2.10 ± 0.71			$-6.6_{-0.8}^{+0.8}$	b:
WR149	WN5o	14.70	13.45	1.20	6.10 ± 0.71			$-4.9_{-0.8}^{+0.8}$	b:
WR150	WC5	13.47	14.71	0.53	3.01 ± 1.01			$-4.3_{-1.1}^{+1.1}$	g
WR151	WN4o+O5V	12.37	13.65	0.65	3.98 ± 1.04	$-5.4_{-1.1}^{+1.1}$	0.76 ± 0.44	$-5.1_{-1.4}^{+2.1}$	b
WR152	WN3(h)	11.67	13.2	0.17	2.02 ± 0.71			$-3.7_{-0.9}^{+0.9}$	g
WR153	WN6o/CE+O6I	9.08	13.04	0.27	2.19 ± 0.96	$-6.2_{-1.0}^{+1.0}$	0.56 ± 0.37	$-5.6_{-1.6}^{+2.2}$	b
WR154	WC6	11.54	13.65	0.36	2.31 ± 1.01			$-4.6_{-1.1}^{+1.1}$	b:
WR155	WN6o+O9II-Ib	8.75	12.38	0.28	2.37 ± 1.07	$-6.1_{-1.1}^{+1.1}$	0.19 ± 0.49	$-4.3_{-2.5}^{+2.9}$	g
WR156	WN8h	11.09	13.07	0.83	4.04 ± 0.71			$-6.1_{-0.8}^{+0.8}$	g
WR157	WN5o(+B1II)	9.91	12.05	0.46	3.11 ± 0.72	$-5.3_{-0.8}^{+0.8}$	0.28 ± 0.16	$-3.9_{-1.3}^{+1.7}$	g
WR158	WN7h	11.46	13.49	0.75	3.71 ± 0.71	$-5.8_{-0.8}^{+0.8}$	0.30 ± 0.94	$-4.5_{-2.1}^{+2.1}$	g

WR Number	Spectral type	$v^{WR} \pm 0.1$ (mag)	μ (mag)	$(b - v)^{WR}$ (mag)	A_v^{WR} (mag)	$M_{V^{sys}}$ (mag)	F_v^{WR} / F_v^{sys}	M_v^{WR} (mag)	Flags
WR159	WN4		11.3						u

Columns: (1) WR Number, (2) Spectral type, (3) v^{WR} apparent magnitude and error, (4) Distance modulus μ , (5) $(b - v)^{WR}$ colour, (6) v^{WR} band extinction A_v , (7) Absolute magnitude of binary system (including companion), (8) Fraction of light contributed to the binary system by the WR component, (9) Absolute magnitude of WR star, (10) Error flags, where $M > \text{upper}_{\text{initial}}$ or $M < \text{lower}_{\text{initial}} = b$, $M > \text{upper}_{\text{final}}$ or $M < \text{lower}_{\text{final}} = b$: (_{initial} denotes the averages calculated before sigma clipping, _{final} are the final absolute magnitude boundaries) and g are results with no issues.

This paper has been typeset from a TeX/LaTeX file prepared by the author.